Universidad
Rey Juan Carlos

Departamento de Biología y Geología, Física y Química Inorgánica

# TESIS DOCTORAL

# Dynamics and Physics of Cancer: Tumor and Immune Cell Interactions

Álvaro García López
Universidad Rey Juan Carlos

May, 2016

**Miguel Ángel Fernández Sanjuán,** Catedrático de Física y
**Jesús Miguel Seoane Sepúlveda,** Profesor Titular de Física

**CERTIFICAN:**

Que la presente memoria de tesis doctoral, titulada *"Dynamics and Physics of Cancer: Tumor and Immune Cell Interactions"*, ha sido realizada bajo nuestra dirección por Álvaro García López para optar al grado de Doctor por la Universidad Rey Juan Carlos.

Y para que conste que la citada tesis reune todos los requisitos necesarios para su defensa y aprobación, firmamos el presente certificado en Móstoles a 25 de Mayo de dos mil dieciséis.

Móstoles, 25 de Mayo de 2016

Fdo. Miguel Ángel Fernández Sanjuán
Catedrático de Física
Universidad Rey Juan Carlos

Fdo. Jesús Miguel Seoane Sepúlveda
Profesor Titular de Física
Universidad Rey Juan Carlos

*En agradecimiento a mis profesores de enseñanza secundaria, Juan Luis García Hourcade y Concepción Rodríguez de Ávila, quienes, con sus lecciones de Física y Química, depositaron la simiente que, con el devenir de los años, acabaría convirtiéndose en ésta mi pasión por la Ciencia.*

# Agradecimientos

*"Quien dice hombre, dice lenguaje, y quien dice lenguaje, dice sociedad."*

-Claude Levi-Strauss (1908-2009)

Esta tesis doctoral no podría haberse llevado a cabo sin la ayuda y consejo de otras personas, algunas de las cuales me han servido de apoyo, tanto material como espiritualmente, a lo largo de todos estos años.

Mi más sincero agradecimiento a los Profs. *Miguel Ángel Fernández Sanjuán* y *Jesús Miguel Seoane Sepúlveda*, por el consejo en la dirección de este trabajo, su paciencia con mis devaneos y la libertad con la que me han permitido desarrollar estas investigaciones. Gracias también a mis queridos compañeros del grupo de investigación en Dinámica No Lineal, Teoria del Caos y Sistemas Complejos de la Universidad Rey Juan Carlos, que me han tendido siempre su mano sin la más mínima vacilación. En particular, quiero mostrar un agradecimiento especial a *Álvar Daza Esteban*, amigo y cómplice de despacho, con quien he mantenido incesantes y acalorados debates: honorable contienda dialéctica, que ha servido para modificar y refinar muchas de las ideas que aquí se vierten, e incluso para deshechar otras de las tantas que, a diario, pasan por mi conturbada mente.

Sea como fuere, la familia es una suerte de simetría en la vida de la inmensa mayoría de los hombres. Una estructura perenne que, a pesar de los avatares y de sus mudanzas, a pesar de sus muchos defectos, se mantiene resuelta y perseverante en su atención y apoyo a uno. En segundo lugar, pues, quiero agradecérselo a toda mi familia, y más en particular a la nuclear, que es la integrada por mis padres *Santiago García Carbajosa* y *Gemma López Gutiérrez*, y mi hermana *Laura García López*. Ellos han provisto infatigablemente el sustento, el amor y, aún si se quiere, el desamor, indispensables para la educación y el desarrollo de todo individuo en sociedad.

Quiero dedicarselo también a esos otros seres queridos, tan importantes; a esa otra familia, la que uno se fragua, con sus amistades. A las que inicié en mi infancia y adolescencia, en la ciudad de Segovia, entre pupitres, atriles, tabernas y plazas.

A las que más tarde, en mi juventud, forjé en la ciudad de Salamanca, donde cursé mis estudios en ciencias Físicas, hace ya cosa de una década. Guardo grato recuerdo de casi todos los que, por aquel entonces, fueron mis compañeros de aula. De entre todos ellos, a *Alfonso Delgado Bonal*, con quien tantos trabajos llevé a cabo durante mis estudios, y con quien di rienda suelta a mi imaginación en innumerables ocasiones, acerca de las diversas materias que son objeto de estudio en la Física. Fue precisamente él quien me advirtió de la beca docente que he tenido el placer de percibir durante cuatro años y por cuya causa me hallo hoy aquí, en la ciudad de Madrid.

Como no puede ser de otra manera, dedico también este trabajo al resto de profesores, muchos formidables, tanto durante mis primeros pasos, en el C. E. I. P. Domingo de Soto, como más tarde, durante la confusa adolescencia por la que transcurrió mi enseñanza secundaria, en el I. E. S. Mariano Quintanilla y, ya por último, durante mi madurez, en la Universidad de Salamanca y en la Universidad de Granada.

El presente trabajo se ha beneficiado de una Beca Iberoamérica del Banco Santander para la realización de una estancia predoctoral en la Universidade Federal do Paraná, de Agosto a Noviembre de 2015. Aprovecho estas últimas líneas, por lo tanto, para manifestar mi agradecimiento a dicha entidad bancaria y a la hospitalidad de los Profs. *Ricardo Luiz Viana* y *Antonio Marcos Batista*, que me acogieron afectuosamente en la ciudad de Curitiba. Finalmente, el trabajo de investigación que ha dado lugar a esta tesis doctoral se ha beneficiado de los proyectos de investigación FIS2009-098981 del Ministerio de Ciencia e Innovación y FIS2013-40653-P del Ministerio de Economía y Competitividad.

Mayo, 2016
Álvaro García López

# Preface

*"Be fruitful and multiply, and fill the Earth and subdue it, and have dominion over the fish of the sea, and over the birds of the heavens and over every living thing that moves on the Earth"*

-Genesis 1:28

The present work constitutes my PhD thesis, which has been accomplished during the last five years in the research group on Nonlinear Dynamics, Chaos Theory and Complex Systems Group at the Universidad Rey Juan Carlos. It is focused on two core subjects, which are the *dynamics of tumor growth* in interaction with the cell-mediated *immune response*, and the application of *control techniques* to avoid the overgrowth of tumors, both from the point of view of Nonlinear Dynamics and Complex Systems. In order to provide a conceptual framework to this work, I develop a general introduction to complex systems, the biology of cancer, and the immune system function. Then, its main body is comprised by an article on the existence and control of chaos in a cancer model of tumor and immune cell interactions, another in which we validate a mathematical model of tumor growth, two works on the establishment of the mathematical equation that governs the lysis of solid tumors and one last article in which we investigate the transient and asymptotic dynamics of tumor-immune aggregates. The thesis has been arranged in seven chapters with the following contents:

**Chapter 1. Introduction**

We begin by introducing the basic notions that are necessary to clearly understand the contents of the whole work. We describe dynamical systems, nonlinearity, and several concepts commonly employed in the study of complex systems. Then we expose the problem of cancer and the current status of cancer theories. An indispensable introduction to immunology and its role in tumor development proceeds. The

fourth last section is devoted to presenting the mathematical tools and techniques that are used in our investigations, both from a historical and a methodological perspective.

**Chapter 2. Chaos and control in a model of tumor-immune interactions**

Here we present our first approach to cancer modelling. We investigate the dynamics of a three-dimensional model describing tumor and immune cell interactions. After inspection of the phase and the parameter spaces, a boundary crisis leading to transient chaotic dynamics is found. To avoid the overgrowth of the tumor, we propose a control technique that has been developed by our research group, which allows to keep the tumor oscillating at a small size population. We also discuss the practical difficulties to apply this technique. The last section of the chapter is devoted to expose other works on the control of chaos.

**Chapter 3. A validated mathematical model of tumor-immune interactions**

In this third chapter our attention turns to the correlation between our models and some experimental results obtained from studies with mice and men. By introducing a mathematical function proposed in other studies of tumor cell lysis, we modify the model presented in the previous chapter, and fit it to the experimental data. Several hypotheses concerning this mathematical function are proposed. Finally, we also validate an experimental chemotherapy protocol applied to mice *in vivo* and study several correlations between the proposed model and the experimental results.

**Chapter 4. The fractional cell kill governing the lysis of solid tumors**

Now we concentrate our efforts in the study of the hypotheses proposed in the foregoing chapter. Using an hybrid cellular automaton model, we show that the mathematical function that describes the velocity at which a tumor is lysed by a population of immune cells, arises from spatial and geometrical constraints. We introduce some crucial modifications, so that the parameters appearing in the mathematical function have a clear biological and physical significance, and also its asymptotic behaviour is well-posed. Moreover, we provide an analytical derivation of the function, using heuristic arguments.

**Chapter 5. The kinetics of tumor lysis**

Having established the mathematical function that governs the lysis of solid tumors, we inspect its different limits in this fifth chapter. Analytical methods are used to determine the rate at which a solid tumor decays in one of such limits, and one last modification is proposed. We test this modification using the cellular automaton previously developed, showing its validity. Finally, we discuss the possibilities of the mathematical function to describe the lysis of non-solid tumors and tumors infiltrated with lymphocytes.

**Chapter 6. Dynamics of tumor-immune interactions**

In this penultimate chapter we investigate the long-range dynamics of tumor and immune cell interactions, using an extension of the cellular automaton. The

possible outcomes of two competing tumor and immune cell populations are put in correspondence with the theory of immunoedition. Diving deep into the parameter space and developing new techniques, we show that a long-lasting tumor mass dormancy uniquely mediated by the immune system is not a very likely event to occur.

**Chapter 7. Conclusions**

The thesis ends summarizing the main results of our investigations.

# Contents

# Chapter 1
# Introduction

*"All truth is simple... is that not doubly a lie?"*

-Friedrich Nietzsche, (1844-1900)

## 1.1 Complex systems

The science of complex systems arises as a response to the reductionist philosophy that dominated science from the 17th century until well into the 20th century. According to this philosophy, all phenomena can and should be explained in terms of fundamental physics. Thus, if cells are made of organelles, and these in turn are made of proteins, which at the same time are composed by atoms, the knowledge of the physical laws governing the atomic scale should suffice to explain the laws governing the dynamics of cells, animals, species and so on. However, experience demonstrates that when a physical system is constituted by numerous parts interacting among them in a complex manner, unexpected and unpredictable properties that can not be inferred from the separated study of such parts appear. Moreover, since the dynamics at a particular scale can be affected by the dynamics at a higher scale, the development of a bottom-up description of nature is simply unrealistic. Given this state of facts, we begin this thesis by introducing some basic definitions concerning nonlinear dynamics and complex systems, and also discussing their importance in the study of physics and biology.

### 1.1.1 Dynamical systems and chaos

As experience reveals, every physical system, whatever is the facet of nature it covers, experiments changes as time goes by. This is to say, the dynamical character of nature is its fundamental or essential feature. Science consists in the study of nature in order to achieve a better understanding that allows us to obtain practical benefits from it. Therefore, a deep knowledge of how things evolve with time is required to reach the mentioned goal. Otherwise we could be arranging things hoping to follow a certain track, and future would mess up all our plans. This is, in fact, what occurs mostly, and it is due to the unpredictability of physical systems under certain circumstances.

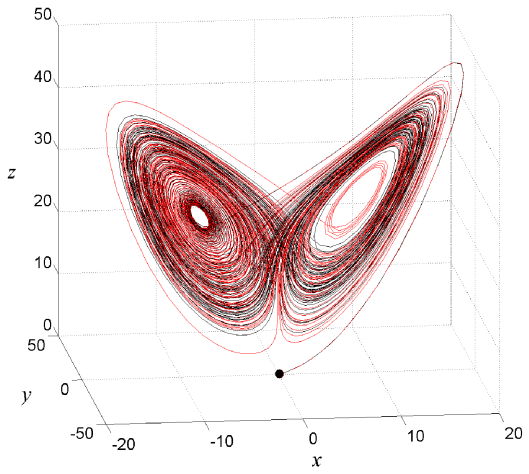


**Figure 1.1. The Lorenz attractor**. Two trajectories for the Lorenz system and almost same initial conditions represented by two overlapping dots. They start together but soon begin to separate exponentially. After a while the red one is in the right wing of the chaotic attractor, while the black one appears on the left side. However, both stay trapped or bounded in a certain region of the phase space.

At a fundamental level, dynamical systems can be described by means of ordinary differential equations. Since this description will be of great importance in our studies, we give some formal definitions in the first place.

**Definition 1.1.** *Given a topological space $X$ a set $E = \mathbb{R}$ or $E = \mathbb{Z}$ and a continuous mapping $\phi : X \times E \to X$, a dynamical system is a list of three elements $(X, E, \phi)$, satisfying:*

- $\phi(0, x) = x \quad \forall x \in X$
- $\phi(t, x) \circ \phi(s, x) = \phi(t + s, x) \quad \forall x \in X \quad t, s \in E$

The topological space $X$ is called *phase space*, and frequently denoted by $\Omega$. The mapping $\phi_t(x)$ is usually called a one-parameter *flow*, and tells us how a particular

initial condition $x$ of the dynamical system evolves with time $t$. If $E = \mathbb{R}$ the dynamical system is said to be *continuous*, while in the other case is said to be *discrete*. In the present work both sort of systems are important, since a common tool used in continuous and bounded dynamical systems is the Poincaré map or return map, which is obtained by observing how trajectories intersect a section of the space. In this manner, an application that maps a certain set in this section into it can be constructed. The time evolution is generally given by a set of equations, called the *equations of motion*, that are written as a system of first order differential equations,

$$\dot{\mathbf{x}} = \mathbf{F}(\mathbf{x}). \tag{1.1}$$

The vector appearing in the previous equation is called a *vector field*, and it is tangent to the flow curves. The flow also obeys the equations of motion and the field represents the tangent at the identity of the flow, which can be simply computed by differentiation

$$\dot{\mathbf{x}} = \left( \frac{d\phi_t(x)}{dt} \right)_{t=0}. \tag{1.2}$$

For discrete systems, equations of motion are written iteratively in the form

$$\mathbf{x_{n+1}} = \mathbf{F}(\mathbf{x_n}), \tag{1.3}$$

where the sequence $\{F^n(x_0)\}_{n\in\mathbb{Z}}$ is called the *orbit* of the initial condition $x_0$.

In summary, a dynamical system is a set of states equipped with a time evolution. Since these equations are deterministic, in principle, given some initial conditions, the future can be predicted from this set of equations. This picture of reality, originated with the discovery of Newtonian mechanics, yields a universe working more or less like a clock. It is traditionally summarized under Pierre Simon Laplace's statement. This statement asserts that, given Newton's laws and the current position and velocity of every particle in the universe, it is possible, in principle, to predict everything for all time. However, the development of the theory of dynamical systems has demonstrated that, because of the nonlinear nature of physical systems, which tend to amplify perturbations [1], the predictive capacity of a model can be hindered and lost for long enough times. Dynamical systems that possess this property are said to be *sensitive to initial conditions*, and are called *chaotic*. Taking up the previous mathematical concepts, a simple, clear and rigorous definition of a chaotic dynamical system can be given as follows

**Definition 1.2.** *A flow $\phi_t(x)$ is said to have sensitive dependence to initial conditions in a compact flow invariant*[1] *subset $\Lambda \subset \Omega$, if there exists $\epsilon > 0$, so that for every $x \in \Lambda$ and any open set $U \subset \Lambda$ containing $x$ there is $y \in U$ and $t > 0$ satisfying $||\phi_t(x) - \phi_t(y)|| > \epsilon$.*

Sensitive dependence to initial conditions means that two arbitrarily close points of phase space separate fast as time goes by. Whenever this sensitive dependence

[1] This means $\phi_t(\Lambda) \subseteq \Lambda$, $\forall t \in \mathbb{R}$.

takes place, we talk about chaos and unpredictability (see Fig. 1.1). In practice, fast means exponentially, and this sensitive dependence is commonly measured by the largest Lyapunov exponent. Note that because the system is bounded, saying that the two points separate does not mean that their distance is always increasing. These two points will certainly come closer again the sooner or the later, but after this re-encounter, they will separate once again. This is in contrast with linear transformations, which transform parallel lines into parallel lines, meeting the fifth postulate of Euclidean geometry. If a linear system expands, *i.e.*, amplifies perturbations, it can not be bounded. In other words, sensitive dependence to initial conditions occurs in a local manner. The big deal with this sensitivity is that any small error or uncertainty in the measure of an initial condition will be exponentially expanded with time evolution. Since our measurement apparatus have a finite resolution, whenever a system is chaotic, long time predictions become impossible. Chaos means unpredictability for far enough future. Therefore, nonlinearity might lead to chaotic dynamics of a physical system, and more sophisticated systems, created from the interaction of nonlinear elements distributed in space, just as those described in the next section, are at the core of the studies of complexity.

### 1.1.2 Characteristics of complex systems

A complex system can be defined as a system "in which large networks of components with no central control and simple rules of operation give rise to complex collective behaviour, sophisticated information processing, and adaptation via learning or evolution" [2]. When pattern and organization appear in a physical system without the guidance of a central controller, it is commonly said that the system *self-organizes* [3]. Generally, the resulting patterns of organization can not be easily deduced from the description of their interconnected parts, and therefore they are said to represent *emergent* properties of the system.

As the field of complex systems has developed, a standard concerning their classification has been widely adopted, splitting this science into two domains: *complex physical systems* and *complex adaptive systems* [4]. Since our works mainly deal with complex physical systems, in the following lines we introduce their fundamental characteristics.

Complex physical systems are usually formed by arrays of elements (atoms, cells, etc.) that occupy several positions in the space. Generally, these elements remain still at their location, and fixed local interactions occur between a particular element and its neighbours. As a result of their interactions, a certain spatio-temporal pattern evolving in time appears. Thus, the three basic ingredients of a complex physical system are: (1) a series of interacting entities that can exist in different states, (2) the geometry representing their spatial distribution and (3) the fixed rules characterizing their interactions.

1. The components of a complex physical system can be diverse, depending on the scale at study. For example, neural networks study interactions between neuron cells. Reaction-diffusion systems study the diffusion and the reaction

of several chemical substances in a spatial domain. In the Ising model, which studies the behaviour of ferromagnetic materials, the lattice points are occupied by particles with a certain spin. But, independently of the nature of these components, all of them must be capable of existing in different states, which change according to deterministic or probabilistic laws.

2. Sometimes the agents of a model are allowed to occupy positions in a continuous space, but most complex systems are modelled using discrete *grids* or lattice-like geometries. The geometry of the lattices varies significantly depending on the model. For simplicity, orthogonal square lattices are frequently assumed, albeit some studies use different Bravais configurations. Non-euclidean geometries are abundant in the literature as well, as for example elements arranged and connected along rings. However, in many situations the geometry is considered unimportant, and the attention is focused on the connections between the model elements. This is a customary approach in the study of networks, where the emphasis is put on the topology of the network.

3. Certainly, the rules that govern the interactions among the elements of a complex system enclose all its "magical" or hard-to-predict features. Of course, these rules are imposed by the specific nature of the interacting parts, but the interactions of complex physical systems obey a particular characteristic that makes these systems deserve their name. Essentially, the interactions are *nonlinear*. As opposed to the superposition principle, this means that the response of the elements of the system to a perturbation is not proportional to it, what endows the system with the capacity to *amplify perturbations*, which can be later propagated to other components of the system. In this sense, complex systems are holistic, a property traditionally referred by saying that "the whole is greater than the sum of its parts".

In some circumstances, the amplification of perturbations due to nonlinear feedback is capable to provoke a rupture of the homogeneity or a *symmetry breaking* of the system. Not surprisingly, *fractal structures* [5] and power-law distributions pervade the study of complexity. Another important property of complex systems is that they can be *self-referential*, meaning by this that the input of an element depends on its own output. In this manner, the line of causality is broken, and complex feedback loops befall. If a negative feedback mechanism is established between a complex system and some environmental variable, in such a way that the input of the dynamical system depends on its output and such variable, the system can exhibit *goal-directed* behaviour, what confers it purposeful or teleological qualities [6]. Therefore, the dynamics of a complex physical system must be understood in terms of a balance between positive feedback mechanisms, which are responsible for the amplification of signals, and the negative feedback mechanisms, that tend to stabilize the system. As a consequence, these systems are frequently found in what has been called *critical states* [7], where small perturbations can destabilize their metastable states, leading to cascade events that are dispersed through the system

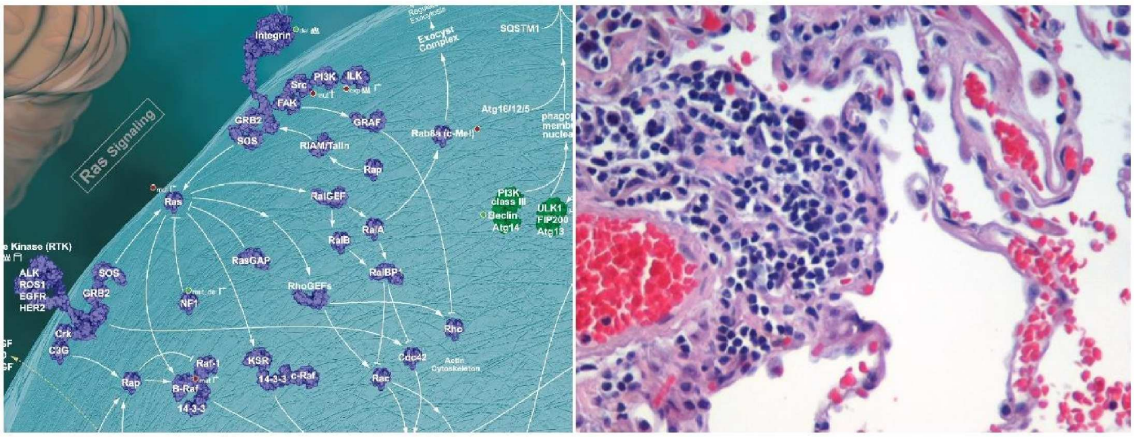


**Figure 1.2. Two complex systems.** (a) A complex network representing the Ras signalling transduction pathway inside a cell. In purple we see the different interacting proteins that comprise these complex network, while the different links representing the positive and negative feedback interactions are shown in white. (b) Microscopic view of an histological specimen of human lung tissue. This complex system is comprised by different types of interacting cells. We can see erythrocytes in red, T cells in blue, and stromal cells in pink. The white regions represent empty space. From Refs. [10, 11], respectively.

in a scale-free manner. Once again, *self-similarity* manifests.

Interestingly, the notion of a single-valued and one-to-one relation between cause and effect in complex systems is ambiguous in other ways. For example, in biological systems, a cause might have several effects (*pleiotropy*) or, on the contrary, different causes might *synergize* to produce a single effect. Another hallmark of complex systems is their *antagonism*. This means that, due to nonlinearity, causality becomes context dependent, and a particular cause might produce one effect or its opposite, depending on its intensity or some other relevant variables of the system. In summary, nonlinearity is the fundamental notion at the core of complexity and *a conditio sine qua non* to observe complex behaviour. However, such condition is not sufficient on its own, and other requisites must be fulfilled. Both necessary and sufficient conditions to observe complex emergent phenomena in physical systems have been mathematically derived and gathered under the term *edge of chaos* [8], a concept that has evolved in the study of complex phenomena [9]. To conclude, and as the introductory definition evidences, every complex system can be regarded as a network (see Fig. 1.2), where the rules of interaction define a topology, linking their interacting elements (*nodes*) in a particular way. In spite of the fact that the interactions or the *links* are often stronger between neighbouring elements, *i.e.*, they act locally, long-range dependencies are commonly found in many complex systems.

Finally, some remarks concerning life and self-organization deserve exposition. As previously noticed, under appropriate conditions, complex physical systems are capable to self-organize into non-homogeneous patterns [12]. This fact seems to defy

the second principle of thermodynamics, which predicts that the ultimate state of an isolated system is an homogeneous state of equilibrium. The solution to this paradox is that the emergence of non-homogeneity and the evolution of a system far from equilibrium requires complex systems to be *open* [13]. It is the constant flow of matter and energy between the system and its environment that allows it to create ordered dynamical structures. Because of their capacity to dissipate gradients and reduce exergy [14], the term dissipative structures was coined by Ilya Prigogine to describe complex physical systems [15]. On the other hand, these structures or dynamical patterns also allow dynamical systems to code and process *information*. Their increasing ability to process information coming from the environment bestow them with the capacity to *adapt* to such environment, by modifying the internal relations among its parts. Therefore, the entropy regulation performed by these systems leads naturally to the concept of *homeostasis* [16], which can be defined as the self-maintenance of a complex system in a similar unstable state in the presence of a fluctuating milieu. From our point of view, it is at this point that complex adaptive systems emerge. Their adaptation is accomplished by constantly rewiring the connections among their constituents and, in this way, the rules that guide the dynamics of the system are constantly evolving, as opposed to complex physical systems.

Even though the dynamical systems modelled in this thesis are evolutionary, the present work focuses on aspects that are rather physical. Therefore, adaptation will not be rigorously represented. Nevertheless, our methods allow to figure out evolutionary features, as for instance in Chapter 7, in which the results are in clear correspondence with the evolutionary theory of immunoedition. Moreover, our models also incorporate some degree of heterogeneity, cell motility and simulate two different scales. Consequently, they include aspects which go beyond models frequently used in the study of complex physical systems and, in a rudimentary sense, are adaptive.

## 1.2 Cancer theories

The ability of cells to proliferate is essential for multicellular organisms, as morphogenesis and wound repair exemplify. However, in such organisms, the ancestral capacities of cells to move and multiply are carefully regulated probably both at the cellular and the tissue level, so that the organization of the tissue displays specific functionalities. When the mechanisms silencing the growth of cells in a tissue fail, an uncontrolled proliferation proceeds, leading to a dysfunctional accumulation of cells, known as a tumor or *neoplasia*. Prior to this agglomeration, tissues evolve from their normal phenotype into a highly abnormal architecture, which is formally known as a *dysplasia*, and that it is not usually harmful to the organism, because of its robustness. During the first steps of carcinogenesis, most tumors (*e.g.*, in situ carcinomas) can not grow beyond the resource limitations imposed by their tissue environment, and it is common to find necrotic cores inside them. It is now very well accepted that solid tumors grow logistically [17]. It is only when tumors cells reach

the circulatory system and colonize the organism that cancers become lethal. These tumors are said to be *invasive*. The extravasation of tumor cells from a primary tumor, their subsequent navigation through the circulatory system and their final landing into other locations of the body, is named *metastasis*. Approximately 90 % of the fatal cancers are metastatic.

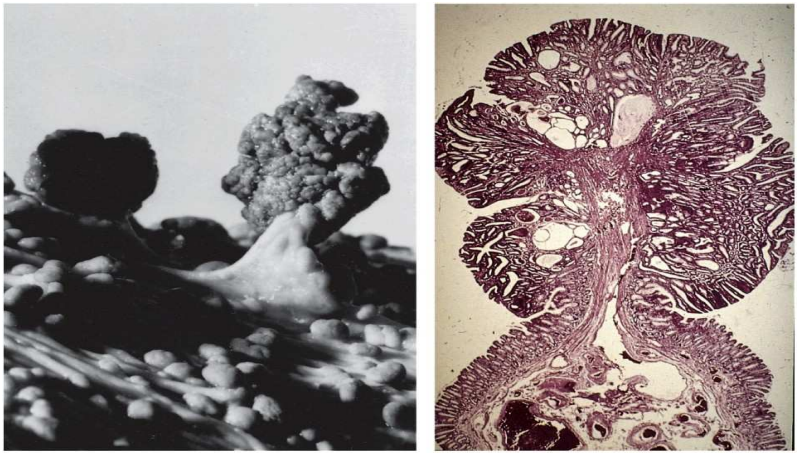

(*a*) (*b*)

**Figure 1.3. A pre-malignant growth in the colon.** (a) A photograph of a pedunculated polyp in the colon. (b) A micrograph of the same polyp. From Ref. [10]

Therefore, cancer is the uncontrolled proliferation and spread of a population of cells through the organism. But, from a physicist point of view, cancer can be defined in a more general and abstract manner. We might define cancer as the *destabilization of an ecosystem due to the overgrowth and overspreading of a certain subset of the species which cohabit in it*. This "unlimited" growth may arise in several manners, but clearly represent an extreme form of liberalism that allows some species to become independent of the environmental constraints that are responsible for their restricted growth.

Concerning the origin of tumors, a theory has dominated the conception of cancer during almost a century [10]. This theory is formally known as the *somatic mutation theory*, and claims that cancer is a *monoclonal expansion* resulting from the accumulation of mutations by a single cell. These mutations arise inevitably as a consequence of stochastic mistakes in the process of replication of the DNA, but can be also produced by several chemicals, commonly known as carcinogens. The mutations of this single renegade cell [18] endow it with the capacity to promote its own proliferation. As the tumor mass grows, further properties must be acquired by the descendants of this aberrant cell, which allow them to circumvent the various homeostatic controls that regulate development in tissues, as well as the natural restrictions imposed from the tissue environment. In this manner, cancer can be seen as an evolutionary Darwinian process [19], in part governed by random drift and natural selection. Waves of clonal expansion and cell death would guide the sculpting of tumors toward their invasive phenotype. Thus, according to this theory, cancer

is a *cell-based* disease, resulting from the accumulation of mutations that concern crucial genes coding proteins that regulate genomic stability and render eukaryotic cells their quiescent default phenotype.

The increasing complexity of the *somatic mutation theory*, together with its inability to provide a substantial progress on the treatment of many cancers (mainly carcinomas), has led to the proposal of an alternative theory, called the *tissue organization field theory*. This theory proposes that cancer is a *tissue-based* disease, affecting the *biophysical* and *biomechanical* communication between the stroma and the epithelium. The proliferation and motility restraints imposed by normal tissue architecture loosen and as a consequence of this disruption, leading to the hyperplasia of the epithelium. Further alteration of the reciprocal interactions between tissue compartments will induce metaplasia, dysplasia, and carcinoma [20].

In conclusion, a lot of movement and conflicting perspectives is currently taking place in the study of carcinogenesis, which legitimate the present work, as well as its methods. Moreover, the National Cancer Institute opened in 2009 twelve centres of Physical Sciences and Oncology, with the aim of enlarging the fight against cancer, and also in order to gain insights from other disciplines. One of them is led by the prestigious physicist Paul Davis. This interdisciplinary spirit has strongly motivated the present work.

## 1.3 Immunosurveillance of tumors

The immune system represents an outstanding example of a complex adaptive system, which comprises many biological processes and cell interactions. It appears in most multicellular organisms (around 98 % have a more or less developed immune system) and evolved to protect such organisms against pathogens, such as viruses, bacteria or fungi. Even though these cells and substances interact among them without the guidance of any central controller, as a building block of an organism, the immune system is a *feedback control* dynamical system. The present thesis mainly deals with the interactions between tumor cells and the cell-mediated immune response. For a detailed description of the immune system, we refer the reader to the Appendix, in which we provide a brief introduction to immunology. In the present section we discuss the role of the immune system in the control of tumor growth.

Paul Ehrlich suggested in 1909 that the immune system might protect an organism from the development of cancer [21]. Around fifty years later, this proposition was more formally reintroduced by Macfarlane Burnet [22, 23] and, later on, by Lewis Thomas [24]. After suffering major setbacks [25, 26], the *immunosurveillance* theory gained renewed consistence close to twenty years ago, thanks to several experimental works with genetically altered mice [27, 28]. Currently, the immunosurveillance of tumors is more properly referred as cancer immunoediting. Given the genetic heterogeneity of tumors, this control system coevolves with them and seems to act as a natural selective force, editing its phenotype by selecting those cells that are unresponsive to immune detection.

Hesitation on the capacity of the immune system to control tumor growth arises

from a quite simple fact. The immune system has evolved to protect the organism against foreign pathogens, while tumor cells originate in the body, and in many aspects, are very similar to normal cells. Since the immune system has tolerance to cells originated in our body, it is reasonable to think that the recognition and destruction of tumor cells is not a very likely event. Even more, it has been observed a great antagonism of the immune system in the control of cancer, since some cells can foster tumor growth, while others can suppress it. Even the same type of cells might show conflicting roles concerning tumor growth. Note that many immune cells promote inflammation by secreting cytokines, some of which can promote cell growth. Nevertheless, several experimental observations support an important role of the immune system in tumor progression, which keeps these tumors in check. For example, histopathological studies reveal the existence of substantial numbers of lymphocytes infiltrating tumor masses, and macrophages engulfing tumor cells at the wound healing site have been observed (see Fig. 1.4).

Even in the case in which the immune cells are effective in the recognition of tumor antigens, experience reveals that tumor cells adapt and find ways to avoid their elimination. These collection of strategies is formally known as *immunoevasion*. We enumerate a few examples:

1. Stop displaying tumor antigens that do not compromise their survival and proliferation, through suppression of their encoding genes.

2. Partial repression of MHC-class I molecules. This occurs through the lack of mRNAs molecules encoding these proteins and post-translational mechanisms, as for example the lack of synthesis of relevant proteins and transporter proteins.

3. Down-regulation of stress ligands, like the NKG2D ligand, by disabling its signalling pathway.

4. Release of ligand proteins in soluble form to the medium.

5. Launching counter-attacks on immunocytes, through the Fas receptor or the release of cytokines, such as TGF-beta and IL-10.

6. Avoiding recruitment through interaction with endothelial cells and adhesion molecules.

7. Inhibition of apoptosis using different signalling pathways.

8. Modifying the mix of immune cells by recruiting T suppressor cells, which inhibit and even kill cytotoxic and helper T cells.

Immunoevasion is of great importance to the present work and, consequently, our models include parameters capable of representing the effectiveness of the immune system in the surveillance of tumors.

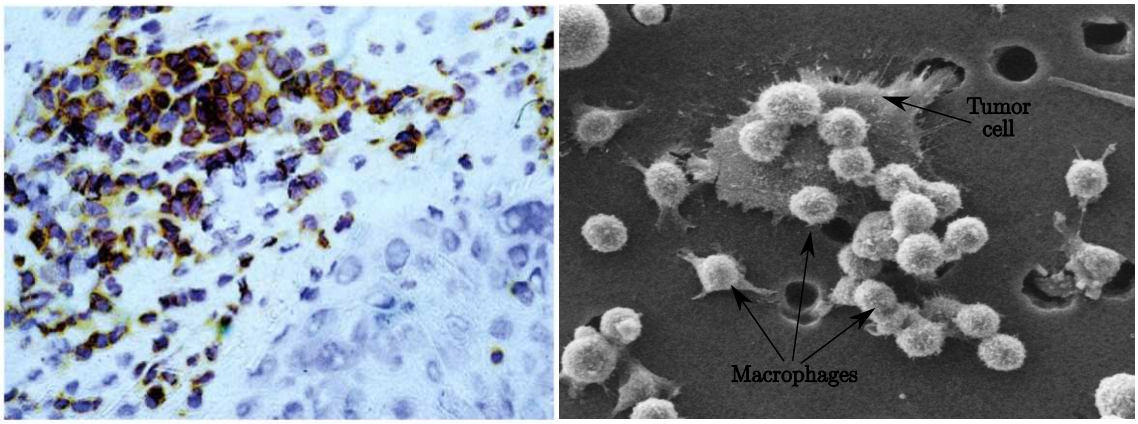


$(a)$ $(b)$

**Figure 1.4. Evidence supporting the immunosurveillance of tumors.** (a) Tumor infiltrating lymphocytes (brown) in an oral carcinoma. From Ref. [10] (b) A group of macrophages fighting a tumor cell. By Susan Arnold, from NCI Vissuals Online.

## 1.4 Mathematical population dynamics

The coda to this introduction is devoted to describe the mathematical context in which our models are developed. Our investigations are accomplished by means of mathematical population models, which have been employed in many domains of science, from chemistry, through population genetics, biology, epidemiology, ecology, evolutionary theory, demography, sociology, or economy, just to cite a few examples. In a first approach, population models are of two types, depending on how they represent the population variable: continuous models and discrete models. Continuous models represent populations through densities or volume fractions, while discrete models assume an integer number of elements. The time variable can also be represented continuously or discretely, and some models also include spatial dependence, again in a discrete or continuous fashion. Other variables can be considered in the model, as for example, the age of the population, and frequently models include stochasticity, in order to account for fluctuations. Finally, different cell populations with specific interactions among them can be considered, forming more or less complex networks. The present thesis mainly deals with two types of models:

- The first are ordinary differential equation (ODE) models, which represent cell populations continuously, are also continuous in time, and they do not explicitly simulate spatial distribution. Nevertheless, the present work demonstrates that these traditional models can account in a tacit manner for spatio-temporal effects.

- The second are hybrid cellular automata models (CA), which are spatio-temporal models in which all variables are treated discretely. However, the diffusion of nutrients in the domain of the tumor and their absorption by the tumor cells, will be treated continuously, through partial differential equations (PDEs).

### 1.4.1 Geometric growth

The oldest mathematical population model of which we have written proof is the Fibonacci's sequence. Leonardo de Pisa was born in 1170 and after preparing to be a merchant, he travelled for business around the Mediterranean Sea, compared the different number systems and studied Arab mathematics. In 1202 he finished writing a book in Latin entitled *Liber abaci*, in which he shows how to use such number systems for accounting, and also gathers many of the results in algebra and arithmetic known to the Arabs. The population problem that he poses in his book tries to compute the number of rabbits after a certain number of months, given the fact that it takes rabbits one month of life to be fertile. Couples of rabbits are then given by the sequence

$$P_{n+1} = P_n + P_{n-1}. \tag{1.4}$$

Interestingly, this old population model incorporates delay, since the number of rabbits at a particular month $n$ does not only depend on the number of rabbits in the previous month, but also on the number of rabbits in the past months. Consequently, two months of history have to be provided as initial conditions. An equivalent time continuous model is given by the delay differential equation $\dot{P}(t) = P(t-\tau)$, which solution is an exponential growth.

Although population models were later used by renowned scientists, such as Edmund Halley, Christiaan Huygens or Gottfried Leibniz, it was the prolific mathematician Leonhard Euler who gave attention to the study of the mathematics of populations in a rigorous and detailed fashion. His first examples are dedicated to the geometric progression, in which a population increases its size at each time step (say a year), at a rate $r$. Mathematically, this linear model is written as

$$P_{n+1} = (1+r)P_n, \tag{1.5}$$

and its continuous counterpart can be written as $\dot{P}(t) = rP(t)$, which as it is well-known, leads an exponential growth, with doubling time $\log(2)/r$. Later on, in 1760, he published other works in which the population is age-structured, and addressed different questions.

### 1.4.2 Limited growth

In 1798, Thomas Malthus, an English priest, seriously considered for the first time the obstacles to geometric growth, arguing that a growing population could only be maintained if its means of subsistence were not comparable [29]. Malthus correctly believed that if the human population grows beyond its capability to produce resources, then part of such population would be inevitably forced to misery, vice and death. Even though Malthus did not introduce any mathematical model so as to properly represent limited growth, conceptually, he set the basis for such models. Certainly, Adolph Quetelet suggested that populations can not grow geometrically over a long period of time because the obstacles mentioned by Malthus act as a resistance. This fact inspired Pierre-François Verhulst, who presented a mathematical

model in 1838. This model is nowadays known as the logistic model, and can be written as follows

$$\dot{P}(t) = rP(t)\left(1 - \frac{P(t)}{K}\right), \tag{1.6}$$

where $r$ is the rate of growth and $K$ has been named the carrying capacity. Note that this model exhibits two terms. The first term represents a geometric growth, while the second stands for the mortality of the population, due to a lack resources as the population increases towards the carrying capacity $P = K$ of its ecosystem. The model exhibits two fixed points, $P = 0$ and $P = K$. The first is unstable and the second is stable. A population that exceeds the carrying capacity of its ecosystem $P > K$, dies at a higher rate than it grows, decaying to stable population levels. This regime precisely represents the circumstances so much feared by Malthus. Logistic growth is very common in solid tumors, and arises as a competition for space and resources, as proposed by the Reverend Malthus.

Alfred Lotka, an American physicist and chemist, independently developed models quite similar to those of Euler, but in a continuous fashion. In the nineteen-twenties, he turned attention to the problem of interacting populations, and developed a two-dimensional biological model, where the variables represent a species of herbivores (predators) and a species of plants (preys). In Fig. 1.5 we exemplify this struggle for life [19]. For this purpose, he used chemical reactions as a conceptual framework, and demonstrated that two species can subsist together performing oscillations. From the Malthusian perspective, these oscillations can be explained in a quite simple manner: the predators grow exponentially, but depend on their preys to subsist. As they keep on growing, the number of plants reduces, and when the population of predators grows beyond a certain limit, plants are very scarce and the predators begin to die. Now, as the predators reduce, the plants regrowth again and the cycle resumes. Perhaps the most important moral of this study, is that the equilibrium of an ecosystem is based on a balance between life and death, leading to oscillatory regimes. A very important Italian mathematician, Vito Volterra, came up with an identical model while investigating the oscillations of cartilaginous fish in the fisheries of the harbours of the Adriatic sea.

The history of population dynamics proceeds up to the present, with very important scientific figures in many disciplines. However, we will detain ourselves here, since the basic concepts required to clearly understand the following chapters have been introduced. For a complete description of mathematical population models and their history we refer the reader to two books [30, 31], which have been very helpful to write the notes that conform this section.

### 1.4.3 Lotka-Volterra models

Since Lotka-Volterra Models are the basis of the cancer ODE models used in this work, in this section we delve deeper into their mathematical nature. Given a species of preys $X(t)$ and another of predators $Y(t)$, the Lotka-Volterra equations can be

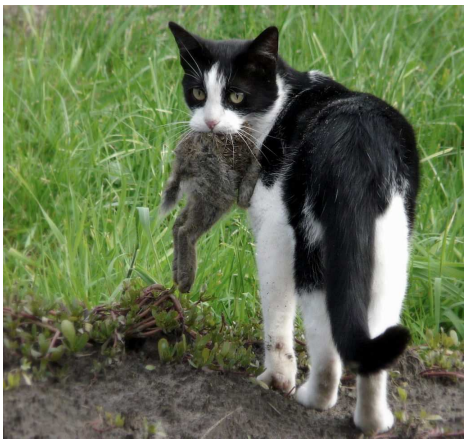

(a)

(b)

**Figure 1.5. The struggle for life**. (a) A feral cat haunting a rabbit. Image by Eddy Van under license CC BY-SA 2.0. (b) Sea anemones engaged in a clone war. The white tentacles are fighting tentacles. After war ends one of them should move. Image by Brocken Inaglory under CC BY-SA 2.0.

written in the form

$$\begin{aligned} \dot{X}(t) &= \alpha X(t) - \beta X(t)Y(t) \\ \dot{Y}(t) &= -\delta Y(t) + \gamma X(t)Y(t). \end{aligned} \tag{1.7}$$

Assuming that in the absence of predators the mortality rate of preys is much smaller than their growth rate, the first equation states that the velocity at which the preys growth or die is the result of the balance between their geometrical proliferation at rate $\alpha$, and the destruction caused by predators, at rate $\beta Y$. Note that predation rate increases with no bound as the number of predators increases, which is unrealistic. Other bounded functional responses have been proposed by ecologists in more realistic attempts [32], and so it is the purpose of the present thesis, concerning tumor-immune interactions. On the other hand, predators multiply when food is available at a rate $\gamma X$, and in its absence die of hunger at rate $\delta$. In the spirit of Alfred Lotka, we can write the Lotka-Volterra equations as an autocatalytic chemical reaction, where the animal species are regarded as molecules. These sort of analogies will be used throughout the text in several chapters. The reactions are

$$A + X \xrightarrow{\kappa} mX \tag{1.8}$$

$$X + Y \xrightarrow{\beta} nY \tag{1.9}$$

$$Y \xrightarrow{\delta} Y^*, \tag{1.10}$$

with $\alpha = \kappa[A]m$ and $\gamma = \beta n$.

More specifically, Lotka-Volterra equations of competition are commonly used in cancer modelling. For example, consider two species of cells which grow logistically up to a carrying capacity, imposed by the homoeostatic controls of the body, and

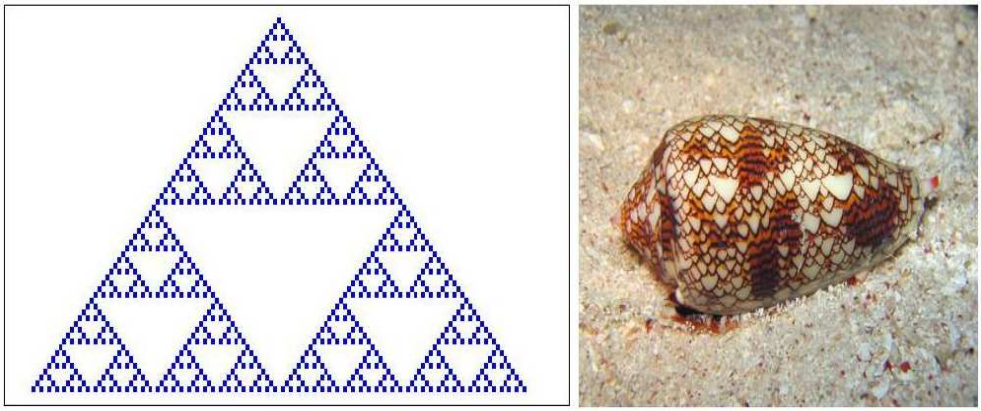

(a) (b)

**Figure 1.6. A one-dimensional cellular automaton**. The horizontal axis represents the space, while the time runs along the vertical one. (a) The Pascal's triangle modulo 2 cellular automaton, generating a Sierpinsky triangle as times goes by. (b) Similar structures in a conus textile shell. Image by John Doe, distributed under CC BY-SA 3.0 license.

compete among them for resources. The differential equations representing this process are

$$\begin{aligned} \dot{X}(t) &= r_1 X(t)\left(1 - \frac{X(t)}{K_1}\right) - a_{12}X(t)Y(t) \\ \dot{Y}(t) &= r_2 Y(t)\left(1 - \frac{Y(t)}{K_2}\right) - a_{21}X(t)Y(t). \end{aligned} \tag{1.11}$$

Now, both cell populations die at a rate that is proportional to the reciprocal species, as a consequence of competition. Depending on the parameter values of the model, two fundamental situations can be addressed: exclusive competition or stable coexistence. In the first case, one species outcompetes the other, while in the second, both stably coexist.

There exists a vast amount of research concerning Lotka-Volterra models. Generalizations such as the Arditi-Ginzburg equations, higher dimensional models exhibiting chaos, time-delayed models, or variants accounting for mutualism or commensalism, and even spatio-temporal reaction-diffusion models, frequently appear in the literature.

### 1.4.4 Cellular automata models

Cellular automata were born in 1950, when John Von Neumann designed a mathematical algorithm to demonstrate the existence of a self-replicating machine. Although he died of cancer before finishing the complete mathematical demonstrations, his proof was finished by his friend Arthur Brooks, who published them in 1966.

A cellular automaton model is a spatio-temporal discrete dynamical model. The

space, which is commonly a square, is divided into suitable units forming a grid. These units are called *cells*, and can exist in different *states*, that are usually represented by integers. Then a set of *rules* is provided, by allowing each cell to interact with its first *neighbours*. Depending on the state of its neighbours and its own value, the cell will perform an action, changing its current state or not. At each *iteration* or time step, all the CA cells are checked and the corresponding rules applied to compute the evolution of the system. Finally, *boundary conditions* must be imposed. Two outstanding examples of cellular automata are the one-dimensional binary cellular automata studied by the British physicist Stephen Wolfram, and also the British mathematician John Horton Conway's "Game of Life". An example is illustrated in Fig. 1.6.

From the point of view of the architecture, the cellular automata used in this work are more sophisticated, since they incorporate multi-scale effects and their rules are probabilistic. The birth and death of the cells will depend explicitly on the nutrient concentration at each point of the space, which is simulated by reaction-diffusion equations. Therefore, "our" cellular automaton can be classified as a probabilistic hybrid cellular automaton.

# References

[1] E.N. Lorenz, "Predictability: does the flap of a butterfly's wings in Brazil set off a tornado in Texas?", 139th Annual Meeting of the American Association for the Advancement of Science, (1972).

[2] M. Mitchell, *Complexity: A guided tour*, (Oxford University Press, New York) (2009).

[3] S. Camazine, *Self-Organizing Systems*, (Encyclopedia of Cognitive Science, Wiley Online Library) (2006).

[4] J.H. Holland, *Complexity: A very short introduction*, (Oxford University Press, New York) (2014).

[5] B. Mandelbrot, *The fractal geometry of nature*, (WH Freeman and Co., New York) (1983).

[6] A. Rosenblueth, N. Wiener, and J. Bigelow, "Behavior, purpose and teleology", *Philos. Sci.* **10**, 18-24 (1943).

[7] P. Bak, C. Tang and K. Wiesenfeld, "Self-organized criticality: an explanation of 1/f noise", *Phys. Rev. Lett.* **59**, 381-384 (1987).

[8] L.O. Chua, "Local activity is the origin of complexity", *Int. J. Bifurcat. Chaos* **15**, 3435-3456 (2005).

[9] S.A. Kauffmann, *The origins of order: Self organization and selection in evolution*, (Oxford University Press, New York) (1993).

[10] R.A. Weinberg, *The Biology of Cancer*, (Garland Science, New York) (2013).

[11] S. Grumelli, D.B. Corry, L.Z. Song, L. Song, L. Green, J. Huh, J. Hacken, R. Espada, R. Bag, D. E. Lewis, and F. Kheradmand, "An immune basis for lung parenchymal destruction in chronic obstructive pulmonary disease and emphysema", *PLoS Med.* **1**, e8 (2004).

[12] A.M. Turing, "The chemical basis of morphogenesis", *Philosophical Transactions of the Royal Society of London B: Biological Sciences* **237**, 37-72 (1952).

[13] E. Schrödinger, *What is life?: With mind and matter and autobiographical sketches*, (Cambridge University Press, New York) (1992).

[14] E.D. Schneider and J.J. Kay, "Life as a manifestation of the second law of thermodynamics", *Math. Comput. Model.* **69**, 25-48 (1994).

[15] I. Prigogine, *Only an illusion*, (Cambridge University Press, New York) (1982).

[16] S.J. Cooper, "From Claude Bernard to Walter Cannon. Emergence of the concept of homeostasis", *Appetite* **51**, 419-427 (2008).

[17] L. Norton, A Gomertzian model of human breast cancer growth, *Cancer Res.* **48** 7067-7071 (1988).

[18] R.A. Weinberg, *One renegade cell: How cancer begins*, (Basic Books, New York) (2013).

[19] C. Darwin, *The origin of species*, (John Murry, London) (1929).

[20] A.M. Soto and C. Sonnenschein, "The tissue organization field theory of cancer: a testable replacement for the somatic mutation theory", *Bioessays* **33**, 332-340 (2011).

[21] P. Ehrlich, "Über den jetzigen Stand der Karzinomforschung", *Nederlands Tijdschrift voor Geneeskunde* **5**, 273-90 (1909).

[22] F.M. Burnet, Cancer-A biological approach: I. The Processes of control. II. The Significance of somatic mutation. *Brit. Med. Jour.* **1**, 779-786 (1957).

[23] F.M. Burnet, "Immunological surveillance in neoplasia", *Transplant Rev.* **7**, 3-25 (1971).

[24] L. Thomas, *Cellular and humoral aspects of the hypersensitive state.* (Lawrence HS, New York, Hober-Harper) (1959).

[25] O. Stutman, "Tumor development after 3-methylcholantrene in immunologically deficient athymic-nude mice", *Science* **183**, 534-536 (1974).

[26] O. Stutman, "Immunodepression and malignancy", *Adv. Cancer Res.* **22**, 261-422 (1975).

[27] D.H. Kaplan, V. Shankaran, A.S. Dighe, E. Stockert, M. Aguet, L.J. Old, and R.D. Schreiber, "Demonstration of an interferon $\gamma$-dependent tumor surveillance system in immunocompetent mice", *Proc. Natl. Acad. Sci. U. S. A.* **95**, 7556-7561 (1998).

[28] V. Shankaran, H. Ikeda, A.T. Bruce, J.M. White, P.E. Swanson, L.J. Old, and R.D. Schreiber, "IFN$\gamma$ and lymphocytes prevent primary tumor development and shape tumor immunogenicity", *Nature* **410**, 1107-1111 (2001).

[29] T. Malthus, *An essay on the principle of population*, (Penguin, New York) (1970)

[30] N. Bacaër, *A short history of mathematical population dynamics*, (Springer Science & Business Media) (2011).

[31] F. Brauer and C. Castillo-Chavez, *Mathematical models in population biology and epidemiology*, (Springer, New York) (2001).

[32] C.S. Holling, "Some characteristics of simple types of predation and parasitism", *Can. Entomol.* **91**, 385-398 (1959).

# Chapter 2

# Chaos and control in a model of tumor-immune interactions

*"The most successful people are those who are good at plan B."*

-James A. Yorke

In this second chapter, we demonstrate the existence of *transient chaotic* dynamics for certain values of the parameter space in a three dimensional cancer model consisting of interacting cell populations, similar to the model used in Refs. [1, 2, 3]. These three populations are the tumor cells, the healthy host cells and the immune effector cytotoxic T-cells present at the tumor site. After examining the phase space of the model for the given parameters, and the boundary crisis leading to transient chaotic dynamics, the partial control method is applied to avoid tumor escape and uncontrolled growth, preventing from extinction of the healthy tissue. We discuss the main difficulties of applying such control method at the present state of the art of cancer treatments, as well as some other inherent to chaotic behavior.

## 2.1 Introduction

As previously discussed, cancer is the result of an uncontrolled proliferation of tumor cells within a tissue, that eventually can spread to new locations in the body. It is believed that the loss of cooperative behavior of cancer cells mainly arises as a consequence of accumulated mutations, and yields a complex evolutionary scenario in which tumor and healthy cells compete for space and scarce resources. Mathematical modeling has proven to be a useful tool for the understanding of many features

concerning the complex interactions between tumor and healthy cells [4, 5, 6, 7]. Just to recall, based on how the tumor tissue is represented, a vast number of cancer growth models fall into two main categories: *discrete* models and *continuum models*. The discrete cell based models are capable of describing biophysical processes in significant detail, considering the individual cells governed by a precise series of rules. However, for large scale systems, this method is very demanding and requires sophisticated computer simulations. An alternative to discrete methods is provided by the continuum aproach, where tumors are treated as a collection of tissue, considering, among other possible elements, the description of densities or cell volume fractions and cell substrate concentrations. More particularly, carcinogenesis population-based models [1, 8, 9, 10] have often been used to study different aspects of tumor progression [11, 12] and settle therapy protocols [13, 14, 15, 16]. As an example, we briefly describe a model which has enormous relevance to the present thesis. The model was engineered in Ref. [6] to suggest a possible dynamical origin of *tumor dormancy* and the *sneaking through* of tumors. These two concepts will be rigorously defined in Chapter 6. It was tested against experimental data, obtained from a $BCL_1$ lymphoma in chimeric mice, and consists of two cell populations: the tumor cells and the immune effector cells. Using enzyme kinetics as a metalanguage, the following differential equations can be derived

$$\begin{aligned} \dot{E} &= s - dE + p\frac{T}{g+T}E - cTE \\ \dot{T} &= rT\left(1 - \frac{T}{K}\right) - bET. \end{aligned} \tag{2.1}$$

Here $r$ is the rate of growth of the tumor cell populations, $K$ is its carrying capacity, and $b$ and $c$ represent Lotka-Volterra competition terms. More specifically, the term represented by $c$ models the *lysis* (destruction) of tumor cells by the immune cells. On the other hand, $b$ can represent any of the several mechanisms that tumor cells utilize to evade the immune system response, described in Chapter 1. Finally, the parameter $s$ models a natural input of cytotoxic cells into the tissue, while $p$ and $g$ comprise the recruitment of cytotoxic cells as a result of tumor-immune interactions. The parameter $d$ represents the rate of inactivation of immune cells, which can only lyse a finite number of times. A possible nondimensional model can be derived by redefining the cell populations in the following manner

$$y = \frac{T}{T_0}, x = \frac{E}{E_0}, \tau = bT_0t, \tag{2.2}$$

with $E_0 = T_0 = 10^6$, which is the typical scale for the the immune and the tumor

cell populations. The resulting nondimensional parameters are re-expressed as

$$\begin{aligned} \sigma &= \frac{s}{bT_0E_0} \quad \rho = \frac{p}{bT_0} \quad \eta = \frac{g}{T_0} \\ \mu &= \frac{c}{b} \quad \delta = \frac{d}{bT_0} \quad \alpha = \frac{r}{bT_0} \\ \beta &= \frac{T_0}{K}, \end{aligned} \tag{2.3}$$

and the equations now read

$$\begin{aligned} \dot{x} &= \sigma - \delta x + \rho\frac{y}{\eta + y}x - \mu yx \\ \dot{y} &= \alpha y\,(1 - \beta y) - xy. \end{aligned} \tag{2.4}$$

A phase space portrait illustrating the dynamics of the model is shown in Fig. 2.1. The phase space clearly exhibits the structure of a Lotka-Volterra model, with "exclusive" competition. Two different regions are distinguished, containing two respective attractors. One of them $A$ is an stable spiral attractor, corresponding to a tumor that is kept at a small size by the immune system. This phenomenon is formally known as *tumor mass dormancy*. The other $B$ is an stable node representing a very big tumor, that has escaped the immune system's vigilance. The fixed point $C$ is a saddle whose stable manifold $W_s$ divides the space into two regions. In the language of dynamical systems, these regions are referred as basins of attraction, since all trajectories inside them ultimately end at their corresponding attractors. Another fixed point, not appearing in the image, occurs for small tumor size populations and a small immune cell population. This fixed point is a repellor. Closer settings in parameter space $(\sigma, d)$ suggest that an increase of immune cells can stimulate tumor growth (immunostimulation) and that initially big tumors can be reduced to a very small size, which later on escape immune surveillance (sneaking through).

We will come back to this model and discuss its main virtues and deficiencies in the last chapter. Nevertheless, this pioneering work served as a foundation for other ODE models, which frequently divide the problem into two clearly differentiated parts. The first one sets and describes the model itself, which commonly consists on some Lotka-Volterra equations describing growth and death of cell populations, as well as competition between them. The second part is devoted to establish a treatment protocol, mainly chemotherapy, immunotherapy or radiotherapy, to reduce in an optimal manner the tumor population. Even though most of these models deal with more than two dimensions, not many of them [2, 3, 17, 18] seriously consider the situation in which cell populations behave in a chaotic fashion. From our point of view, the main reason why this occurs is that, in spite of the fact that there is experimental evidence of deterministic chaos in tumor cell populations [19], in general this evidence is not abundant and clear enough. Although chaotic dynamics of a growing tumor seems to be uncommon, it is more probable to appear when

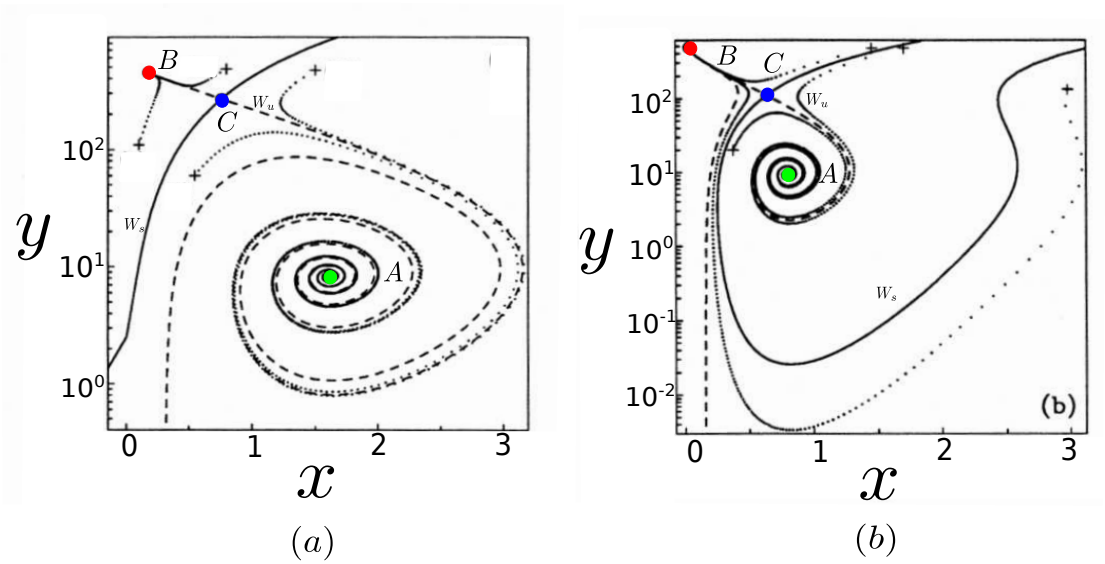


**Figure 2.1. The phase space**. We show the phase space of the model presented in Eq. (2.4), for the set of parameters $\sigma = 0.1181$, $\rho = 1.131$, $\eta = 20.19$, $\mu = 0.0033$, $\delta = 0.3743$, $\alpha = 1.636$ and $\beta = 0.0020$. (a) Two stable attractors $A$ and $B$, representing a dormant tumor and an escaping one respectively. The third fixed point shown $C$ is unstable, with its invariant manifolds $W_s$ and $W_u$. (b) In this second case the value of $\mu$ has been increased to 0.0055. The system experiences a bifurcation through a heteroclinic connection. Now we see that high immune cell population values do not lead to the dormant tumor state $A$. After being reduced, the tumors persist at small cell populations and sneak through until they escape. Adapted from Ref. [6].

therapies are considered. Therefore, we think that chaos should not be disregarded in the study of tumor progression. In particular, as far as we are concerned, no one has mentioned the possibility of finding transient chaos in the populations of these tumor models. We believe that, since complex interactions take place between neoplastic, stromal and immune response cells, it is likely for transient chaotic dynamics to happen before tumor dominates the struggle. On the other hand, several methods to control transient chaos have been proposed along the last decades [20, 21, 22, 23, 24]. Among them, the partial control method [25, 26, 27, 28] aims to control systems displaying chaotic transients in the presence of certain external disturbances (usually noise), using smaller controls. The main idea of partial control is to take advantage of the Cantor set structure embedded in a region of phase space containing the remnant of a chaotic attractor to avoid escaping from it by small perturbations. In this manner, we prevent the occurrence of a particular dynamics.

## 2.2 Model description and phase space analysis

We now introduce an ODE mathematical model of tumor-immune interactions and describe the phase space.

### 2.2.1 The model

We develop our investigations with a model used in Refs. [2, 3]. It is the same three dimensional Lotka-Volterra model than the one described in Ref. [1], with the only difference that no constant input of effector immune cells is considered. Such input can be used to model innate immunity [10] or an immunotherapy protocol [9]. Each of the variables represents a cell population, namely: $T(t)$ the tumor cells, $H(t)$ the healthy host cells near the tumor site, and $E(t)$ the effector immune cells. The growth of cancer and host cells is assumed to be logistic with growth rate $r_i$ and carrying capacity $k_i$. Both compete with each other, being the competition terms given by $a_{ij}$. The production of immune cytotoxic T-cells is triggered by antigen presenting cells. Assuming that this process occurs at a enough smaller time scale than the one corresponding to tumorigenesis, the stimulation of the immune system by the tumor specific antigens can be considered to act instantly and modelled by a Michaelis-Menten law. The immune effector cell production rate in response to the presence of tumor cells is given by $r_3$, and the steepness of the response curve is associated to $k_3$, the value of the tumor cells at which the immune response rate is half of the maximum production, where the response curve saturates. These cells only compete with cancer cells and in their absence they die off with a constant per capita rate $d_3$. Therefore, the system of differential equations is

$$\begin{aligned}
\dot{T} &= r_1 T\left(1-\frac{T}{k_1}\right) - a_{12}TH - a_{13}TE \\
\dot{H} &= r_2 H\left(1-\frac{H}{k_2}\right) - a_{21}HT \\
\dot{E} &= r_3\frac{ET}{T+k_3} - a_{31}ET - d_3E.
\end{aligned} \tag{2.5}$$

The nondimensionalization and parameter reduction of this system is thoroughly studied in Ref. [2], yielding the set of equations

$$\begin{aligned}
\dot{x} &= x\,(1-x) - a_{12}xy - a_{13}xz \\
\dot{y} &= r_2 y\,(1-y) - a_{21}yx \\
\dot{z} &= r_3\frac{zx}{x+k_3} - a_{31}zx - d_3z.
\end{aligned} \tag{2.6}$$

### 2.2.2 Equilibria of the system

An exhaustive phase space analysis has been carried out in the previously cited references [1, 2]. In the following, we restrict our attention to a particular set of parameter values, for which the system has a chaotic attractor close to a boundary crisis. The choice of parameters in Eq. 2.6 is: $a_{12} = 0.5$, $a_{21} = 4.8$, $a_{13} = 1.2$, $a_{31} = 1.1$, $r_2 = 1.20$, $r_3 = 1.291$, $d_3 = 0.1$ and $k_3 = 0.3$. The only significant differences of this setting compared to the one arranged in Ref. [1] are given by

parameters $a_{12}$ and $r_3$, which take higher values in the present case. The biological meaning of this choice is that tumor cells are more agressive in their competition with normal cells, and that the recruitment or response of the immune effector cells due to the presence of tumor cells is much stronger.

We now describe all the nullclines and equilibria for the current set of parameters. The fixed points of the system are given by $\dot{x} = \dot{y} = \dot{z} = 0$, what yields the set of equations

$$\begin{aligned} 0 &= x\,(1 - x - a_{12}y - a_{13}z) \\ 0 &= y\,(r_2 - r_2 y - a_{21}x) \\ 0 &= z\,((r_3 - k_3 a_{13} - d_3)x - a_{31}x^2 - k_3 d_3)\,. \end{aligned} \tag{2.7}$$

Nullclines can be read directly from Eq. 2.7. There is a total of six nullclines: the $x-y$, $y-z$ and $x-z$ planes, the plane $\Pi_1$, represented by the implicit equation $x + a_{12}y + a_{13}z = 1$, the plane $\Pi_2$, given by $r_2 y + a_{21}x = r_2$, and the planes $\Pi_3$ and $\Pi_4$ for $x$ the constant solutions of the quadratic equation $a_{31}x^2 - (r_3 - k_3 a_{13} - d_3)x + k_3 d_3 = 0$. If we focus on the positive octant $\mathbb{R}^+ \times \mathbb{R}^+ \times \mathbb{R}^+$, the intersections of the different nullclines yield six different fixed points $x_i^*$, as shown in Fig. 2.2. We give the numerical values of the fixed points and also analyze their stability by examining the eigenvalues of the Jacobian at each of them.

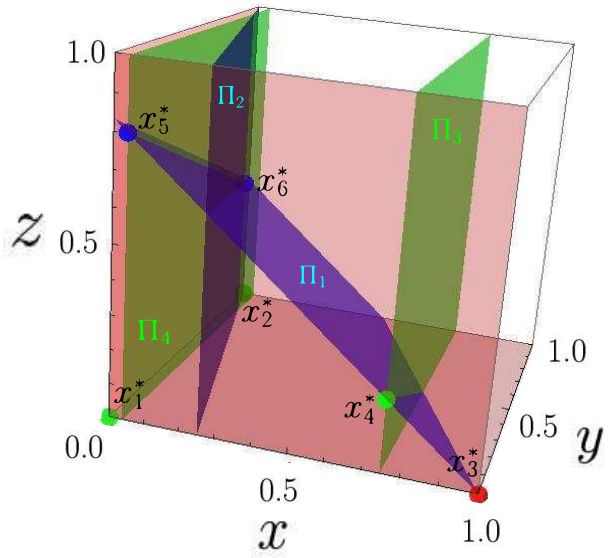


**Figure 2.2. Phase space with the nullclines and the fixed points**. The planes are the different nullclines, with the fixed points placed at some of their intersections. The green points are saddle fixed points, the red point is the tumor stable fixed point and the blue points are the two spiral-saddles that give rise to chaotic motion.

The point $x_1^*$ is the origin $(0, 0, 0)$, a saddle with two positive eigenvalues corresponding to the $x$-axis and the $y$-axis, and a negative eigenvalue along the $z$-axis. The point $x_2^* = (0, 1, 0)$ represents the healthy state, for which there are only normal cells. This fixed point is a saddle point too, but with two stable directions (negative eigenvalues) and one unstable (positive eigenvalues). The stable eigenvectors

are contained in the $x = 0$ plane, so if the dynamics enters this plane, it eventually reaches the healthy solution. The point $x_3^* = (1, 0, 0)$ has its three eigenvalues smaller than zero, representing a stable solution for which there are only tumor cells. Since this point is the one we want to avoid falling into, we have colored it in red. The fixed point $x_4^* = (0.75, 0, 0.21)$ is also a saddle fixed point with two stable and one unstable directions. A stable and an unstable direction are in the plane $y = 0$, while the remaining stable direction is given by the eigenvector $(0.23, 0.97, 0.02)$. The two stable directions are related to the stable manifold separating the basins of attraction of the chaotic attractor and the tumor stable fixed point. The fixed points $x_5^* = (0.04, 0, 0.8)$ and $x_6^* = (0.04, 0.85, 0.45)$ are two spiral-saddles. For $x_5^*$ the spiral is stable and is contained in the $y = 0$ plane, while the unstable direction is given by the eigenvector $(-0.02, 1.00, -0.03)$, almost pointing parallel to the $y$-axis. The other spiral-saddle shows opposite stability, *i.e.*, the spiral is unstable and the stable direction is given by the eigenvector $(-0.02, -1.0, 0.02)$. The interplay of these two "facing" spiral-saddles is responsible for the heteroclinic chaotic motion of the system, which is the reason why we paint them blue. The attractor together with the fixed points are shown in Fig. 2.3(a). The Lyapunov exponents of the system are $\lambda_1 = 0.022$, $\lambda_2 = 0$ and $\lambda_3 = -0.76$, so the Kaplan-Yorke dimension of the chaotic attractor is $d_L = 2.027$.

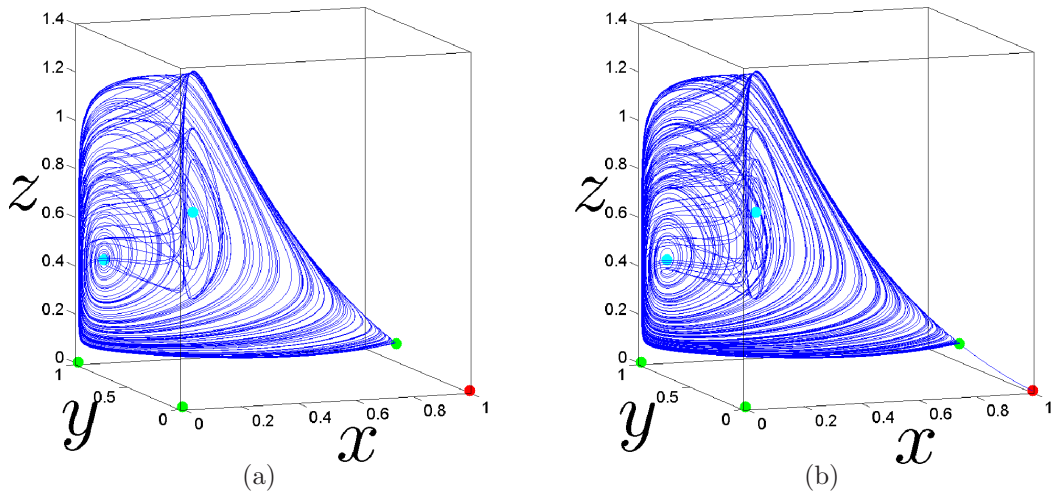


**Figure 2.3. Chaotic attractors and boundary crisis.** (a) Chaotic attractor before the crisis. Again saddle fixed points are marked in green, the tumor attractor is shown in red, and the spiral-saddles are painted blue. (b) The same chaotic attractor and fixed points after the crisis. Now trajectories do not stay forever in the chaotic attractor, but fall into the tumor stable equilibrium after a long transient.

### 2.2.3 Boundary crisis and transient chaos

It would be expected that, decreasing the level of the immune response to tumor cells, the cancer state $x_3^*$ should asymptotically prevail over the chaotic attractor. As is well known, whenever two attractors coexist in phase space, the stable manifold of a saddle fixed point between them separates their basins of attraction. If one of these attractors is chaotic, when we vary a parameter, it might happen that it collides with the stable manifold of the saddle. Such phenomenon is formally known as a boundary crisis, and allows the chaotic attractor to access the basin of the stable attractor, falling into it. Indeed, when we decrease the value of the immune respone $r_3$ from 1.291, the chaotic attractor collides with the stable manifold of $x_4^*$ at an approximated critical value $r_3^c = 1.2909$. For values of $r_3$ below the critical value, the dynamics of the system eventually sinks into $x_3^*$. However, if the value of the parameter is close to the boundary crisis, the chaotic attractor persists as a remnant (or ghost), so larger or shorter chaotic transients are observed before escaping into the stable attractor, as shown in Fig. 2.3(b). The use of the partial control method to avoid ending in that attractor, which corresponds to the tumor-only state, is the pursued objective through Sec. 2.4. In Fig. 2.4 we show a two-dimensional fold of the parameter space, corresponding to the rate of production of immune cells $r_3$ and the rate of growth of healthy cells $r_2$, making a clear distinction between parameter regions before and after the crisis.

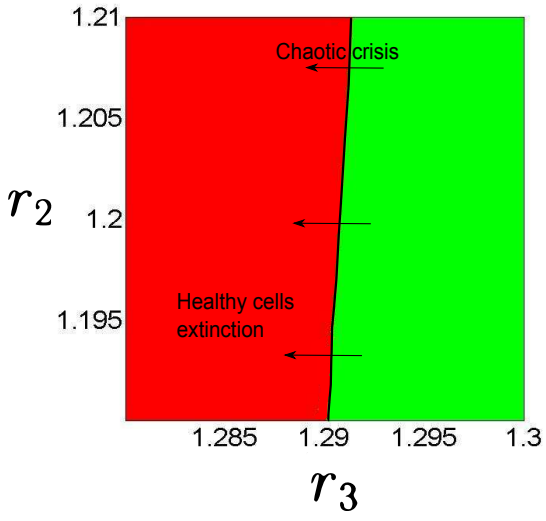


**Figure 2.4. A region of the parameter space**. We see how the variation of the parameter $r_3$ induces the crisis for many different values of the parameter $r_2$. The boundary between the two regions contains the critical values of $r_3^c$.

## 2.3 The partial control method

### 2.3.1 Basic aspects

Transient chaos is a physical phenomenon that occurs in systems for which trajectories behave chaotically during some finite amount of time in a region $Q$ of the phase space, until they move toward a final state outside $Q$. The underlying topological structure in $Q$ responsible for that type of motion is a Cantor set-like structure known as the chaotic saddle. Manifestations of transient chaos are wide, and many examples can be found in the literature [29, 30, 31]. We show transient chaotic dynamics for our model in Fig. 2.3(b). Partial control is a feedback control method aimed to mantain the transient chaotic dynamics as long as desired, avoiding the escape from $Q$. Things get even more complicated if we consider the existence of some unpredictable external disturbances acting on the system. Since most physical systems interact with their environment, realistic situations always have to deal with a certain amount of noise. The striking advantage of the partial control technique is that it allows the avoidance of the undesired event sometimes using smaller controls than the disturbances. If we consider a map $f$ modeling the dynamics of the system, the whole process is mathematically expressed as

$$q_{n+1} = f(q_n) + \xi_n + u_n, \tag{2.8}$$

where $\xi_n$ is the noise at step $n$, and $u_n$ is the feedback control applied at the same iteration. In our case we have a continuous system, and a Poincaré map must be arranged to apply partial control. In addition, the noise and the control are bounded and moreover the upper control bound is smaller than the upper noise bound, that is,

$$\xi_0 > u_0 > 0 \qquad |u_n| \leq u_0 \qquad |\xi_n| \leq \xi_0. \tag{2.9}$$

Noises and controls obeying these conditions are called admissible, and trajectories fulfilling Eq. 2.8 are equally named.

### 2.3.2 The safe set and the asymptotic safe set

Consider a point $q_0$ in the set $Q$, the one we want to keep the dynamics in. We say that such point is safe if for any iteration $q_n$ of this point and any admissible disturbance $\xi_n$ there exists an admissible feedback control $u_n$ such that $q_{n+1}$ remains in $Q$. Note that if $q_0$ is safe, any of its iterations is safe as well. More generally, if any point in $S \subset Q$ is a safe point, we say $S$ is a *safe set*. Examples of safe sets for different systems can be seen in Ref. [27]. The following lines are devoted to describe the computation of the safe set.

The computation of the safe set can be achieved by means of the *Sculpting Algorithm* [27], which proceeds iteratively in the following manner. A point in the safe set has to verify that any of its images under Eq. 2.8 is in $S$, so, beginning with $Q$, we compute the fattend set $Q + u_0$, this is to say, we add to $Q$ all points that are at a distance $u_0$ from its boundary. Then we eliminate every point in $Q + u_0$

that is at a distance $\xi_0$ from its boundary, obtaining $Q + u_0 - \xi_0$ (see Fig. 2.5). All points in $Q$ whose images are in $Q + u_0 - \xi_0$ are safe for one iteration. We call this set $Q_1 \subset Q$ and insist that every point in $Q_1$ can be kept in $Q$ for one iteration. Now we repeat the proceedure starting with $Q_1$ and obtain $Q_2$, the set of points that are safe for two iterations. The set $Q_\infty$ is the largest safe set in $Q$. Topological properties granting the convergence of the iterates are given in Ref. [28]. Here we just recall that if $Q$ is compact, all $Q_n$ are compact and that the infinite intersection of non-empty compact sets $\bigcap_n^\infty Q_n$ is non empty. In practice we have to use a grid with limited resolution to compute $S$, so the procedure converges for some finite $n$.

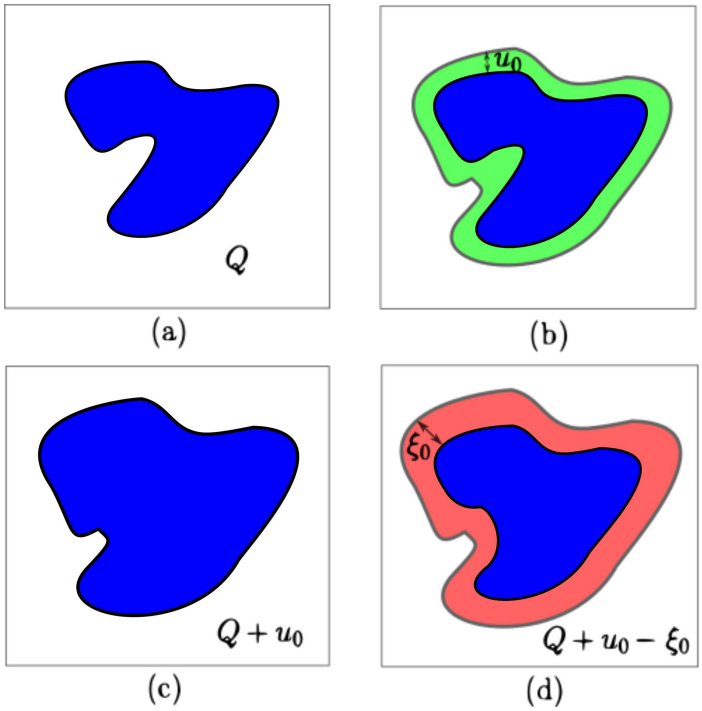


**Figure 2.5. An iteration of the Sculpting Algorithm**. (a) An initial set $Q$ to apply partial control. (b) Fattening realized by the addition of points at a distance $u_0$ from the boundary of $Q$. (c) The resulting set $Q + u_0$. (d) The set $Q + u_0 - \xi_0$, result of the shrinking of $Q + u_0$, which is performed by eliminating the points that are at a distance $\xi_0$ from it. The set $Q_1$ would consist on all the points in $Q$ whose images are in $Q + u_0 - \xi_0$ in one iteration. Even though $\xi_0 > u_0$, as long as we sculp the sucessive sets $Q_n$, the Cantor construction of the chaotic saddle, or equivalently, the sets of points that do not escape from the region $Q$ after some particular iteration, are glued together by the control if such iteration is high enough, what is related to the convergence of the Sculpting Algorithm.

Intuitively, if noises are not too high, all the partially controlled trajectories must end in some region around the original attractor (or the ghost). This means that there exists a trapping region where trajectories enter after a sufficiently high number of partially controlled iterations and never leave. This idea leads to the definition of the largest *asymptotic safe set* $A$. Such set is invariant under Eq. 2.8, so any of its points must be accessible from any other point in it by a partially controlled

iteration. Clearly stated, the largest asymptotic safe set is the largest invariant set under partial control. For the rigorous mathematical formalism see Ref. [28]. The asymptotic safe set can be computed using a similar Sculpting Algorithm to the one described in the previous paragraph. Starting with $S$, we compute all of the accessible points under partial control from every point in it, this is to say, we compute $(f(S)+u_0+\xi_0)\bigcap S$. We call this new set $S_1$ and use it to compute $S_2$, and so on until obtaining $S_\infty$. Another algorithm used in Ref. [28], called the *Growing Algorithm*, operates locally starting at some point $q$ in $S$ and computing all the points accessible by any partial control iteration $(f(q)+u_0+\xi_0)\bigcap S$. However, it might happen that $A$ contains other invariant subsets in it, so that the Growing Algorithm starting at some particular point $q$ in $A$ gives, as a result, a set that is smaller than the largest one. In the next section we introduce the smallest asymptotic safe set computed with the Growing Algorithm, and show that partially controlled trajectories cover it densely. Therefore, such set is the attractor of the partially controlled system.

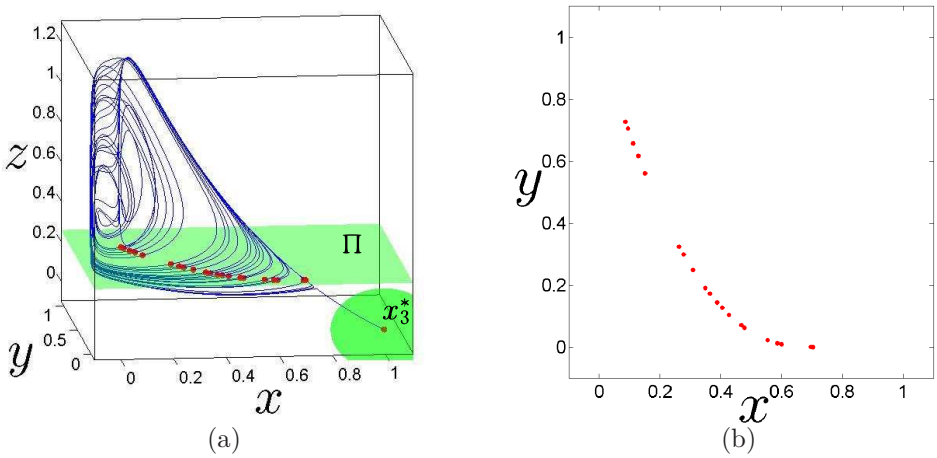


**Figure 2.6. The Poincaré section**. (a) A Poincaré section Π for $z = 0.255$. The trajectory returns to it several times (red points) before escaping to the attractor $x_3^*$, contained in the green ball. (b) The return map associated to the green section in (a).

## 2.4 Avoiding extinction of healthy cells

Although partial control could be carried out in the whole phase space, computational efficiency exhorts to use some subspace with a dimension as small as possible. This way, the first thing we have to do to apply partial control is to select a Poincaré section. Any two-dimensional manifold intersecting the chaotic attractor serves for this purpose, but for simplicity, we choose a plane Π at some fixed value of the immune cell population, *i.e.*, at a constant $z$ value. According to the reasons explained ahead, we use $z = 0.255$. This Poincaré section appears in green in Fig. 2.6(a) and the associated Poincaré map is shown in Fig. 2.6(b). The value of $r_3$ after the crisis

is set to 1.2907. Since we know that eventually trajectories approach $x_3^*$, a simple way to avoid this event is to assure that any iteration comes back to the Poincaré section $\Pi$. With this purpose, we take $Q$ as the set of all points in that plane that come back to it at least once before escaping to the attractor. In fact, this set resembles very much the basin of attraction of the chaotic attractor for a parameter value of $r_3$ above the critical value. The set $Q$ is shown in Fig. 2.7. The reason why we choose $z = 0.255$ is that for such value of the immune effector cell population the set $Q$ is the biggest, and the control/noise ratio is the smallest.

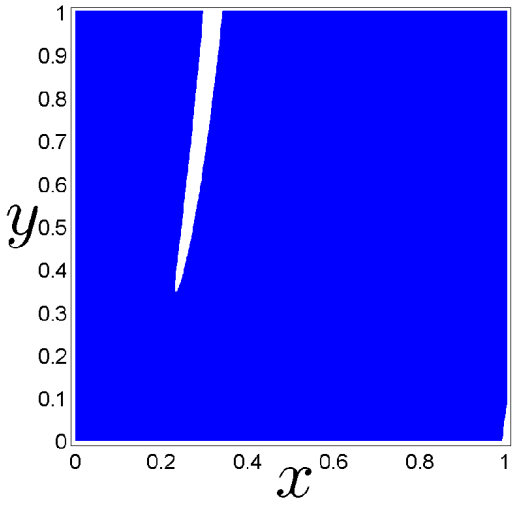


**Figure 2.7. The set $Q$.** A subset of $[0,1] \times [0,1]$ formed by all initial conditions on $z = 0.255$ that return at least once to the Poincaré section before escaping to the attractor. The purpose of partial control is to mantain trajectories in the blue region, avoiding the escape through the long white tusk that transverses it and the small white piece on the bottom right corner.

Concerning disturbances on the system, these models usually use multiplicative noises [32], so that external perturbations acting on them modify the cell populations through some parameter fluctuations. Note that the use of additive noises could lead to negative values of populations, which have no physical/biological meaning. Nevertheless, partial control acting on some parameter of a dynamical system is still to be attained. For the moment, we take additive noises, considering that those leading to negative values of the cell populations are meaningless, and therefore rejected. If preferred, one can think that the noise probability distribution varies as we approach to a zero value of any coordinate of the system, what is somehow equivalent to considering multiplicative noises. Anyway, this does not require modifying the noise and control conditions given in Eq. 2.9, since they cover the rejected cases. Another important issue is that the use of continuous noises modifies the set $Q$, because some points in the non-disturbed case that would come back to $\Pi$ do not return when disturbances are present. Nevertheless, to simplify things, we will suppose that noises act only on the Poincaré section and assume a correspondence

between the maximum continuous noise amplitude and the discretized one, which are related by $e^{\lambda_1 \tau_{max}}$, being $\lambda_1$ the maximum Lyapunov exponent and $\tau_{max}$ the maximum recurrence time of a point in the set $Q$. The probability distribution of the noise is then considered uniform and takes values according to Eq. 2.9, with bounds $\xi_0 = 0.02$ and $u_0 = 0.013$, which means a control/noise ratio $\rho = 0.65$.

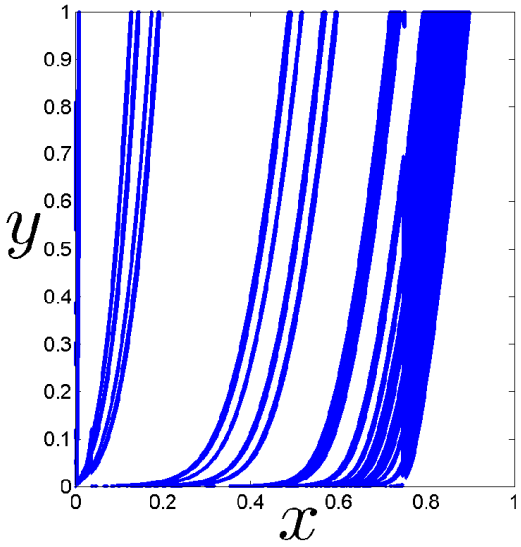


**Figure 2.8. The safe set $S$ obtained from $Q$.** We have used a maximum admissible noise of $\xi_0 = 0.02$ and a maximum admissible control $u_0 = 0.013$.

The Sculpting Algorithm is applied to a $3000 \times 3000$ grid to obtain the safe set, which is shown in Fig. 2.8. Any trajectory starting in $S$ can be controlled to stay in $S$ as much time as desired. Using this safe set, we compute the largest asymptotic safe set $A$ and also the smallest asymptotic safe set $I \subset A \subset S$. The former is computed with the Sculpting Algorithm, while the later uses the Growing Algorithm starting with a point in $A$. Both sets are shown in Fig. 2.9. As stated in Ref. [28], potentially there could be more that one asymptotic safe set. In fact, we have found up to four asymptotic safe sets with the growing procedure. One of them is the smallest asymptotic safe set, which is contained in all the remaining. We claim that there is not a smaller invariant set under partial control. Rigorously stated, $I$ is irreducible under partial control transformations. After a sufficient amount of time trajectories enter in $I$ and do not escape, covering it densely, as shown in Fig. 2.10. We perform a simulation of the partially controlled system for 6000 iterations, proving its success to prevent escape from the chaotic attractor towards the stable tumor fixed point.

In spite of this mathematical and numerical achievement, it is important to give biological and medical significance to controls. The idea of tumor therapies relies on a very simple fact: kill by all possible means the tumor cells. Three well known methods to accomplish it are chemotherapy, which tries to destroy cancer cells by the injection in the body of a chemical agent designed for the purpose; immunotherapy,

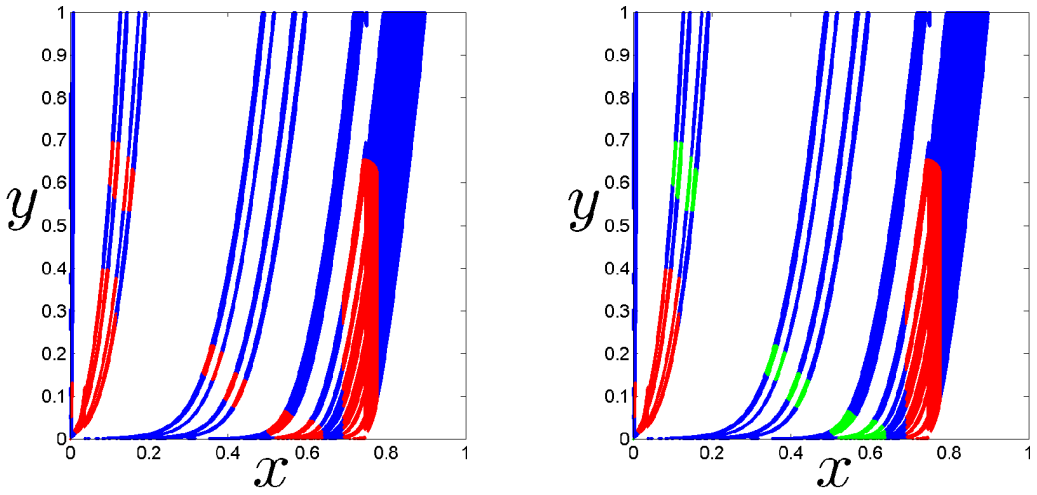


**Figure 2.9. The asymptotic safe set $A$ and the irreducible asymptotic safe set $I$.** (a) The safe set in blue containing the largest asymptotic safe set (red) obtained with the Sculpting Algorithm. (b) The smallest asymptotic safe set (green) obtained with the Growing Algorithm starting at some point in the largest asymptotic safe set, close to the original attractor. Note how this safe set encloses the attractor in Fig. 2.6(b).

that kills cells by a reinforcement of the immune system; radiotherapy, that attacks cells by means of ionizing radiation, breaking their chromosomes. The process of chemotherapy is very complex, since drugs have to be absorbed, reach the tumor site and then be eliminated from the organism. These pharmacokinetical aspects have to be modelled dynamically. It is for these reasons that the mathematical modeling of chemotherapy is generally attained by means of another variable representing the concentration of the drug at the tumor site, with the inclusion of an extra ordinary differential equation and curve responses of the cell populations to the drug [1]. Also the process of radiotherapy is rather sophisticated, even though the time dependence of the dose is more precisely defined than in chemotherapy, as pharmacokinetics or other accessibility matters do not really arise. Once a dose of radiation is applied, cells start a repair process to rehabilitate chromosomes. The model that explains the effects of radiation on cells is the well known linear quadratic model (LQM) that also includes an additional variable representing the average double strand breaks of chromosomes [8]. For short exposure to radiation compared to the time between therapy sessions, a Dirac's delta discrete approximation can be performed [14]. Nevertheless, both of these medical treatments destroy all types of cells with a variable killing rate depending on each case and cell population. Immunotherapy affects the production of immune effector cells that kill tumor cells, and also requires new variables associated to different substances that stimulate the immune system, as for instance the lymphokine concentration (e.g. IL-2) [12].

Since partial control treats cells separately and requires to increase and decrease

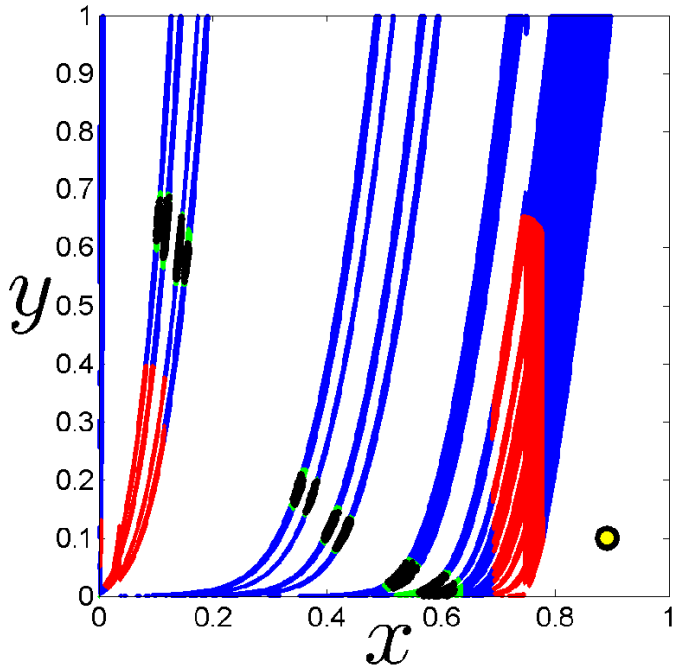


**Figure 2.10. A partially controlled trajectory**. We represent 6000 iterations starting at a point close to the original attractor. The black points are the iterates, which cover densely the smallest asymptotic safe set (green). We see that the trajectory stays close to the attractor avoiding escape. The radius of the two circles in the bottom-right part of the image represent the maximum control $u_0$ (yellow) and the maximum noise $\xi_0$ (black).

populations according to the safe sets, none of these procedures serve. Nevertheless, the great advance of biomedical engineering suggests that a day may come for which selective drugs allow to control cell populations in a totally independent way. On stimulation of cellular growth there is also research [33, 34], so the possibility of increasing cell populations is not harebrained. In fact, this is a rather counter-intuitive thing, since as we have shown, occasionaly we have had to increase the number of cancer cells to control the tumor escape.

Another interesting point is that the chaotic attractor in Fig. 2.3(a) oscillates between regions where there is a very low number of cancer cells and a high number of healthy ones to others where the opposite situation is found. A similar oscillatory regime also appears in other works with this model [2, 3], and it is characteristical of Lotka-Volterra predator-prey systems. Whenever this happened at some stage of tumorigenesis, the precise instant of the application of a therapy would be crucial. This means that a single therapy session applied at the right time might be enough to annihilate the tumor, while many sessions wrongly applied could result in a great damage to the patient. Furthermore, the chaotic behavior of the system implies that periodic controls acting on it might not have the desired effect. Finally, supposing that we could perform the required controls, a physician would ask how much time do

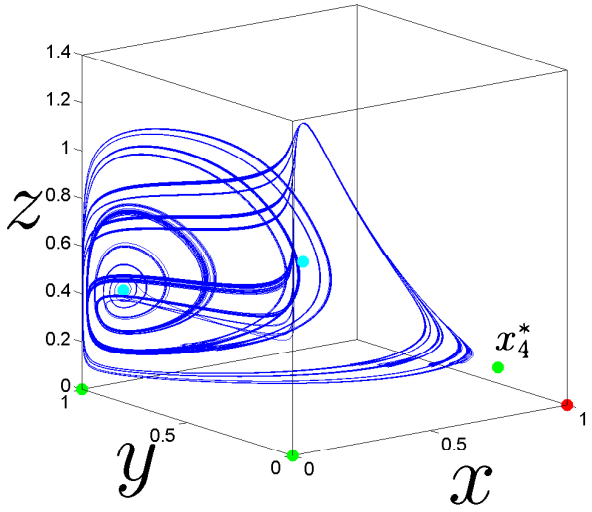


**Figure 2.11. The partially controlled attractor**. We show 1000 iterations (of the Poincaré map) of the controlled trajectory. Note that it does not get as close to the saddle fixed point $x_4^*$ as it does without control.

we have to wait until we reach the Poincaré section again, or equivalently, how often therapy controls need to be applied. Certainly, as we have stated, the recurrence time of each point is different, so, the way we have tackled the problem, no periodic or continuous protocols can be used. We show the recurrence time of every point in the Poincaré section in Fig. 2.12. The idea of using non periodic protocols is not new, and cases can be found in the literature, as for example the optimal therapy protocols used in Ref. [1], or the modeling of intermittent hormone therapy of prostate cancer developed in Refs. [35, 36, 37].

## 2.5 Other tecniques for controlling dynamical systems

To not deviate the attention from the main topic of this work, which is the dynamics of cancer, and because this chapter deals with the control of chaos in dynamical systems, we include here other contributions to this research area. In particular, we briefly discuss a general method developed to test the experimental possibilities that a dynamical system offers to suppress an undesired chaotic dynamics. This is pertinent because, as the reader might have noticed, the control technique applied in the previous sections operates directly on the dynamical variables, which in general are not accessible to an experimenter. Moreover, many other control techniques are used in the study of dynamical systems, which are more alike to cancer treatments, and which operate by manipulating one or more of the accessible parameters of the model. The main idea of these techniques is to introduce a perturbation in the system to control its dynamics. However, for this purpose, a deep knowledge of the system response to the parameters of the perturbation is required. The tools we introduce in this section provide a nice example of how this knowledge can be

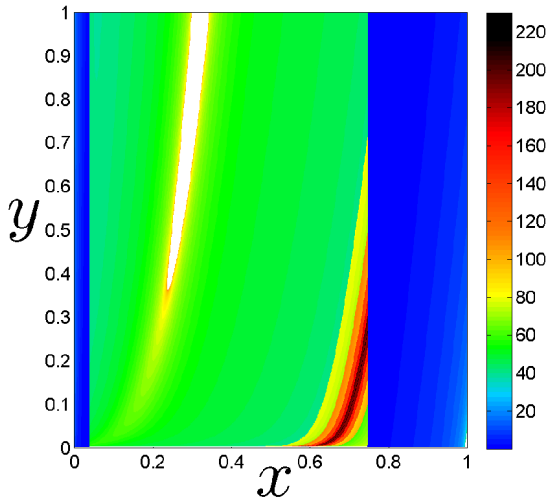


**Figure 2.12. The recurrence time of each point in the Poincaré section**. The color bar represents the time it takes a point $(x, y)$ in the section to return to it.

acquired.

Sometimes chaotic dynamics represents an advantage because it makes systems more adaptable. Precisely, in the previous sections we have shown how chaos can be used to avoid the occurrence of an undesired dynamics. However, in other situations chaos is an undesirable effect. For example, chaos restricts the operating range of many electronic and mechanic devices. This is a good enough reason to justify the attention that *chaos suppression* has received in the study of dynamical systems [38, 39, 40, 41]. In the case of nonlinear oscillators, such a suppression can be accomplished by introducing a time periodic perturbation depending on a set of predetermined parameters, which can be chosen to cause an stabilization of the chaotic system toward a periodic state. In chemotherapy, for example, drugs are commonly administered periodically (every three weeks) as well. Thus, contrary to some *feedback* control methods, as the partial control or, for example, the celebrated OGY [42], the present case is of the essence of some *nonfeedback* control methods, as for example the phase control [43, 44]. In the phase control method typically time independent variations of a phase difference between the periodic perturbations acting on a certain nonlinear oscillator is used to achieve chaos suppression. Sometimes anharmonic periodic perturbations have been used, as it is the case of Jacobi elliptic functions [40, 45], for which the elliptic parameter has been selected as the control parameter. Whatever the perturbation is, it always depends on one or more parameters, so studying the response of the dynamical behavior for the perturbed system to their variations is required. This task can be managed analytically or numerically. In the former case, one of the commonly used methods is the Melnikov analysis [40], while in the last one bifurcation diagrams or chaotic parameter sets are computed [45, 46]. A chaotic parameter set informs us if the asymptotic dynamics of a system is chaotic or not when varying two system parameters. This set is a basic and useful

tool in the study of dynamical systems [47] since it easily allows to visualize the asymptotic behavior of the system in a certain region of the parameter space. The asymptotic behavior of a dynamical system can be studied by computing the largest Lyapunov exponent, whenever it exists. As is well known, Lyapunov exponents measure the exponential rates of contraction and expansion along the orbits of dynamical systems. Given two available parameters of a particular system, the *chaotic parameter set* is defined as the set of the largest Lyapunov exponent computed for every pair of parameter values in a planar grid (see Fig. 2.13). The fact that it involves two parameters makes this set specially useful, what explains its frequent use in the study of chaos suppression. The ultimate usefulness of this set is that they might be later used in experimental settings [48] as guides to suppress chaotic dynamics. Nevertheless, in experimental situations, parameters are measured with a finite accuracy. This means that a certain parameter variation, appearing in a bifurcation diagram or a chaotic parameter set as adequate, could be uneffective in practice due to the limited precision with which such a parameter is measured.

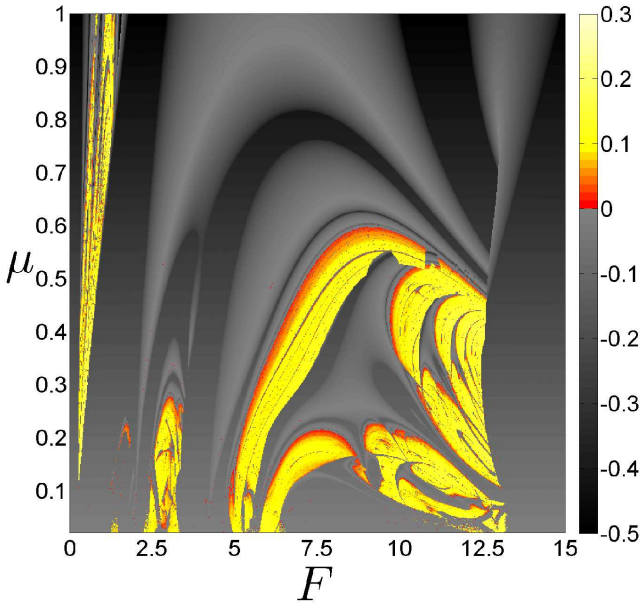


**Figure 2.13. The chaotic parameter set**. Chaotic parameter set for the Duffing oscillator $\ddot{x} + \mu\dot{x} - x + x^3 = F\sin t$ in the $(F, \mu)$ parameter space. The colorbar shows the value of the largest Lyapunov exponent, computed for a grid of $720 \times 720$ points, and using as initial condition $(x, \dot{x}) = (1, 0)$. Both periodic (gray colored) and chaotic (non-gray colored) motions are displayed.

Therefore, we now study when it is in practice possible to turn the asymptotic dynamics of a system from chaotic to periodic by variations of a parameter. Having settled a domain for that parameter, we want to know if suppression is in fact feasible for many different values spread over it, and if it is carried out with small variations of the parameter or not. For such purpose, we define the *suppressibility*,

a measure that takes into account all these matters. Sometimes it occurs that chaotic parameter sets exhibit highly fractal patterns. In those situations we have no security of reaching one asymptotic behavior or the opposite, due to the limited precision with which we measure a parameter. For this reason we have to provide a way to not consider them when defining and studying effective suppression. As we will see, our numerical study can be carried out in the parameter space by means of the chaotic parameter set.

The basic idea of suppression is to vary a free parameter, the *suppressing parameter*, from a particular value for which chaos rules, to another value for which periodic regime exists. Since we are only interested in the sign of the largest Lyapunov exponent, we represent chaotic parameter sets as binary sets, assigning black color to chaos and white to periodic dynamics. In this manner, we have an $R \times R$ matrix of grid points (being $R$ the resolution with which we compute the chaotic parameter set), and black or white squares centred in them. For convenience, we identify the square and its centre and simply refer to it as a pixel. Each of these pixels $(i, j)$ is related to a point in the parameter space $(F_i, \mu_j)$, with $i, j = 1, ..., R$. Chaos suppression in the chaotic parameter set simply corresponds to a *transition* from a black pixel to a white one, both contained in a line parallel to the axis associated to the suppressing parameter. We call each of these lines in a chaotic parameter set a *suppressing line*. Returning to our model, we take $F$ as the suppressing parameter and fix the value of $\mu$. If there is a particular point in the parameter space $(F_i, \mu_j)$ for which chaotic dynamics occurs, we can switch it to periodic by varying the suppressing parameter, *i.e.*, by making a transition to a different point in the same suppressing line $(F_k, \mu_j)$. Therefore, pixels in a suppressing line provide a natural way to measure how much a particular chaotic attractor can be suppressed. Simply count all the transitions from that black pixel to all the white ones contained in such line.

At this point, an important objection arises. The chaotic set is a delicate tool for several reasons. The most remarkable one is that chaotic parameter sets usually display fractal structure, so that chaotic regions hide "periodic lakes" inside them at any scale. Moreover, in some sort of systems, even periodic regions reveal chaotic states at any scale as one zooms in. It could happen that many (possibly infinite) periodic lakes were hidden in a black pixel, allowing transitions to a regular regime by smaller variations of the parameter. This is certainly true, but in such a case a smaller region of the chaotic parameter set should be computed. Then the same objection would arise again and again due to the fractal character of the chaotic parameter set. However, even if this was the case, experimentally there is a limitation on the measurement of the suppressing parameter $F$, imposed by the experimental uncertainty $\Delta F$. This implies a restriction in the range of values of the suppressing parameter used to compute the chaotic parameter set. The reason is that if a white pixel is at a distance from a black one smaller than the uncertainty, suppression can not be guaranteed by a transition to that pixel. We define transitions that do not assure suppression as *unsafe transitions*. On the contrary, those that guarantee suppression are named *safe transitions*. Pixels involved in safe (unsafe) transitions

are referred as safe (unsafe) too. We also define the length of a suppressing line $L$ as the distance used to compute the chaotic parameter set in the suppressing direction. In the example shown in Fig. 2.13 this length corresponds to the width of the chaotic parameter set $L = |F_{max} - F_{min}| = 15$. This width must be chosen according to the uncertainty in the measurement of the suppressing parameter. In particular, it must never be smaller than the uncertainty, because in that case we would not be able to guarantee suppression by any specific transition. In other words, all transitions would be unsafe. Even more, it is convenient that the uncertainty of the suppressing parameter be much smaller than the length of the suppressing lines. For instance, an adequate length could be such that we assign an uncertainty $\Delta F$ of one pixel. This means $\Delta F = L/R$. If this is the case, only transitions to white pixels one pixel away from black ones would be unsafe. Concerning uncertainty, all the transitions can be considered as safe for $\Delta F < L/2R$.

Suppose now we compute a chaotic parameter set with an uncertainty of just one pixel, and we are in a black (chaotic) pixel located at position $(i, j)$. If the first coordinate $i$ corresponds to the suppressing direction and a neighbouring pixel $(i \pm 1, j)$ is white, we should not make a transition to it, because it is unsafe. Even worse, we can not even assure that the first was certainly chaotic. Therefore boundaries in the direction of the suppressing parameter must be redefined by marking as inaccessible all the pixels that are at a distance equivalent to the the parameter uncertainty from the boundary. The remaining pixels in that suppressing line are safe, and so are all the transitions from one of those black pixels to the white ones in the same line. We define all the transitions from a safe black pixel $(i, j)$ to all the safe white ones in a specific suppressing line $j$ as the *set of accessible transitions* $\mathcal{A}_{ij}$ corresponding to that initial chaotic attractor. These transitions are called safe or effective in the sense that for the initial pixel chaos occurs and the final white pixel guarantees suppression.

The distance between two elements involving a transition, or in a similar fashion, how much the parameter must be varied to achieve a certain transition, is also a very important fact when measuring how much can be suppressed the dynamics of a particular black pixel. If we have two possible or accessible transitions, one of them implying a variation of the parameter of two pixels, while another meaning a variation of eight pixels, it seems reasonable to prefer the first one. Hence the next step is to find a way of considering preferably transitions involving shorter variations of the parameter. The problem is to establish a mechanism to tell how much preferable are short transitions to large ones. Certainly here one has to deal with some arbitrariness, which is going to depend on the conditions we settle to achieve suppression. For instance, we might want to weight very high short transitions and then very low long ones. Or maybe we prefer to weight the same transitions up to a certain distance and then let their weight decrease slowly, etc. Therefore, given two pixels in a suppressing line, $(i, j)$ and $(k, j)$, we define the *order* of the transition $(i, j) \to (k, j)$ as the distance between them $|i - k|$, considered as matrix elements in a suppressing line $j$. Then we assign a *weight* $w_{ik}$ to every transition, through a monotonically decreasing function $w : \mathbb{N} \to \mathbb{R}$ depending on the order of the transi-

tion $w_{ik} = w(|i-k|)$. For example, if we take $w(n) = 1/n$, a black pixel $(i, j)$ and a white pixel $(k, j)$, the transition between them has a weight $w_{ik} = 1/|i-k|$. In this case first order transitions have weight 1, second order transitions have weight $1/2$, and, in general, the $n$th order transition has weight $1/n$. We also require that $w(1) = 1$, what simply gives unit value to the highest possible weight. Finally, we define the suppressibility $\chi_{ij}$ on a black pixel $(i, j)$ as the sum of all the weights over the set of accessible transitions $\mathcal{A}_{ij}$, *i.e.*, the weights related to all the safe transitions to white pixels in the same suppressing line

$$\chi_{ij} = \sum_{k \in \mathcal{A}_{ij}} w_{ik}. \tag{2.10}$$

Now, given two chaotic situations and some particular suppressing conditions coded in $w$, we can quantitatively compare them to know which one offers more and better possibilities of being suppressed in a certain region of the parameter space. As an example, we consider the two chaotic attractors for parameter choices $(F_{387}, \mu_{132}) = (8.0625, 0.1797)$ and $(F_{555}, \mu_{298}) = (11.5625, 0.4057)$ in Fig. 2.13. We recall that $(F_{387}, \mu_{132})$ corresponds to the values of the forcing amplitude and damping associated to the grid point given by the coordinates $(387, 132)$ in the computed chaotic parameter set, whose resolution is $720 \times 720$. Keep $F$ as the suppressing parameter and suppose it is experimentally measured with a precision $\Delta F = 0.021$, what corresponds to one pixel in the mentioned figure. What is the suppressibility for each of those two attractors if we want to use no more than thirty pixels (variations of the suppressing parameter less or equal than 0.6241) to suppress chaos and consider all transitions equally weighted? These conditions impose an assignment of weights according to a Heavyside function of the form

$$w_{ik} = \begin{cases} 1 & |i-k| \leq 30 \\ 0 & |i-k| > 30 \end{cases} . \tag{2.11}$$

Computation of the suppressibility yields $\chi_{(387,132)} = 8$ and $\chi_{(555,298)} = 7$. This means that under the experimental conditions stated in the previous paragraph, the first attractor offers more possibilities of being suppressed. Now that this is well understood, we define the *suppression parameter set* as the value of the suppressibility computed for every safe black pixel in the chaotic parameter set. This set shows where chaos can be more easily and in more ways suppressed, as shown in Fig. 2.14. Note that many chaotic attractors have disappeared, since they can not be suppressed under the specified experimental restrictions imposed by $w$ and $\Delta F$.

Some more information can be extracted from the chaotic parameter set, and other considerations must be taken into account under special circumstances, but we detain ourselves here, since the main concepts of our method have been illustrated.

## 2.6 Conclusions and Discussion

In summary, the present chapter shows the possibility of preventing a tumor escape in a chaotic cancer model in the presence of some external disturbances, applying

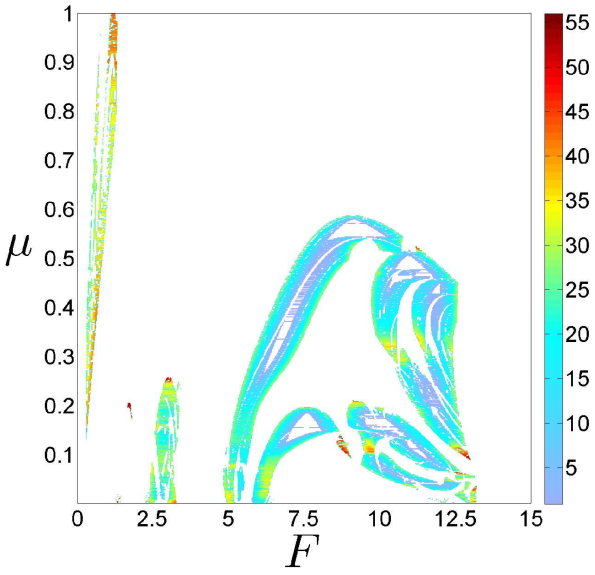


**Figure 2.14. The suppression parameter set**. Suppression parameter set for $\ddot{x}+\mu\dot{x}-x+x^3 = F\sin t$ in the $(F,\mu)$ parameter space, with suppressing parameter $F$, uncertainty $\Delta F = 0.021$ and $w_{ik} = 1-\Theta(|i-k|-30)$, where $\Theta(x)$ is the Heavyside function. This set shows all the safe chaotic events for which chaos can be suppressed, and which ones offer better possibilities of being suppressed, according to the conditions imposed by $w$. It is obtained by computing the suppressibility $\chi_{ij}$ for every safe black pixels $(i,j)$ and assigning each chaotic event a color depending on its value. The colorbar goes from cold colors to hot ones, corresponding respectively to the lower (1) and higher (56) values of the the suppressibility measure.

small controls to the cell populations. This has been achieved by means of the partial control method, which applies to transient chaotic situations in presence of external disturbances. The fact that controls are smaller than the external disturbances is promising, since the side effects of drugs and radiation are well known. On the other hand, the main difficulties at the current stage of development of the partial control method to maintain healthy cell populations arise from two simple facts. It requires to be able to modify cell populations directly and all of a sudden, implying an enormous accessibility to the system, and different cell populations have to be treated independently. This is in contrast to the regular procedure of most cancer treatments, that usually decrease all cell populations by complex processes. Other investigations concerning the control of chaos in dynamical systems have been described at the end of the chapter. This method reveals that the most feasible way to control a dynamical system is, perhaps, by varying one ore more of its relevant parameters. Therefore, we conclude that the implementation of partial control to parameter variations is convenient. Another surprising aspect is that sometimes it has been required to increase cell populations. Although striking, if we consider common tumor therapies, this reveals important consequences of chaotic dynamics on tumor progression and therapy protocols.

# References

[1] L.G. De Pillis and A. Radunskaya, "The dynamics of an optimally controlled tumor model: a case study", *Math. Comput. Modelling* **37**, 1221-1244 (2003).

[2] M. Itik and S. Banks, "Chaos in a three dimensional cancer model", *Int. J. Bifurcation and Chaos* **20**, 71-79 (2010).

[3] C. Letellier, F. Denis, and L.A. Aguirre, "What can be learned from a chaotic cancer model?" *J. Theor. Biol.* **22**, 7-16 (2013).

[4] N. Bellomo, N.K. Li, and P.K. Maini, "On the foundations of cancer modelling: selected topics, speculations, and perspectives", *Math. Mod. Meth. Appl. S.* **18**, 593-646 (2008).

[5] Ž. Bajzer, M. Marušić, and S. Vuk-Pavlović, "Conceptual frameworks for mathematical modelling of tumor growth dynamics", *Math. Comput. Modelling* **23**, 31-46 (1996)

[6] V.A. Kuznetsov, I.A. Makalkin, M.A. Taylor, and A.S. Perelson, "Nonlinear dynamics of immunogenic tumors: Parameter estimation and global bifurcation analysis", *Bull. Math. Biol.* **56**, 295-321 (1994).

[7] A. d'Onofrio, "A general framework for modelling tumor-immune system competition and immunotherapy: Mathematical analysis and biomedical inferences", *Physica D* **208**, 220-235 (2005).

[8] R.K. Sachs and L.R. Hlatky, "Simple ODE models of tumor growth and anti-angiogenic or radiation treatment", *Math. Comput. Modelling* **33**, 1297-1305 (2001).

[9] D. Kirschner and J.C. Panetta, "Modelling immunotherapy of the tumor-immune interaction", *J. Math. Biol.* **37**, 235-252 (1988).

[10] L.G. De Pillis, A.E. Radunskaya, and C.L. Wiseman, "A validated mathematical model of cell-mediated immune response to tumor growth", *Cancer Res.* **6**, 235-252 (2005).

[11] L.G. De Pillis, W. Gu, and A.E. Radunskaya, "Mixed immunotherapy and chemotherapy of tumors: modelling, applications and biological interpretations", *J. Theor. Biol.* **238**, 841-862 (2006).

[12] S.T.P. Pinho, H.I. Freedman, and F. Nani, "A chemotherapy model for the treatment of cancer with metastasis", *Math. Comput. Modelling.* **36**, 773-803 (2002).

[13] F. Nani and H.I. Freedman, "A mathematical model of cancer treatment by immunotherapy", *Mathematical Biosciences* **163**, 159-199 (2000).

[14] R. Placeres Jiménez and E.O. Hernández, "Tumor-host dynamics under radiotherapy", *Chaos, Solitons & Fractals* **44**, 685-692 (2011).

[15] H.I. Freedman, and S.T.R. Pinho, Stability criteria for the cure state in a cancer model with radiation treatment, *Nonlinear Analysis: Real Word Applications* **10**, 2709-2715 (2009).

[16] J.C. Panetta and J. Adam, "A mathematical model of cycle-specific chemotherapy", *Math. Comput. Modelling* **22**, 67-82 (1995).

[17] M. Saleem and T. Agrawal, "Chaos in a tumor growth model with delayed feedback responses of the immune system", *J. Appl. Math.* 891095 (2012).

[18] E. Ahmed, "Fractals and chaos in cancer models", *Int. J. Theoret. Phys.* **32**, 353-355 (1993).

[19] C. Wolfrom, N.P. Chau, J. Maigné, J.C. Lambert, B. Ducot, S. Guerroui, and J. Deschatrette, "Evidence for deterministic chaos in aperiodic oscillations of proliferative activity in long-term cultured Fao hepatoma cells", *Journal of Cell Science* **113**, 1069-1074 (2000).

[20] T. Tèl, "Controlling transient chaos", *J. Phys. A: Math. Gen* **24**, L1359-L1368 (1991).

[21] I.B. Schwartz and I. Triandaf, "Sustaining chaos by using basin boundary Saddles", *Phys. Rev. Lett.* **77**, 4740-4743 (1996).

[22] T. Kapitaniak and J. Brindley, "Preserving transient chaos", *Phys. Lett. A* **241**, 41-45 (1998).

[23] W. Yang, M. Ding, A.J. Mandell, and E. Ott, "Preserving chaos: Control strategies to preserve complex dynamics with potential relevance to biological disorders", *Phys. Rev. E* **51**, 102-110 (1995).

[24] J. Aguirre, F. d'Ovidio, and M.A.F. Sanjuán, "Controlling chaotic transients: Yorke's game of survival", *Phys. Rev. E* **69**, 016203 (2004).

[25] S. Zambrano and M.A.F. Sanjuán, "Exploring partial control", *Phys. Rev. E* **79**, 026217 (2009).

[26] J. Sabuco, S. Zambrano, and M.A.F. Sanjuán, "Partial control of chaotic transients using escape times", *New Journal of Physics* **12**, 113038 (2009).

[27] J. Sabuco, S. Zambrano, M.A.F. Sanjuán, and J.A. Yorke, "Finding safety in partially controllable chaotic systems", *Commun. Nonlinear Sci. Numer. Simulat.* **17**, 4274-4280 (2012).

[28] J. Sabuco, M.A.F. Sanjuán, and J.A. Yorke, "Dynamics of partial control", *Chaos* **22**, 047507 (2012).

[29] T. Tèl and Y. Lai, "Chaotic transient in spatially extended systems", *Phys. Rep.* **460**, 245-275 (2008).

[30] L. Chen and K. Aihara, "Chaotic simulated annealing by a neural network model with transient chaos", *Neural Networks* **8**, 915-930 (1995).

[31] T. Tèl, A. de Moura, C. Grebogi, and G. Károlyi, "Chemical and biological activity in open flows: A dynamical systems approach", *Phys. Rep.* **413**, 91-196 (2005).

[32] B. Spagnolo, A. Fiasconaro, and D. Valenti, "Noise induced phenomena in a Lotka-Volterra system", *Fluct. Noise Lett.* **3**, L177 (2003).

[33] S.R. Seong, J.W. Lee, T.I. Kim, D.J. Son, Y.W. Yun, D.C. Moon, Y.W. Yun, D.Y. Yoon, and J.T. Hong, "Stimulation of cell growth by erythropoietin in RAW264.7 cells: association with AP-1 activation", *Arch. of Pharm. Res.* **29**, 218-223 (2006).

[34] C.T. Cottage, L. Neidig, B. Sundararaman, S. Din, A.Y. Joyo, B. Bailey, N. Gude, N. Hariharan, and M.A. Sussman, "Increased mitotic rate coincident with transient telomere lengthening resulting from Pim-1 overexpression in cardiac progenitor cells", *Stem cells* **30**, 2512-2522 (2012).

[35] A.M. Ideta, G. Tanaka, T. Takeuchi, and K. Aihara, "A mathematical model of intermittent adrogen suppression for prostate cancer", *J. Nonlinear Science* **18**, 593-614 (2008).

[36] Y. Hirata, N. Bruchovsky, and K. Aihara, "Development of a mathematical model that predicts the outcome of hormone therapy for prostate cancer", *J. Theor. Biol.* **264**, 517-527 (2010).

[37] T. Suzuki, N. Bruchovsky, and K. Aihara, "Mathematical modelling of prostate cancer growth and its application to hormone therapy", *Transactions of Royal Society A* **368**, 5045-5059 (2010).

[38] Y. Braiman and I. Goldhirsch, "Taming chaotic dynamics with weak periodic perturbations", *Phys. Lett.* **66**, 2545-2548 (1991).

[39] R. Chacón and J. Díaz Bejarano, "Routes to suppressing chaos by weak periodic perturbations", *Phys. Lett.* **71**, 3103-3106 (1993).

[40] R. Lima, and M. Pettini, "Suppression of chaos by resonant parametric perturbations", *Phys. Rev. A* **31**, 726-733 (1990).

[41] F. Rodelsperger, Y.S. Kivshar and H. Benner, "Reshaping-induced chaos suppression", *Phys. Rev. E* **51**, 869-872 (1995).

[42] E. Ott, C. Grebogi, and J.A. Yorke, "Controlling chaos", *Phys. Rev. Lett.* **64**, 1196-1199 (1990).

[43] J.M. Seoane, S. Zambrano, S. Euzzor, R. Meucci, F.T. Arecchi, and M.A.F. Sanjuán, "Avoiding escapes in open dynamical systems using phase control", *Phys. Rev. E* **78**, 016205 (2008).

[44] M.A.F. Sanjuán, "Using nonharmonic forcing to switch the periodicity in nonlinear systems", *Phys. Rev. E* **58**, 4377-4382 (1998).

[45] S. Zambrano, E. Allaria, S. Brugioni, I. Leyva, R. Meucci, M.A.F. Sanjuán and F.T. Arecchi, "Numerical and experimental exploration of phase control of chaos", *Chaos* **16**, 013111 (2006).

[46] S. Zambrano, J. Seoane, I.P. Mariño, M.A.F. Sanjuán, S. Euzzor, R. Meucci, and F. T. Arecchi, "Phase control of excitable systems", *New Journal of Physics* **10**, 073030 (2008).

[47] E. Barreto, B.R. Hunt, C. Grebogi, and J.A. Yorke, "From High Dimensional Chaos to Stable Periodic Orbits: The Structure of Parameter Space", *Phys. Lett.* **78**, 4561-4564 (1997).

[48] L. Fronzoni, M. Giocondo, and M. Pettini, "Experimental evidence of suppression of chaos by resonant parametric perturbations", *Phys. Rev. A* **43**, 6483-6487 (1991).

# Chapter 3

# A validated mathematical model of tumor-immune interactions

*"It doesn't matter how beautiful your theory is, it doesn't matter how smart you are. If it doesn't agree with experiment, it's wrong"*

-Richard P. Feynman (1918-1988)

We continue our investigation developing and validating an ODE model of tumor progression with three interacting cell populations representing the healthy tissue, the neoplastic tissue and the immune effector cells. By means of the least-squares fitting method, we adjust the model to experimental data [1], verifying that the lysis of cancer cells by the effector constituents of the immune system is accurately reproduced by the model. As a completely new feature regarding previous modelling of this nature, we also introduce a chemotherapy protocol validated with *in vivo* experiments in mice [2]. To reproduce the time evolution of the experimental *fractional tumor cell kill* by the chemotherapeutic agents a new method is proposed, that avoids dealing with complex pharmacokinetical models. The study is closed with the examination of correlations between the model and the experiments.

## 3.1 Introduction

It is increasingly apparent that the growth deregulation within a tumor can only be explained once we understand the contributions of the host healthy cells present with it, which play key roles in driving tumor cell proliferation. Signaling interactions between the stromal and the neoplastic tissue may ultimately prove to be as important as the cancer cell autonomous mechanisms in explaining tumor cell pro-

liferation [3]. The importance of the immune system fighting the growth of tumors is undeniable, to the point that immunotherapy is lately focusing major attention of cancer therapists and researchers [4]. Adoptive cell transfer using chimeric antigen receptors [5, 6] or the modulation of CTLA-4 activity by means of monoclonal antibodies [7] are two outstanding examples [4]. Also chemotherapy treatments are under constant examination, in the pursuit of better distribution mechanisms that diminish the toxicity of the anti-cancer drugs [8], as well as protocols that evade the resistance of tumor cells to such cytotoxic substances [9]. Mathematical modelling of tumor growth [10] has been widely used to explain different aspects of tumor progression, such as tumor dormancy, sneaking through, angiogenic switch, invasion, morphology, etc. Therefore, the development of validated and simple mathematical models representing several types of tissues and the nonlinear interactions among them, as well as therapy protocols, is of paramount importance.

We derive the dynamical system equations from a similar validated model describing immune and tumor dynamics [11], but that considers different cell populations for innate and specific immune responses and disregards tumor-host interplay. Here, the immune response is integrated in a single cell population, as it was the case of older models [12], allowing us to include a population representing the healthy tissue and still to visualize in a simple manner their dynamical phase space.

## 3.2 Model development

All the biological assumptions considered to set up the model equations are based on both accepted knowledge of basic laws governing tumor growth and the immune system function [1, 11, 12]. The tumor-host competition for space and resources is developed following previous modelling [13, 14, 15, 16], while the law governing the fractional tumor cell kill by the chemotherapeutic drugs is derived from the exponential kill model [17], developed in accordance with *in vitro* experiments.

The growth of the cell populations is assumed to be logistic for both the tumor $T$ and the healthy cells $H$, with growth rates $r_1$ and $r_2$, and carrying capacities $K_1$ and $K_2$. Other types of laws, such as Gompertz law, have no relevant consequences in the dynamics, and might be used as well. We use ordinary competition terms frequently appearing in Lotka-Volterra models, identical to those used in Refs. [12] and [14]. Finally, the immune response and the destruction of the neoplastic tissue is built up from the one presented in Ref. [11], which was validated with data from published mouse [1] and human [18] studies. The model of cell-mediated immune response described in that work consists of a tumor cell population $T$ interacting with two immune cell populations, the natural killers $N$ and the $CD8^+$ T lymphocytes $L$. The fractional tumor cell kill by T cells is given by a Hill function $D(L,T)$ depending on $L/T$, while the fractional tumor cell kill by NK cells is proportional to the number of such cells. The NK cells dynamics is modelled with four terms: a constant input $\sigma$ responsible for innate immunity, a recruitment contribution $gT^2/(h+T^2)N$, a competition term $pNT$ with tumor cells, and a decay term representing the death $fN$ of the natural killers, which after several interactions with the tumor cells become

inactivated. The CTLs dynamics is governed by analogous laws, but there is no constant input of cells, since they correspond to acquired immunity. On the other hand, it includes the stimulation of T lymphocytes in response to the interaction between NK and tumor cells $rTN$. The activation term is $jD^2T^2/(k+D^2T^2)L$, the death term is $mL$ and the competition one is $qLT$.

It can be numerically shown that for many initial conditions and not long times these two immune cell populations are more or less related in a linear fashion. In this manner, we identify them and linearly combine their equations, simply referring to them as effector cells $E$. The resulting model is

$$\begin{aligned}
\dot{T} &= r_1 T\left(1-\frac{T}{K_1}\right) - a_{12}HT - a_{13}ET - D(E,T)T \\
\dot{H} &= r_2 H\left(1-\frac{H}{K_2}\right) - a_{21}TH \\
\dot{E} &= \sigma - d_3 E + \tilde{g}\frac{T^2}{\tilde{h}+T^2}E + g\frac{D^2(E,T)T^2}{h+D^2(E,T)T^2}E - a_{31}TE,
\end{aligned} \tag{3.1}$$

with

$$D(E,T) = d\frac{(E/T)^\lambda}{s+(E/T)^\lambda}. \tag{3.2}$$

This fractional cell kill law was a novel feature discovered and introduced in Ref. [11], so it deserves some comments. To give some hints on the significance and possible explanations of this law we rewrite it in the following form

$$D(E,T) = d\frac{E^\lambda}{sT^\lambda+E^\lambda}. \tag{3.3}$$

Written this way, the law states that the more effector cells, the greater the fractional cell kill, but bearing in mind the saturation of antigen-mediated immune response, which depends on the tumor load. The value for which the fraction cell kill is half of its maximum is given by $E_{hm} = s^{1/\lambda}T$, what means that bigger tumors are harder to fight by T lymphocytes. If two tumors of the same nature and different size at a certain time instant, are lysed at the same rate by the immune system, the bigger tumor will require more effector cells. This is because an immune cell destroys tumor cells one by one and the number of encounters is limited by the inactivation of the effector cells. Or equivalently, if two tumors of different size are reduced to a particular fraction of its size after a certain period of time, the bigger tumor will require more effector cells. On the other hand, and as we develop in the next chapter, the saturation effect in this law is tacitly including *geometrical* properties of the tumor and their consequences (*e.g.*, *crowding* effects and accessibility of the immune cells). We believe that it would be desirable to propose a general law of the form

$$D(E,T) = d\frac{E^\lambda}{h(T)+E^\lambda}, \tag{3.4}$$

and study different functions depending on the tumor load $h(T)$ for different tumors. In the cited work $h(T) = sT^{\lambda}$ is used. We have tested the importance of the parameter $\lambda$ by studying deviations from this function in the form $h(T) = sT^{\lambda+\Delta\lambda}$, and we have found that shifts $\Delta\lambda/\lambda$ even higher than one are still capable of validating in an accurate manner the immune response by simply decreasing the value of the parameter $s$. The precise relation between $\Delta\lambda$ and $s$ is depicted in Fig. 3.1, and it is explained by noting that the function $h(T)$ can be thought as a surface in the parameter space $(\lambda, s)$, so that changes in the parameters along a level curve $sT^{\lambda} = c(T)$ are also capable of validating the experimental results. This means that the rational form $E/T$ appearing in Eq. (3.2) may not generally hold, and can not be derived solely from the experiments used in Ref. [11]. What can be safely deduced from such experiments is that $h(T)$ increases with the tumor size. Therefore, the dePillis-Radunskaya-Wiseman law (PRW law) states that the number of the T cells for which the fractional tumor cell kill is half of its maximum, increases monotonically with the tumor burden. It remains unexplained why the same does not happen for the NK cells as well. As pointed out in Ref. [11], this might be due to the fact that NK cells are less effective destroying tumor cells. Generally, a T lymphocyte is able to destroy more tumor cells during its life cycle than a natural killer cell [19]. Note also that to obtain similar values for the lysis of tumor cells by T cells and NK cells, much higher values of the Effector:Target ratio are required for the last [11]. This hypothesis is also supported by the fact that the PRW law fits better the experimental results for which the immune system is more effective, as can be seen in Fig. 3.2.

The model shown above fits the data accurately, but it is quite hard to manage when investigating its dynamical properties. A simplified version of this model capable of reproducing experimental data can be obtained by neglecting the recruitment and lysis of the NK cells, which are more ineffective fighting the tumor cells. Note however, that the role of the NK cells is indirectly present in the model, in the background source rate $\sigma$. The equations are now

$$\begin{aligned}
\dot{T} &= r_1 T\left(1 - \frac{T}{K_1}\right) - a_{12} HT - D(E,T)T \\
\dot{H} &= r_2 H\left(1 - \frac{H}{K_2}\right) - a_{21} TH \\
\dot{E} &= \sigma - d_3 E + g\frac{D^2(E,T)T^2}{h + D^2(E,T)T^2}E - a_{31} TE.
\end{aligned} \tag{3.5}$$

The chemotherapy treatment is here described by the exponential kill model, which proposes the fractional cell kill law $k_i(C) = b_i(1 - e^{-\rho_i C})$, with $i = 1, 2, 3$, and $C$ the drug concentration at the tumor site, which dynamics is given by a single compartment model and first order pharmacokinetics. Therefore, the whole set of

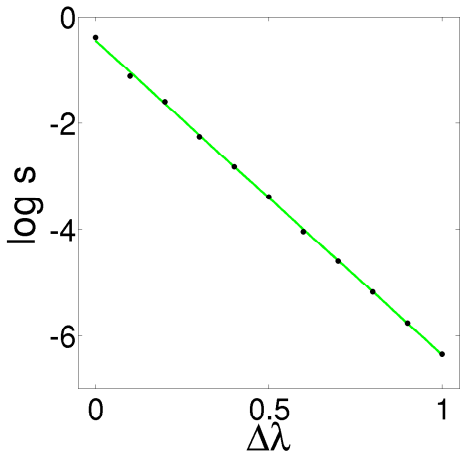


**Figure 3.1. Level curve in the parameter space**. In this figure, we show the changes in the parameter $s$ required to validate the model when the parameter $\lambda$ in the function $h(T) = sT^{\lambda}$ is changed to $\lambda+\Delta\lambda$. The case $\Delta\lambda = 0$ corresponds to the $(ll)$ values shown in Table 3.1. The relation is explained by the level curves of the function $sT^{\lambda}$ in the parameter space $(\lambda, s)$, which can be expressed in the form $\log s = \log c(T) - \lambda \log T$. Averaging this equation in time, we obtain the equation $\log s = a - b\lambda$. A linear regression has been performed to confirm the previous assertion, obtaining the relation $\log s = -0.46 - 5.79\Delta\lambda$, with a coefficient of determination $R^2 = 0.9996$.

equations reads

$$\begin{aligned}
\dot{T} &= r_1 T\left(1 - \frac{T}{K_1}\right) - a_{12}HT - D(E,T)T - k_1(C)T \\
\dot{H} &= r_2 H\left(1 - \frac{H}{K_2}\right) - a_{21}TH - k_2(C)H \\
\dot{E} &= \sigma - d_3 E + g\frac{D^2(E,T)T^2}{h + D^2(E,T)T^2}E - a_{31}TE - k_3(C)E \\
\dot{C} &= I(t) - k_e C,
\end{aligned} \tag{3.6}$$

with $I(t)$ the input of drug and $k_e$ the rate of elimination of the drug from the body. In fact, to reproduce *in vivo* experiments the fractional cell kill law $k(C)$ is modeled depending on the time-delayed concentration of drug $C(t-\tau)$.

Finally, the cooperation between the healthy and the tumor tissues is not modelled here. The reason is that the paracrine signals stimulating tumor growth come from ancillary cells (*e.g.* fibroblasts), different from the host cells (*e.g.* epithelial cells) from which the tumor evolves [20]. Moreover, the stromal cells cooperating with the tumor differ from the normal stromal cells. Therefore, a model with several healthy cell populations representing the different types of tissues should be considered to rigorously represent the tumor microenvironment.

## 3.3 Fitting the model to experimental data

We fit both, the model and its simplified version, to four experimental situations, proving that the tumor-immune interaction is again validated with accuracy. The data used to arrange the equations and fix the parameters of our mathematical model are obtained from Ref. [1]. In this work the authors study the effects of ectopically expressing NKG2D ligands in three tumor cell lines, which resulted in the rejection of the tumors by syngeneic B6 mice. Such rejection was mediated by NK cells and $CD8^+$ T cells. Their experimental results demonstrate that a high enough expression of these ligands creates a significant barrier to the tumor establishment in mice. In particular, the data borrowed from this work and used to fit the model correspond to the point where the authors address whether prior immunization with tumor cells that express ligands of the NKG2D receptor induces protective immunity to ligand-negative tumor cells. The NK and $CD8^+$ T cells lysis of a T-cell lymphoma after primary challenging with ligand-expressed cell transductants and being again challenged with ligand-transduced or ligand-negative-transduced cells is reported. More specifically, we deal with four possible scenarios: a primary challenge with control-transduced cells followed by a secondary challenge with ligand or control cells, and a primary interaction with ligand-transduced cells followed again by ligand or ligand-negative rechallenges.

Firstly, we give a summary of the parameters used, which are listed in Table 3.1 and Table 3.2, together with the corresponding sources in which the parameter estimation methods are explained. As in Ref. [14], we consider similar carrying capacities $K_i$ for the tumor and the healthy tissue, assuming that generally the tumor occupies a region that otherwise would be filled with normal cells. Also the rates of growth $r_i$ of both cell populations take very close values, following the same reference, but we assume that the tumor grows faster in the absence of competition and immune surveillance, since its dependence on cell to cell signaling for growth is smaller [3]. These four parameters, the recruitment rates and steepnesses, the constant input, as well as the inactivation rate of the effector cells, are borrowed from Refs. 6 and 10. It has been demonstrated that the Gompertz law of growth of tumor cell populations is a robust emergent feature of cancer dynamics under nutrient competition among tumor cells [21]. It is commonly considered [12] that the competition between the neoplastic and the healthy tissues is indirect, what means that cells do not kill each other, but struggle for territory and nutrient resources. However, a very important source of competition between the tumor and the healthy host cells is due to the acidic environment in which tumor cells develop, which is a consequence of the primitive metabolic pathways they use [14, 22, 23]. In fact, if we neglect spatial dependence in the equation governing the excess of $H^+$ ions in the model presented in Ref. [14], the stationary state gives a fixed point for ion concentration proportional to the number of tumor cells. Clearly stated, the more tumor cells, the lower the pH and the worse for the healthy tissue. When substituted in the reaction-diffusion equation governing the dynamics of the healthy host cells, we obtain another competition term between the host and the tumor cells.

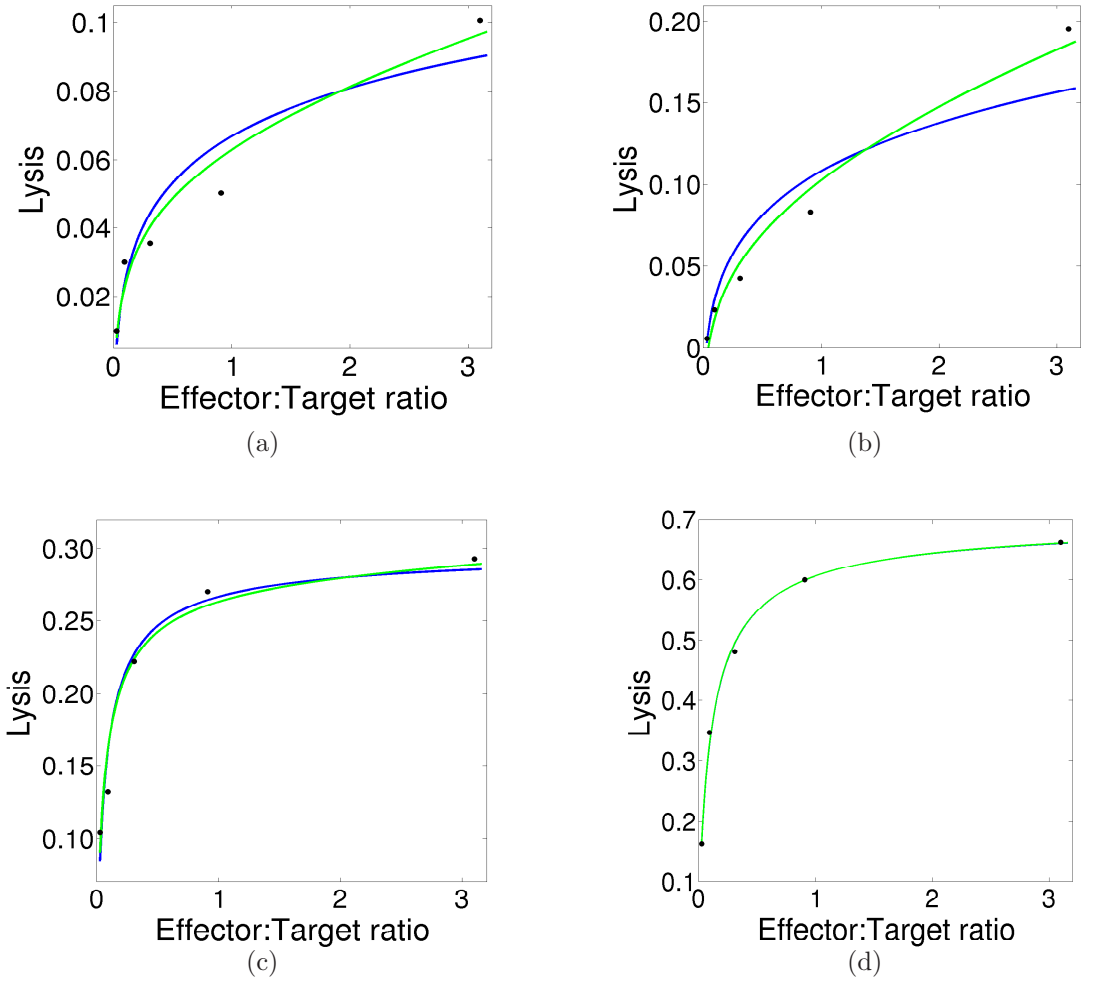


**Figure 3.2. Least-squares fitting of the model**. The data and the predicted curves from the models for the lysis of tumor cells by the effector cells. The green curve represents the general model, while the blue corresponds to its simplified version. (a) The experiment where the effector cells are primary challenged with ligand-negative-transduced cells and then rechallenged again with control-transduced cells ($nn$). (b) The case for which the effector cells are primary challenged with ligand-negative-transduced cells and then rechallenged with ligand-transduced cells ($nl$). (c) In this case the effector cells are primary challenged with ligand-transduced cells and then rechallenged with control-transduced cells ($ln$). (d) The experiment where the effector cells are primary challenged with ligand-transduced cells and then rechallenged again with ligand-transduced cells ($ll$).

Therefore, we assume that the tumor cells compete in a more aggressive manner and set $a_{12} < a_{21}$. The effects of changing these parameters is reported in Sec. 3.4, and rough estimates are provided in Sec. 3.6.

According to the experiments taken from Ref. [1], the model validation should be carried out in two separate steps, one for each type of effector cells. For instance, the first could involve the validation of the results concerning NK cells to obtain

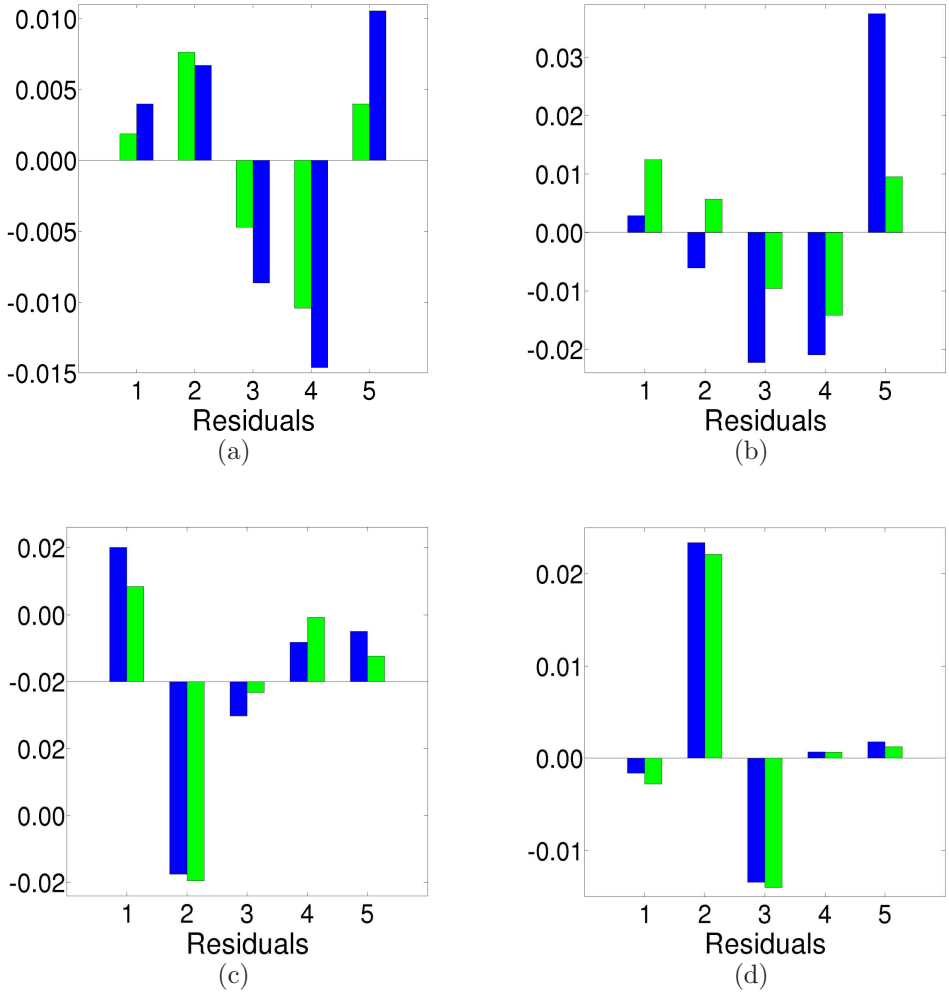


**Figure 3.3. The residuals of the fitting**. The differences between the experimental data and the model estimated values (residuals) obtained from the predicted curves for the lysis of tumor cells by effector cells. The green bars correspond to the the general model, while the blue bars belong to its simplified version. They are more or less randomly distributed. (a) The $(nn)$ case represented in Fig. 3.2(a). (b) The $(nl)$ case represented in Fig. 3.2(b). (c) The $(ln)$ case represented in Fig. 3.2(c). (d) The $(ll)$ case represented in Fig. 3.2(d).

the value of the parameter $a_{13}$ for the ligand and ligand-negative transduced cells. Then, after setting $a_{13}$ to zero, the experimental lysis of $CD8^+$ T cells should be fitted for the different cases. Finally, both contributions would be added to the model. However, another possibility is to fit only CTLs results and let the parameter $a_{13}$ take diverse values. This procedure allows more accurate fittings and has the advantage of suggesting a generalization of the PRW law, as explained at the end of the present section. To avoid the risks of overfitting because of using too many parameters, we have to proceed carefully. Since the model is derived from an original

validated model, we take the values of $a_{13}$ used in such work and modify them the least as possible to obtain curves that resemble the ones shown there. The same procedure is followed for the steepness $s$ of the saturation term in the PRW law. Then, the curves are fitted using the parameters $d$ and $\lambda$. Trajectories are runned up to a maximum time of four hours $t_{max} = 0.167$ days, at which the lysis of tumor cells $1 - T/T_0$ is measured in the experiments. Initial conditions are chosen to guarantee that the experimental Effector:Target ratios $E_0/T_0$ belong to the computed interval. The lysis of the tumor cells is obtained at $t_{max}$ for the various initial conditions and optimization is achieved by the least-squares method using a grid of values for the two parameters. The fitted curves for the model and its simplified version are shown in Fig. 3.2, while the residuals are depicted in Fig. 3.3. The general model fits the data nicely, with randomly distributed residuals. As expected, the reduced version gives worse results, specially for the control-transduced cells. The first four points in Fig. 3.2(a) and Fig. 3.2(b) can be fitted with exactness, but not the last one. Hence, a combination of a nonsaturating law with the PRW law gives considerably better results for the cases in which the immune response is less effective. These results suggest extending the PRW law by considering a fractional cell kill $F(E,T)$ given by the sum of a power law function and a Hill function

$$F(E,T) = cE^{\nu} + d\frac{E^{\lambda}}{h(T) + E^{\lambda}}. \tag{3.7}$$

Two limits can be clearly distinguished in this law. On the one hand, we have the situation in which the immune response is more or less effective $c \approx 0$, as shown in Figs. 3.2(c) and 3.2(d). On the other hand, an ineffective immune response is given by $d \approx 0$, which corresponds to the NK cell lysis in Ref. [11]. Intermediate situations are better represented by Eq. (3.7), as shown in Figs. 3.2(a) and 3.2(b). An heuristic explanation as to why less effective cells do not show saturation in practice can be given as follows. Suppose that we have two identical tumors of size $T$ in presence of the same number of effector cells, but the first $E$ being very effective recognizing and lysing tumor cells, while the second $\tilde{E}$ being ineffective. The difference between these two cell populations can be represented by considering that in the second case only a small fraction $f$ of the effector cells are interacting with the tumor $\tilde{E} = fE$. Therefore, the PRW law becomes

$$D(\tilde{E},T) = d\frac{f^{\lambda}E^{\lambda}}{h(T) + f^{\lambda}E^{\lambda}} = d\frac{E^{\lambda}}{\tilde{h}(T) + E^{\lambda}}, \tag{3.8}$$

where $\tilde{h}(T) = h(T)/f^{\lambda}$. In the case $f \ll 1$, and as long as $E$ is not much higher than $T$, we get $\tilde{h}(T) \gg E^{\lambda}$, what yields the fractional cell kill $D(E,T) = E^{\lambda}/\tilde{h}(T)$. If the variation of $T$ is small or $h(T)$ varies slowly with $T$, then the approximation $cE^{\lambda}$ holds. For example, if we consider the parameter values of the $(ll)$ experiment in Tab. 3.1 and take $f = 10^{-4}$, then we get a value for $\tilde{h}(T)$ two or three orders of magnitude higher than $E^{\lambda}$, depending on the values of the Effector:Target ratio.

| Parameter | Units | Value | Description | Source |
|---|---|---|---|---|
| $r_1$ | $\text{day}^{-1}$ | $5.14 \times 10^{-1}$ | Tumor cells growth rate | (6) |
| $K_1$ | cell | $9.8 \times 10^{8}$ | Tumor carrying capacity | (6) |
| $a_{12}$ | $\text{cell}^{-1}\ \text{day}^{-1}$ | $1.1 \times 10^{-10}$ | Competition of host cells with tumor cells | |
| $a_{13}(nn)$ | $\text{cell}^{-1}\ \text{day}^{-1}$ | $5.2 \times 10^{-8}$ | Fractional tumor cell kill of the power law | (6) |
| $a_{13}(nl)$ | | $1.6 \times 10^{-7}$ | | (6) |
| $a_{13}(ln)$ | | $3.2 \times 10^{-8}$ | | (6) |
| $a_{13}(ll)$ | | $8.5 \times 10^{-9}$ | | (6) |
| $d(nn)$ | $\text{day}^{-1}$ | 2.20 | Saturation level of fractional tumor cell kill of the PRW law | |
| $d(nl)$ | | 3.47 | | |
| $d(ln)$ | | 2.60 | | |
| $d(ll)$ | | 7.86 | | |
| $s(nn)$ | None | 1.6 | Steepness coefficient of the PRW law | |
| $s(nl)$ | | 2.5 | | |
| $s(ln)$ | | $1.4 \times 10^{-1}$ | | |
| $s(ll)$ | | $4.0 \times 10^{-1}$ | | |
| $\lambda(nn)$ | None | $1.2 \times 10^{-1}$ | Exponent of the PRW law | |
| $\lambda(nl)$ | | $2.1 \times 10^{-1}$ | | |
| $\lambda(ln)$ | | $7.0 \times 10^{-1}$ | | |
| $\lambda(ll)$ | | $7.0 \times 10^{-1}$ | | |
| $r_2$ | $\text{day}^{-1}$ | $1.80 \times 10^{-1}$ | Host cells growth rate | (6,11) |
| $K_2$ | cell | $1.0 \times 10^{9}$ | Host cells carrying capacity | (6,11) |
| $a_{21}$ | $\text{cell}^{-1}\ \text{day}^{-1}$ | $4.8 \times 10^{-10}$ | Competition of tumor cells with host cells | |
| $\sigma$ | $\text{cells day}^{-1}$ | $7.5 \times 10^{4}$ | Constant source of effector cells | (10) |
| $d_3$ | $\text{day}^{-1}$ | $6.12 \times 10^{-2}$ | Inactivation rate of effector cells | (6) |
| $\tilde{g}(n)$ | $\text{day}^{-1}$ | $2.5 \times 10^{-2}$ | Maximum recruitment rate related to the power law | (6) |
| $\tilde{g}(l)$ | | $2.0 \times 10^{-1}$ | | (6) |
| $g(nn)$ | $\text{day}^{-1}$ | $3.75 \times 10^{-2}$ | Maximum recruitment rate related to the PRW law | (6) |
| $g(nl)$ | | $3.75 \times 10^{-2}$ | | (6) |
| $g(ln)$ | | $1.13 \times 10^{-1}$ | | (6) |
| $g(ll)$ | | $3.00 \times 10^{-1}$ | | (6) |
| $\tilde{h}$ | $\text{cell}^2$ | $2.02 \times 10^{7}$ | Steepness coefficient for recruitment related to the power law | (10) |
| $h$ | $\text{cell}^2$ | $2.02 \times 10^{7}$ | Steepness coefficient for the recruitment related to the PRW law | (10) |
| $a_{31}$ | $\text{cell}^{-1}\ \text{day}^{-1}$ | $2.8 \times 10^{-9}$ | Immune-tumor competition | (10) |

**Table 3.1. The non-simplified model parameters**. The values of the parameters used to compute the curves representing the lysis of cancer cells by the effector cells, for the general model given by Eq. (3.1). The parameters of the PRW law, $\lambda$ and $d$, are obtained by a least-squares fitting of the solutions of the system of differential equations to the experimental data. The parenthesis represent four different cases: a primary challenge with control-transduced cells followed by a secondary one with ligand ($nl$) or control ($nn$) cells, and a primary interaction with ligand-transduced cells followed again by ligand ($ll$) or ligand-negative ($ln$) rechallenges.

## 3.4 Parameter and phase space analysis

Even though the simplified model fits better the experiments where cells are primary challenged with ligand-transduced cells, to study the dynamics we concentrate on the control-transduced choice of parameters. The reason is that the cell lines used in the experiments do not normally express ligands of the NKG2D receptor [1]. We begin by nondimensionalizing Eq. (3.5), redefining the cell populations and the time

$$\tilde{T} = \frac{T}{K_1}, \tilde{H} = \frac{H}{K_2}, \tilde{E} = \frac{r_1 E}{\sigma}, \tilde{t} = t r_1. \tag{3.9}$$

| Parameter | Units | Value | Description | Source |
|---|---|---|---|---|
| $r_1$ | $\text{day}^{-1}$ | $5.14 \times 10^{-1}$ | Tumor cells growth rate | (6) |
| $K_1$ | cell | $9.8 \times 10^{8}$ | Tumor carrying capacity | (6) |
| $a_{12}$ | cell $^{-1}$ day $^{-1}$ | $1.1 \times 10^{-10}$ | Competition of host cells with tumor cells | |
| $d(nn)$ | $\text{day}^{-1}$ | 2.6 | Saturation level of fractional tumor cell kill of the PRW law | |
| $d(nl)$ | | 7.1 | | |
| $d(ln)$ | | 2.7 | | |
| $d(ll)$ | | 7.9 | | |
| $s(nn)$ | None | 1.8 | Steepness coefficient of the PRW law | |
| $s(nl)$ | | 5.0 | | |
| $s(ln)$ | | $1.4 \times 10^{-1}$ | | |
| $s(ll)$ | | $4.0 \times 10^{-1}$ | | |
| $\lambda(nn)$ | None | $2.2 \times 10^{-1}$ | Exponent of the PRW law | |
| $\lambda(nl)$ | | $2.5 \times 10^{-1}$ | | |
| $\lambda(ln)$ | | $7.3 \times 10^{-1}$ | | |
| $\lambda(ll)$ | | $7.0 \times 10^{-1}$ | | |
| $r_2$ | $\text{day}^{-1}$ | $1.80 \times 10^{-1}$ | Host cells growth rate | (6,11) |
| $K_2$ | cell | $1.0 \times 10^{9}$ | Host cells carrying capacity | (6,11) |
| $a_{21}$ | cell $^{-1}$ day $^{-1}$ | $4.8 \times 10^{-10}$ | Competition of tumor cells with host cells | |
| $\sigma$ | cells $\text{day}^{-1}$ | $7.5 \times 10^{4}$ | Constant source of effector cells | (10) |
| $d_3$ | $\text{day}^{-1}$ | $6.12 \times 10^{-2}$ | Death of effector cells | (6) |
| $g(nn)$ | $\text{day}^{-1}$ | $3.75 \times 10^{-2}$ | Maximum recruitment rate related to the PRW law | (6) |
| $g(nl)$ | | $3.75 \times 10^{-2}$ | | (6) |
| $g(ln)$ | | $1.13 \times 10^{-1}$ | | (6) |
| $g(ll)$ | | $3.00 \times 10^{-1}$ | | (6) |
| $h$ | $\text{cell}^2$ | $2.02 \times 10^{7}$ | Steepness coefficient for the recruitment related to the PRW law | (10) |
| $a_{31}$ | cell $^{-1}$ day $^{-1}$ | $2.8 \times 10^{-9}$ | Immune-tumor competition | (10) |

**Table 3.2. The simplified model parameters**. The values of the parameters used to compute the curves representing the lysis of cancer cells by the effector cells, for the simplified model given by Eq. (3.5). The parameters of the PRW law, $\lambda$ and $d$, are obtained by a least-squares fitting of the solutions of the system of differential equations to the experimental data. The parenthesis again represents four different cases: a primary challenge with control-transduced cells followed by a secondary one with ligand ($nl$) or control ($nn$) cells, and a primary interaction with ligand-transduced cells followed again by ligand ($ll$) or ligand-negative ($ln$) rechallenges.

The new parameters are related to the previous ones in the following way

$$\begin{aligned}
&\tilde{a}_{12} = \frac{a_{12}K_2}{r_1} \quad \tilde{d} = \frac{d}{r_1} \quad \tilde{s} = s\left(\frac{K_1 r_1}{\sigma}\right)^{\lambda} \\
&\tilde{r}_2 = \frac{r_2}{r_1} \quad \tilde{a}_{21} = \frac{a_{21}K_1}{r_1} \\
&\tilde{d}_3 = \frac{d_3}{r_1} \quad \tilde{a}_{31} = \frac{a_{31}K_1}{r_1} \quad \tilde{g} = \frac{g}{r_1} \quad \tilde{h} = \frac{h}{(K_1 r_1)^2}.
\end{aligned} \tag{3.10}$$

Dropping the tildes, our nondimensionalized system becomes

$$\begin{aligned}\dot{x} &= x(1-x) - a_{12}yx - D(x,z)x \\ \dot{y} &= r_2 y(1-y) - a_{21}xy \\ \dot{z} &= 1 - d_3 z + g\frac{D^2(x,z)x^2}{h + D^2(x,z)x^2}z - a_{31}xz.\end{aligned} \tag{3.11}$$

The rescaled parameters are $a_{12} = 0.195$, $d = 5.0$, $\lambda = 0.21$, $s = 11.5$, $r_2 = 0.35$, $a_{21} = 0.954$, $d_3 = 0.112$, $g = 0.29$, $h = 7.95 \times 10^{-11}$ and $a_{31} = 5.25$. Unless specified, these parameters are used all along our study.

We now describe all the nullclines and equilibria for the current set of parameters. The fixed points of the system are given by $\dot{x} = \dot{y} = \dot{z} = 0$, which yields the system of equations

$$\begin{aligned}0 &= x\left(1 - x - a_{12}y - D(x,z)\right) \\ 0 &= y\left(r_2 - r_2 y - a_{21}x\right) \\ 0 &= 1 - d_3 z + g\frac{D^2(x,z)x^2}{h + D^2(x,z)x^2}z - a_{31}xz.\end{aligned} \tag{3.12}$$

Nullclines can be read directly from Eq. (3.12). There is a total of five nullclines: the $x-z$ and $y-z$ planes, the surface $S_1$ represented by the implicit equation $1 - x - a_{12}y - D(x,z) = 0$, the plane $\Pi$ given by $r_2 - r_2 y - a_{21}x = 0$, and the surface $S_2$, which implicit equation is given by the last of the three equations shown above. If we restrict our attention to the biologically meaningful region, which is the positive octant $\mathbb{R}^+ \times \mathbb{R}^+ \times \mathbb{R}^+$, the intersections of the different nullclines yield five different fixed points $x_i^*$, as shown in Fig. 3.4. We give the numerical values of the fixed points and also analyze their stability by examining the eigenvalues of the Jacobian at each of them.

The first fixed point is $x_1^* = (0, 0, d_3^{-1})$, in particular $(0, 0, 8.93)$, a saddle with two positive eigenvalues corresponding to the $x$-axis and the $y$-axis, and a negative eigenvalue along the $z$-axis. The point $x_2^* = (0, 1, 8.93)$ represents the healthy state, for which there are only healthy and immune cells. Therefore, we represent it in green color. This fixed point is stable, being one of the attractors of the dynamical system. The other stable fixed point is $x_3^* = (0.65, 0, 0.31)$, representing a stable solution for which there are only tumor and immune cells. As in previous works [14], we associate this fixed point to malignant growth, so we have colored it in red. The fixed point $x_4^* = (0.06, 0, 6.55)$ is a saddle fixed point with two unstable and one stable directions, separating the stable tumor attractor and the state $x_1^*$, which is attractive in such plane, and for which there are only immune cells. A stable and an unstable direction are in the plane $y = 0$, while the remaining unstable direction is given by the eigenvector $(0.01, 0.08, 1)$. The last fixed point is $x_5^* = (0.1, 0.74, 3.02)$, corresponding to the saddle fixed point, which two dimensional stable manifold separates the basins of attraction of the healthy and the tumor stable states. Hence,

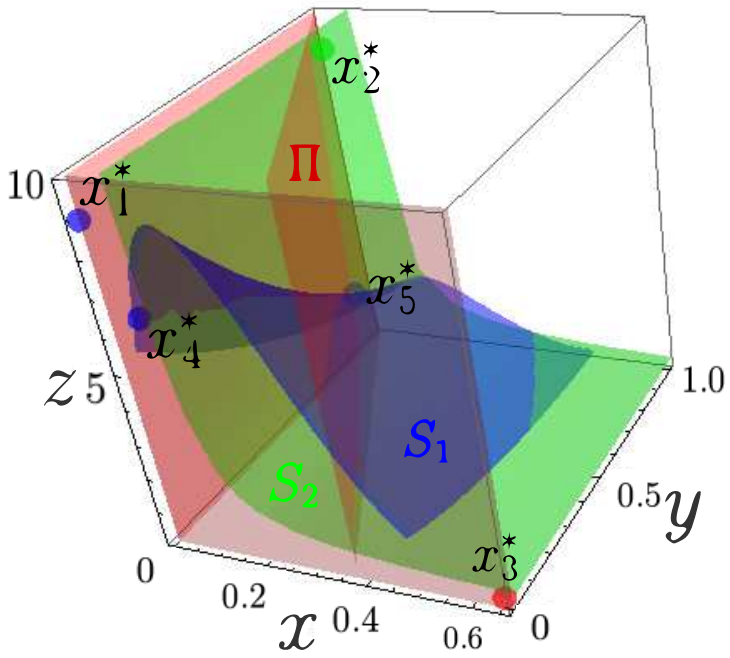


**Figure 3.4. The phase space**. The positive octant of the phase space with the nullclines and the fixed points. The surfaces represent the different nullclines, with the fixed points placed at some of their intersections. Every fixed point is the intersection of three surfaces. The surface $S_2$ has not been ploted completely for clarity, but it also intersects the $y-z$ plane. The green point is the healthy state, while the red point is the tumor stable fixed point. The other three fixed points are saddles.

the system is bistable. The evolution of the three cell populations for an initial condition leading to the malignant tumor state is shown in Fig. 3.5(d).

We begin the parameter analysis studying the effects of varying $d$, that affects the intensity with which the immune system destroys cancer cells. In Figs. 3.5(a) and 3.5(b) we depict the change in the basins size due to increasing such parameter to a value of $d = 6.5$, while in Fig. 3.6(a) a bifurcation diagram is computed, showing the evolution of the fixed points as such parameter is varied. Starting from high values of $d$, for which there is only a healthy stable state and the fixed point $x_1^*$, the parameter reaches a critical value of $d_c = 7.4185$ and a saddle-node bifurcation occurs. Another similar bifurcation appears for $d_c = 7.4095$. In total, four fixed points are born: three unstable and one stable. Only two of them are in the positive octant, the tumor fixed point $x_3^*$ and $x_4^*$, both unstable. As we keep on decreasing the immune strength, for a value of $d_c = 7.2650$, the stable fixed point enters the positive octant and a transcritical bifurcation occurs, through which the malignant state switches its stability with the stable fixed point. These results are in agreement with Ref. [1], where cells that express ligands reject tumors, while control cells do not. The existence of a critical value $d_c$ beyond which there is not a malignant tumor attractor constitutes an important prediction of the model, and might be used to estimate

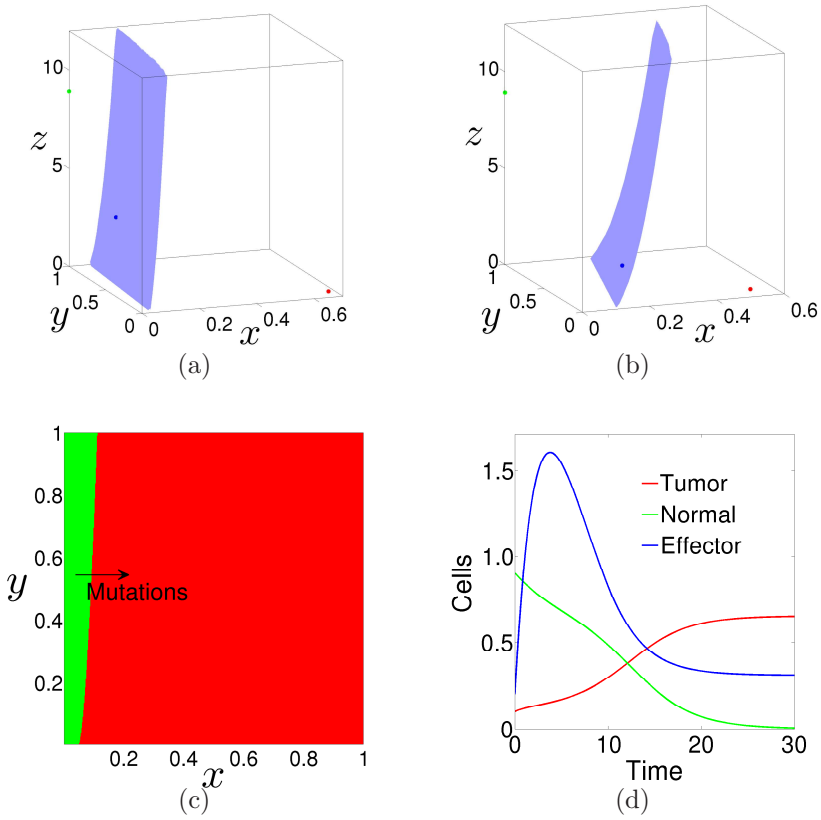


**Figure 3.5. The basins of attraction**. (a) The stable manifold of the fixed point $x_5^*$ (blue) separating the basins of attraction of the healthy $x_2^*$ (green) and the tumor $x_3^*$ (red) stable fixed points for $d = 5.0$. (b) Same figure but for $d = 6.5$. As the immune system response is stronger, the healthy basin enlarges and the tumor coordinate of the malignant attractor becomes smaller. (c) A section of the basins of attraction for $z = 3.5$. Oncogenic mutations can be understood as a crossing from the green basin to the red one. (d) Time series with the evolution of the three cell populations (nondimensional variables). As the tumor starts growing and replacing the normal tissue, the immune system orchestrates his response, activating the effector cells to counteract the proliferation of tumor cells. However, the effort is insufficient.

the minimum level of ligands required to ensure tumor regression through ligands expression. Also the parameter $s$ is important in the model. Its behavior is opposed to the previous. As it is decreased, for a value of $s_c = 7.55$, a transcritical bifurcation occurs, turning unstable the malignant attractor. It again disappears through a saddle-node bifurcation for the critical value $s_c = 7.35$. However, the parameter $\lambda$ does not change the stability of our dynamical system after considerable variations (even twenty times), although its increase leads to more negative eigenvalues of the tumor attractor, making this fixed point more attractive.

Looking at the basin of attraction in Fig. 3.5(c), it might result surprising that a healthy state is always stably preserved. The reason is that cancer is the result

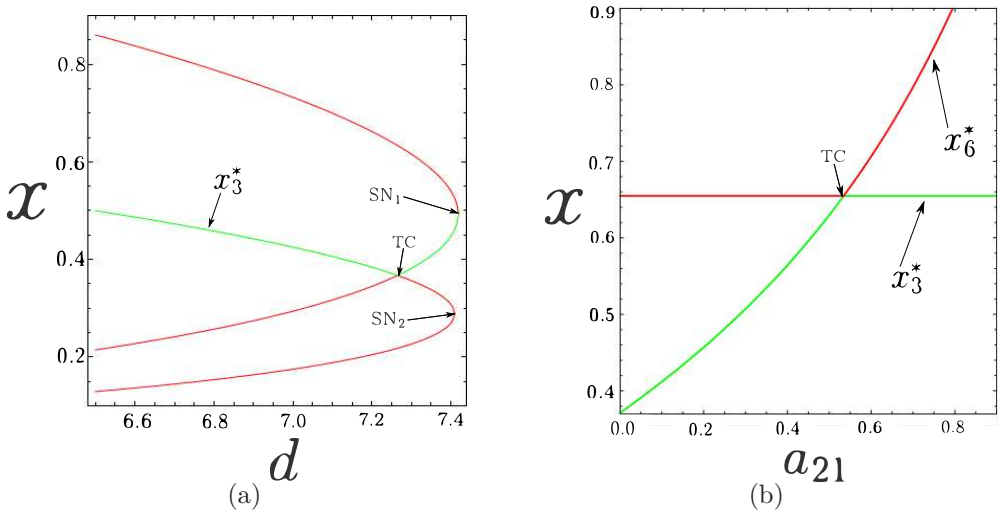


**Figure 3.6. Bifurcation diagrams**. (a) The bifurcation diagram for the tumor coordinate as we vary the parameter $d$, associated to the maximum fraction cell kill of the effector cells. As such parameter is decreased from values $d > 7.4$, for which there is only a healthy state, two saddle-node ($SN_1$ and $SN_2$) bifurcations occur, giving birth to four fixed points, among which figures the tumor one, still unstable. Later on, a transcritical bifurcation (TC) turns the tumor stable fixed point $x_3^*$ stable, by switching stability with another fixed point. The stable attractor is shown in green, while the unstable saddles are painted in red. (b) The bifurcation diagram for the tumor coordinate as we vary the parameter $a_{21}$. For high values of $a_{21}$, the fixed point $x_6^*$, corresponding to an equilibria for which all the cell populations coexist, is unstable and placed out of the positive octant. As we decrease $a_{21}$, it enters the positive octant and switches stability with the malignant tumor fixed point $x_3^*$ through a transcritical bifurcation (TC). The tumor shrinks as we keep on decreasing the value of $a_{21}$.

of accumulated mutations and no mutations between healthy and cancerous phenotypes have been considered in the present model. This is in accordance, but also in contrast, with a simple logistic growth model, for which the zero value of the tumor cell population is a fixed point, but it is unstable, so that any small perturbation pulls the dynamics away from it. The homologous to such zero cell population fixed point in the present model is $x_1^*$, which is always unstable. However, as we argue in detail in the next paragraph, a healthy stable state will be preserved unless the action of the immune system and the competition of the healthy cells with the cancer cells are negligible, what is in consonance with the fact that apoptosis is a major barrier to tumor growth that must be circumvented [3]. The effect of mutations can be associated to a passage from one basin to the other. The smaller the basin of attraction of the healthy point is, the easier for a tumor to be born. Mutations can be modeled in several manners, for example, considering multiplicative noises on some parameters of the model, or introducing balanced decay and growth terms in the host and the tumor cell differential equations respectively [24, 25], like in the quasispecies formalism [26].

Concerning the tumor-host competition terms $a_{12}$ and $a_{21}$, the following behavior is observed. In an ordinary Lotka-Volterra competition model with two populations ($N_1$,$N_2$) (no immune response), the stability of the fixed point $(0, K_2)$ depends upon the competition term $a_{12}$ affecting the other population, and vice versa. In such a model, if $a_{12} > r_1/K_2$, then the fixed point $(0, K_2)$ is stable, while if it is smaller, the point becomes unstable. The immune system introduces an innovation in this scenario as long as $d$ is not very small, since no matter how small $a_{12}$ is made, the effector cells are killing tumor cells, what means that there is always a healthy state. On the other hand, if we decrease the parameter $a_{21}$ more than the critical value 0.535, a transcritical bifurcation occurs for which the tumor fixed point $x_3^*$ becomes unstable and a equilibria $x_6^*$ representing the coexistence of the three species arises in the positive octant, becoming stable. As can be seen in Fig. 3.6(b), for $a_{21} = 0.5$ such equilibria is $x_6^* = (0.63, 0.10, 0.32)$. A big tumor coexists with the healthy tissue. As we keep on decreasing the value of $a_{21}$, the tumor shrinks and the healthy tissue swells, what corresponds to a more benignant state. Thus, the maximum size a tumor can reach according to our model, depends noticeably on its capability to reduce the host healthy cells living with it, which in part is related to aerobic glycolysis.

## 3.5 Fitting the chemotherapy treatment to experiments

Therapies are the main practical reason for studying tumor growth. Two important restrictions in the application of chemotherapy are the toxicity of the drugs and the resistance of tumor cells to such cytotoxic agents. In order to properly model and understand these two processes in our context, a realistic modelling of chemotherapy must be attained in the first place. Depending on their particular mechanism of action (alkylation, topoisomerase inhibition, antimetabolism, etc.), cytotoxic chemotherapeutic agents can be classified in two main groups: cell cycle specific (CS) and nonspecific (CNS). Both types of drugs appear commonly combined in many therapies. For example, locally advanced breast cancer uses cyclophosphamide, doxorubicin and docetaxel. Therefore, we shall utilize a model capable of reproducing CS and CNS drugs, preferably not requiring explicit modelling through several cell populations in different stages of the cell cycle, as in other works [27]. A mechanistic model that has been tested with *in vitro* experiments for both types of drugs is the exponential kill model. This model has been already used [11, 25, 28], and proposes a fractional cell kill law of the form

$$k(C) = b(1 - e^{-\rho C}), \tag{3.13}$$

where $C$ is the drug concentration at the tumor site, and for CS drugs $b$ depends on the fraction of cells in a vulnerable part of the cell cycle at a certain time instant, and the cells rate of entry and abandon of such phase of the cycle. In the case of CNS drugs such parameter is equal to one. The scaling parameter $\rho$ is related to the levels of drug resistance. This factional cell kill law means that for a given dose of drug, after a certain period of time the tumor is reduced to a particular fraction of its size,

no matter how big or small it was initially [2]. Survival fractions can be analytically obtained assuming exponential growth and constant concentrations of the drug [17], but neither of these two situations generally hold for *in vivo* experiments. We have modified this law so that it depends on the time-delayed concentration. This is the simplest modification we have been able to elucidate that permits to fit the data. The significance of this method will be discussed ahead. In this first approach, to fit the experiments we neglect the cytotoxic effects of the drug on the healthy tissue. The resulting nonautonomous dynamical system reads

$$\begin{aligned} \dot{x} &= x(1-x) - a_{12}yx - D(x,z)x - b(1-e^{-\rho u(t-\tau)})x \\ \dot{y} &= r_2 y(1-y) - a_{21}xy \\ \dot{z} &= 1 - d_3 z + g\frac{D^2(x,z)x^2}{h + D^2(x,z)x^2}z - a_{31}xz, \end{aligned} \tag{3.14}$$

with $u(t) = u_0 e^{-k_e t}$ for $t \geq 0$ and zero if $t < 0$. Hence, a single dose of drug is administered at $t = 0$, but it starts to cause its effect at time $\tau$. The relations between the chemotherapy parameters of the nondimensional model and the originals shown in Eq. (3.6) are

$$\tilde{b} = \frac{b}{r_1} \quad \tilde{\tau} = \tau r_1 \quad \tilde{k_e} = \frac{k_e}{r_1}, \tag{3.15}$$

where tildes have been excluded again in Eq. (3.14).

The data used to fix the parameters of the chemotherapy treatment are borrowed from Ref. [2]. In this study a plasmacytome is inoculated into BALB/c mice and allowed to grow up to a certain size. Then the animals receive cyclophosphamide, a cell cycle nonspecific alkylating agent, and tumor regression is observed days later. To validate the modelled chemotherapy treatment, we use the results from two experiments. In the first one, five mice are given subcutaneous injections of $1 \times 10^3$ viable MOPC 104E cells, and the tumor is allowed to grow up to 0.09 g (1 g equals $1 \times 10^9$ tumor cells). Cyclophosphamide is given at a single dose after palpable nodules are present. In the second experiment three mice receive intravenous injections of $1 \times 10^6$ cells of the same cell line, and the tumor is allowed to proliferate up to maximum size of 2.90 g. They use three mice as control with mescaline treatment and three more with a single dose of cyclophosphamide. They are able to estimate the size of the tumor from the immunoglobuline M levels using a linear model $\dot{M} = T - kM$, being $M$ the IgM levels and $T$ the tumor size, which is assumed to grow exponentially $T(t) = T_0 e^{\alpha t}$, with $\alpha$ a function of the doubling time of tumor cells. The parameter $k$ represents the removal rate of IgM from circulation. The dose of drug administered in the experiments is 200 mg/kg, and the mice weight around 20 g, so we take $u_0 = 4$ mg. We consider that the drug elimination rate is $k_e = 2.5$ day$^{-1}$, what approximately corresponds to a half-life of 6.5 h. In the first experiment in Ref. [2], the averages of the tumor weight and the mass percentage of the tumor respect to the total mass are reported. In the second experiment the same magnitudes are addressed for each of the three mice. We limit ourselves to the first

mouse results, which tumor grows bigger. Because no data concerning the tumor-immune interaction is provided in these two experiments, we can not properly fit the model given by Eq. (3.5). For this reason, we use the nondimensional model with the parameter values given in Sec. 3.4, and the mass percentage of the tumor measured in the experiments, and set the initial conditions $(x_0, y_0, z_0)$ proceeding as follows. In the first experiment the therapy begins at day 22, when the tumor size reaches the 4 % of the total body weight. Therefore, we consider that the $x$ coordinate of the fixed point associated to the malignant tumor state $x_3^*$, represents a size of 5 % of the total body, *i. e.*, $x_0 = x_3^* \cdot 0.4/0.5$. An identical prescription is followed with the second experiment, for which the tumor reaches a size of 12 % of the total body weight. Now we make $x_0 = x_3^* \cdot 12/15$. Since in the second experiment large implants of intravenously disseminated tumors are studied, while the first experiment deals with small localized subcutaneous tumors, we consider different initial conditions concerning the effector cells for each experiment, assuming that in the second one the immune response is stronger. In particular, the values we use are respectively $z_0 = 7.0$ and $z_0 = 1.0$. The initial condition for the healthy tissue is taken $y_0 = 0.5$ in both experiments. These initial conditions lead to the tumor stable fixed point in the absence of treatment, and other choices might be used as well. The parameter values $\tau$ and $\rho$ arranged to fit the fractional tumor cell kill by cyclophosphamide are obtained following the same method as in Sec. 3.3. We show them in Table 3.3 for both cases. The time-delay is longer in the first experiment, probably because small localized tumors are harder to reach than large implants. The levels of drug resistance are certainly low (high values of $\rho$), and similar for the two experiments.

In Fig. 3.7 and Fig. 3.8, we can see that the model validates well the experimental results. During the first three/four days the drug has little effect on the tumor, and from this day on a severe decrease is observed. Along these first days, we recognize that the curves are slightly concave and then rise up, before cyclophosphamide starts to be effective. This is a consequence of the immune system, that is destroying proliferating tumor cells. After this first period of time the drug starts to cause its effect and dominates the dynamics during the next five/six days. From this day on, the immune system takes care of the remaining part of the tumor and the healthy tissue regenerates. The action of chemotherapy can be thought as a passage from the red basin to the green one in Fig. 3.5(c). We believe that the lag in the action of the drug is due to complex pharmacokinetics. In general, it takes a time for the drugs to reach the tumor site and be absorbed, as well as to inflict damage to the proliferating cells through its cytotoxic mechanism. In particular, it might happen that different drugs have different time-delays, what might play a role in modelling combination therapy when studying tumor resistance to chemotherapeutic agents, and also their toxicity.

The dynamical response to chemotherapy mainly consists in a change of the basin size. The higher the dose, the bigger the healthy basin. The manifold separating the basins of attraction moves to the right and rotates clockwise. The results are similar to those shown in Fig. 3.5(a) and Fig. 3.5(b), and also in previous works [12], so we do not show them. It is important to recall that the nonautonomous system given by

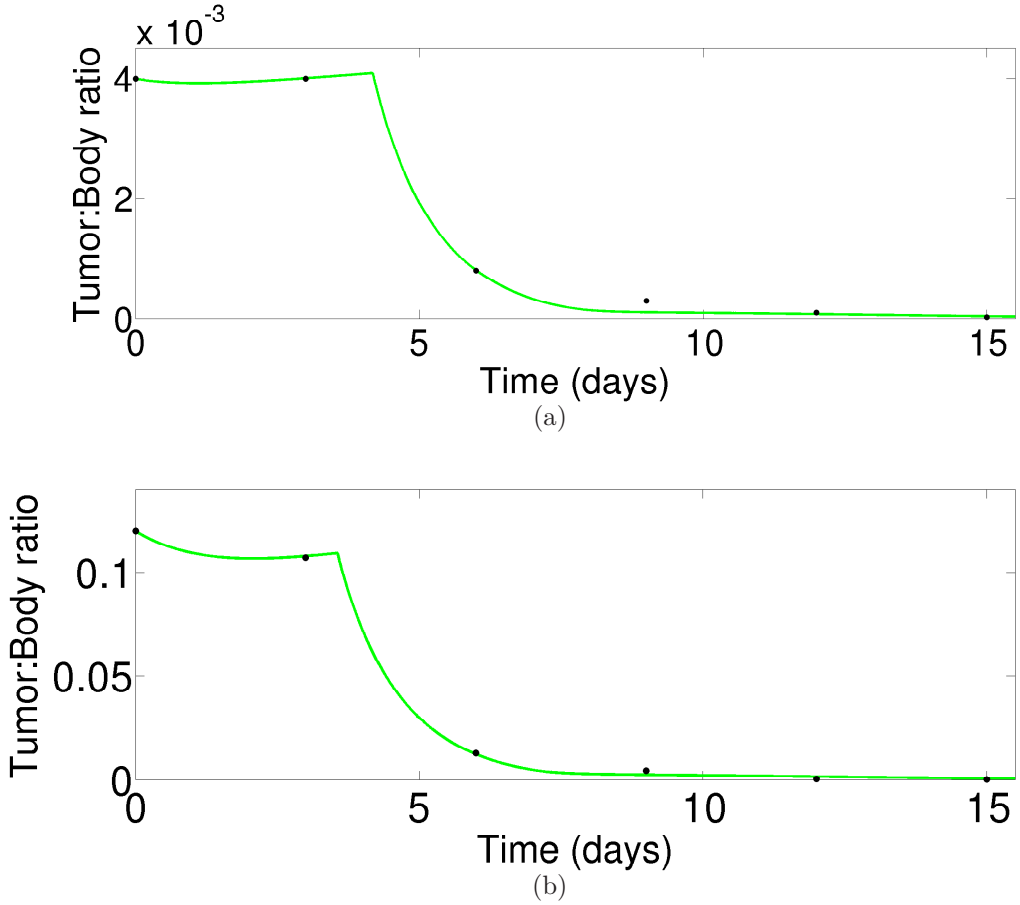


**Figure 3.7. Least square fitting of the chemotherapeutic protocol**. (a) Data in the first experiment and the model predicted curve for the tumor decay after a single dose injection of cyclophosphamide is delivered into the mice. The $y$-axis represents the fraction of tumor cells in the body. During the first days, the drug has little effect on the host, and then the tumor cells are strongly reduced. (b) Data for the second experiment and the model predicted curve for the tumor decay after a single dose injection of cyclophosphamide is delivered into the mice.

Eq. (3.14) tends to the original system asymptotically. This means that although the basins structure and size change during the treatment, once the drugs are eliminated, the original dynamical system is restored, and so they are its stability properties. Consequently, a tumor relapse requiring to resume the chemotherapeutic treatment would be expected. On the other hand, as shown in Sec. 3.4, therapies implying a change in the parameter values of the dynamical system, as it is the purpose of immunotherapeutic vaccines [1, 28], are obviously more advantageous, because they can change the stability properties of the dynamical system permanently, preventing the disease from recurring.

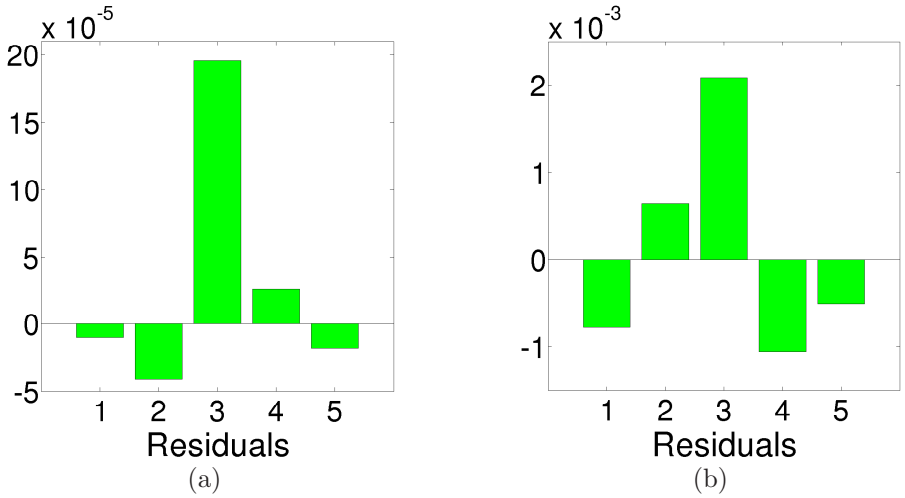


(a) (b)

**Figure 3.8. The residuals of the fitting**. (a) Residuals of the fitted data in the first experiment, corresponding to Fig. 3.7(a). (b) Residuals of the fitted data in the second experiment, corresponding to Fig. 3.7(b).

## 3.6 Experimental correlations with the model

This section is devoted to expose some correlations between the model and the experimental data appearing in Ref. [2], with the aim of obtaining rough estimations of the parameters $a_{12}$ and $a_{21}$. In particular, the experimental results correspond to the same experiment as those shown in Fig. 3.7(b), but now we focus on the growth of the tumor before therapy is applied. In that experiment, the actual body weight, which is defined as the difference between the total weight of each mouse and the weight of their respective tumors, is computed. For the cyclophosphamide treated group, the data are registered at days 10, 18 and 21, the last corresponding to the beginning of the treatment (see Fig. 3.9). It is hard to know if these variations are due to differences in the tumor cells and the healthy cells interacting with them, consequence of other cells in the body, changes in the metabolism or, more simply, nourishment. Nevertheless, we believe that it is good to show that our model is compatible with such results, mainly to assure ourselves that the parameter values of the competition terms are biologically reasonable. For these reasons and because no data concerning the tumor-immune interaction is available in these experiments, we do not fit the curves.

We relate the total body weight to the sum of the three cell populations, while the actual body weight is considered to be the sum of the healthy and the immune cell populations. Since the last is considerably smaller than the former, the actual population of cells looks like the normal cells population. We also consider the approximation $d = 0$ (otherwise small tumor sizes lead to the healthy attractor), which is reasonable during the first days of tumor growth, since it takes the body some time to develop an immune response. The plots in Fig. 3.9 show similar behaviors of the experimental data and the theoretical predicted values by the model

| Experiment 1 | | | |
|---|---|---|---|
| Parameter | Units | Value | Description |
| $\rho$ | $mg^{-1}$ | $4.04 \times 10^3$ | Level of drug resistance |
| $\tau$ | day | 4.18 | Time-delay |
| Experiment 2 | | | |
| Parameter | Units | Value | Description |
| $\rho$ | $mg^{-1}$ | $4.03 \times 10^3$ | Level of drug resistance |
| $\tau$ | day | 3.56 | Time-delay |

**Table 3.3. The parameters of the chemotherapeutic protocol**. The values of the level of drug resistance and the time it takes the drug to start causing its cytotoxic effect. They are obtained through a least-squares fitting of the solutions of Eq. (3.14) to two different experimental situations were mice are treated with cyclophosphamide.

at days 18 and 21 for the three mice. In some cases the correspondence is not only qualitative, but also quantitative.

As we can see in Fig. 3.9, for the first mouse there is a decrease of the healthy cell population, what implies a decrease of the actual and total populations at day 18. Later on, the tumor increases and the total population rises, while the healthy host cells keep on being destroyed. Interestingly, in this case, a better correlation between the experimental data and the theoretical predicted curves at day 21 can be achieved if saturation of the competition term given by $a_{21}$ with the tumor load is considered. This saturation would be explained by the fact that competition for space occurs between nearby cells, and competition for nutrients occurs along the direction of the gradient of nutrient concentration. For the second mouse the tumor grows very slowly, so the cell populations remain almost constant. In the third case, since the mouse has smaller weight, we choose a smaller value of the healthy cell population as an initial condition. The population starts to increase, and so does the tumor. A maximum actual weight is observed at day 18, and then the healthy cell population starts to decrease due to the growth of the tumor. However, the total weight at day 21 is almost the same, because the tumor has grown considerably. The parameters we have had to change from the ones settled in Eq. (3.5) to reproduce the experiments are shown in Table 3.4. Note that for every mouse $a_{21} > a_{12}$ holds, as conjectured in Sec. 3.3.

## 3.7 Conclusions and Discussion

We have developed a model of tumor growth taking into account the heterogeneity of the tissue as a complex interaction between several types of cells. The model includes tumor-immune and tumor-host interactions, which are in conformity with experimental data. We have examined the dynamical properties of the model, showing its correlation with theoretical and empirical knowledge of tumor progression. Also chemotherapy has been studied and a way to overcome the problem of modelling complex drug dynamics has been proposed. We believe that the model might be useful when attempting to embark the study of tumor growth. Of course, ODE-based modelling and the present model itself are both far away from being definitive.

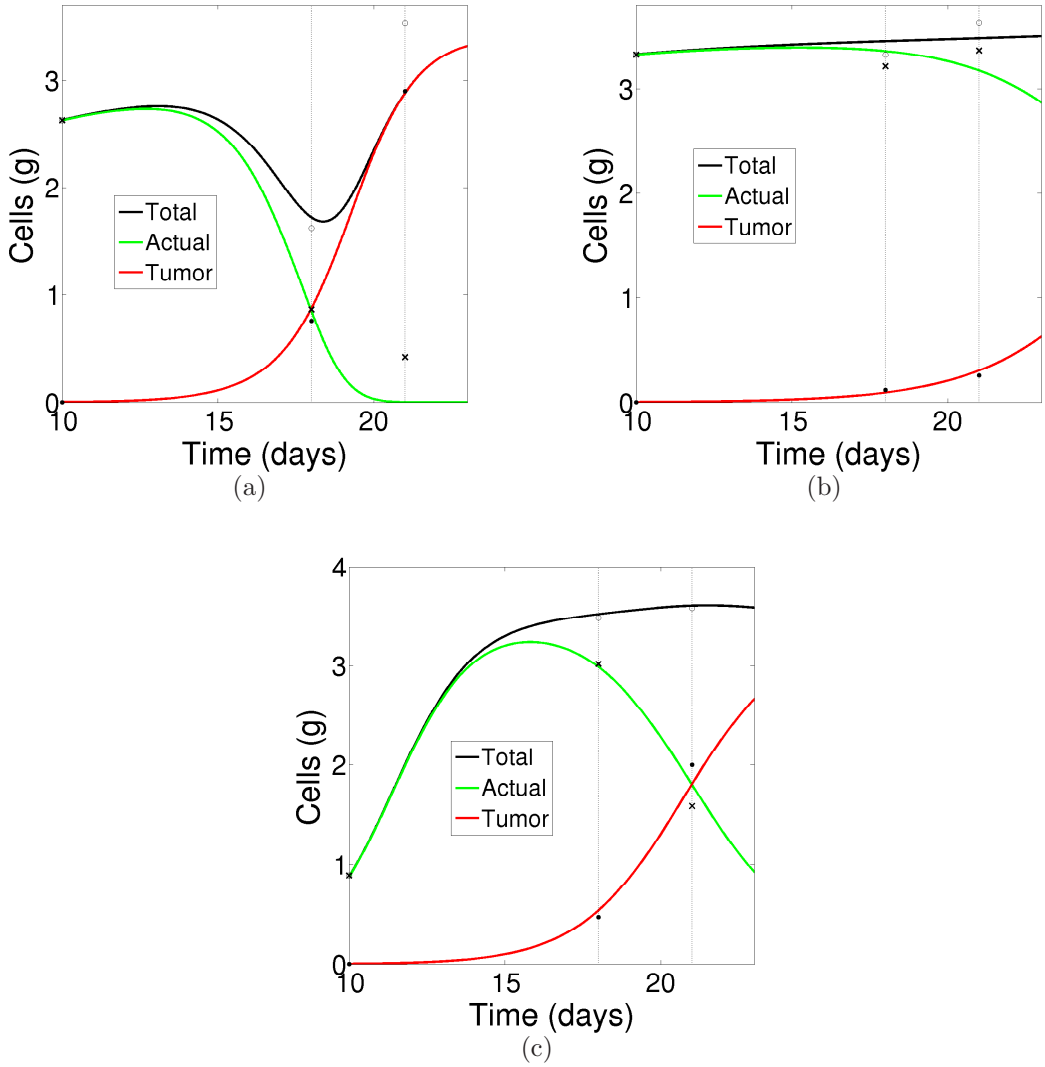


**Figure 3.9. Correlations between the model and experimental data**. The time series given by the model (solid curves) and the experimental data of the tumor (•), the actual (×) and the total (○) cell populations for the three mice in the second experiment in Ref. [2]. The first points are used to fix initial conditions. (a) For the first animal the actual and the total sizes first decrease because the healthy tissue is being destroyed. Then the growth of the tumor rises and the total and the tumor cell populations become equal. (b) In the second animal the tumor grows very slowly and the cell populations are almost constant. (c) In the third case the healthy cells start to grow together with the tumor, but as the tumor increases the normal cells reach a peak and begin to die.

Rather, they might be used as a foundation upon which to build up different and increasingly more sophisticated models, capable of reproducing the many aspects of the tremendously complex dynamics of cancer inception and evolution at its different, but inextricably related, scales. In the next chapter more sophisticated models

| Mouse 1 | | | |
|---|---|---|---|
| Parameter | Units | Value | Description |
| $K_1$ | cells | $3.4 \times 10^9$ | Carrying capacity of tumor cells |
| $K_2$ | cells | $3.5 \times 10^9$ | Carrying capacity of healthy cells |
| $r_1$ | $\text{day}^{-1}$ | 0.95 | Rate of growth of tumor cells |
| $r_2$ | $\text{day}^{-1}$ | 0.06 | Rate of growth of normal cells |
| $a_{12}$ | $\text{cells}^{-1}\text{day}^{-1}$ | $4.8 \times 10^{-11}$ | Competition of healthy cells with tumor cells |
| $a_{21}$ | $\text{cells}^{-1}\text{day}^{-1}$ | $6.0 \times 10^{-10}$ | Competition of tumor cells with healthy cells |
| Mouse 2 | | | |
| Parameter | Units | Value | Description |
| $K_1$ | cells | $3.4 \times 10^9$ | Carrying capacity of tumor cells |
| $K_2$ | cells | $3.5 \times 10^9$ | Carrying capacity of healthy cells |
| $r_1$ | $\text{day}^{-1}$ | 0.62 | Rate of growth of tumor cells |
| $r_2$ | $\text{day}^{-1}$ | 0.13 | Rate of growth of normal cells |
| $a_{12}$ | $\text{cells}^{-1}\text{day}^{-1}$ | $4.8 \times 10^{-11}$ | Competition of healthy cells with tumor cells |
| $a_{21}$ | $\text{cells}^{-1}\text{day}^{-1}$ | $1.3 \times 10^{-10}$ | Competition of tumor cells with healthy cells |
| Mouse 3 | | | |
| Parameter | Units | Value | Description |
| $K_1$ | cells | $3.4 \times 10^9$ | Carrying capacity of tumor cells |
| $K_2$ | cells | $3.5 \times 10^9$ | Carrying capacity of healthy cells |
| $r_1$ | $\text{day}^{-1}$ | 0.82 | Rate of growth of tumor cells |
| $r_2$ | $\text{day}^{-1}$ | 0.49 | Rate of growth of normal cells |
| $a_{12}$ | $\text{cells}^{-1}\text{day}^{-1}$ | $3.7 \times 10^{-11}$ | Competition of healthy cells with tumor cells |
| $a_{21}$ | $\text{cells}^{-1}\text{day}^{-1}$ | $2.3 \times 10^{-10}$ | Competition of tumor cells with healthy cells |

**Table 3.4. The simplified model parameters**. The values of the parameters in the simplified model that were required to change in order to describe the growth of the plasmacytome, the time evolution of the body weight and the time evolution of the actual body weight, for the three mice in the second experiment in Ref. [2].

are used to ascertain the validity of the hypotheses presented above.

# References

[1] A. Diefenbach, E.R. Jensen, A.M. Jamieson and D.G. Rauelt, "Rae1 and H60 ligands of the NKG2D receptor stimulate tumor immunity", *Nature* **413**, 165-171 (2001).

[2] R.N. Hiramoto and V.K. Ghanta, "Chemotherapy and rate of kill of tumor cells in a mouse plasmacytome", *Cancer Res.* **34**, 1738-1742 (1974).

[3] D. Hanahan and R.A. Weinberg, "Hallmarks of Cancer". *Cell* **100**, 57-70 (2000).

[4] J. Couzin-Frankel, "Cancer immunotherapy", *Science*, **342** 1432-1433 (2013).

[5] L. Gattinoni, D.J. Powell Jr., S.A. Rosenberg, and N.P. Restifo, "Adoptive immunotherapy for cancer: building on success", *Nat. Rev. Immunol.* **6**, 383-393 (2006).

[6] M. Kalos, B.L. Levine, D.L. Porter, S. Katz, S.A. Grupp, A. Bagg, and C.H. June, "T cells with chimeric antigen receptors have potent antitumor effects

and can establish memory in patients with advanced leukemia", *Sci. Transl. Med.* **3**, 95ra73 (2011).

[7] A. Ribas, L.H. Camacho, G. Lopez-Berestein, D. Pavlov, C.A. Bulanhagui, R. Millham, B.Comin-Anduix, J.M. Reuben, E. Seja, C.A. Parker, A. Sharma, J.A. Glaspy, J. Gomez-Navarro, "Antitumor activity in melanoma and anti-self responses in a phase I trial with the anti-cytotoxic T lymphocyte-associated antigen 4 monoclonal antibody CP-675,206", *J. Clin. Oncol.* **23**, 8968-8977 (2005).

[8] F. Pastorino, C. Brignole, D. Di Paolo, B. Nico, A. Pezzolo, D. Marimpietri, G. Pagnan, F. Piccardi, M. Cilli, R. Longhi, D. Ribatti, A. Corti, M.T. Allen, and M. Ponzoni, "Targeting liposomal chemotherapy via both tumor cell-specific and tumor vasculature-specific ligands potentiates therapeutic efficacy", *Cancer Res.* **66**, 10073-10082 (2006).

[9] O. Lavi, M.M. Gottesman, and D. Levy, "The dynamics of drug resistance: A mathematical perspective", *Drug Resistance Updates* **15**, 90-97 (2012).

[10] N. Bellomo, N.K. Li, and P.K. Maini, "On the foundations of cancer modelling: selected topics, speculations, and perspectives", *Math. Models Methods Appl. Sci.* **18**, 593-646 (2008).

[11] L.G. De Pillis, A.E. Radunskaya, and C.L. Wiseman, "A validated mathematical model of cell-mediated immune response to tumor growth", *Cancer Res.* **65**, 235-252 (2005).

[12] L.G. De Pillis and A. Radunskaya, "The dynamics of an optimally controlled tumor model: a case study", *Math. Comput. Modelling* **37**, 1221-1244 (2003).

[13] V.A. Kuznetsov, I.A. Makalkin, M.A. Taylor, and A.S. Perelson, "Nonlinear dynamics of immunogenic tumors: parameter estimation and global bifurcation analysis", *Bull. Math. Biol.* **56**, 295321 (1994).

[14] R.A. Gatenby and E.T. Gawlinsky, "A reaction-diffusion model of cancer invasion", *Cancer Res.* **56**, 5475-5753 (1996).

[15] D. Kirschner and J.C. Panetta, "Modelling immunotherapy of the tumor-immune interaction", *J. Math. Biol.* **37**, 235-252 (1988).

[16] S.T.P. Pinho, H.I. Freedman, and F. Nani, "A chemotherapy model for the treatment of cancer with metastasis". *Math. Comput. Modelling* **36**, 773-803 (2002)

[17] S.N. Gardner, "A mechanistic, predictive model of dose-response curves for cell cycle phase-specific and nonspecific drugs", *Cancer Res.* **60**, 1417-1425 (1996).

[18] M.E. Dudley, J.R. Wunderlich, P.F. Robbins, J.C. Yang, P. Hwu, D.J. Schwartzentruber, S.L. Topalian, R. Sherry, N.P. Restifo, A.M. Hubicki, M.R. Robinson, M. Raffeld, P. Duray, C.A. Seipp, L. Rogers-Freezer, K.E. Morton, S.A. Mavroukakis, D.E. White, and S. A. Rosenberg, "Cancer regression and autoimmunity in patients after clonal repopulation with antitumor lymphocytes", *Science* **298**, 850-854 (2002).

[19] D.G. Mallet and L.G. De Pillis, "A cellular automata model of tumor-immune system interactions", *J. Theor. Biol.* **239**, 334-350 (2006).

[20] A.F. Olumi, D.G. Gary, S.W. Hayward, P.R. Carrol, R.D. Tlsty, and G.R. Cunha, "Carcinoma-associated fibroblasts direct tumor progression of initiated human prostatic epithelium", *Cancer Res.* **59**, 5002-5011 (1999).

[21] S.C. Ferreira Jr., M.L. Martins, and M.J. Vilela, "Reaction-diffusion model for the growth of avascular tumor", *Phys. Rev. E* **67**, 051914 (2002).

[22] O. Warburg, "On the origin of cancer cells", *Science* **123** 309-314 (1956).

[23] M.G. Van der Heiden, L.C. Cantley, and C.B. Thompson, "Understanding the Warburg effect: the metabolic requirements of cell proliferation", *Science* **324**, 1029-1033 (2009).

[24] A.M. Ideta, G. Tanaka, T. Takeuchi, and K. Aihara, "A mathematical model of intermittent androgen suppression for prostate cancer", *J. Nonlinear Science* **18**, 593-614 (2008).

[25] S.M. Gardner, "Modeling multi-drug chemotherapy: tailoring treatment to individuals, *J. Theor. Biol.* **214**, 181-207 (2002).

[26] M.A. Nowak, "What is quasispecies?", *Trends Ecol. Evol.* **7**, 118-121 (1992).

[27] J.C. Panetta and J. Adam, "A mathematical model of cycle-specific chemotherapy", *Math. Comput. Modelling* **22**, 67-82 (1995).

[28] L.G. De Pillis, W. Gu, and A.E. Radunskaya, "Mixed immunotherapy and chemotherapy of tumors: modelling, applications and biological interpretations", *J. Theor. Biol.* **238**, 841-862 (2006).

# Chapter 4

# The fractional cell kill governing the lysis of solid tumors

*"To play life you must have a fairly large checkerboard and a plentiful supply of flat counters of two colors"*

-Martin Gardner. *Scientific American* (October 1970)

In this chapter we focus our attention on the *fractional cell kill* exposed in the previous one, and which governs the lysis of tumor cells by cytotoxic cells. We use *in silico* simulations to ascertain the validity of the hypotheses previously given. In order to achieve this goal, we redefine the nature of this mathematical expression. Our results indicate that this law emerges from *spatial and geometrical* restraints. In particular, simulations are provided in the limit of *immunodeficient* environments, showing the disappearance of the saturation of the lysis of tumor cells for high effector-to-target ratios as the immune system becomes more and more ineffective.

## 4.1 Introduction

The progress of tumor immunotherapy with T lymphocytes mainly relies on our capacity to uncover and understand the molecular and cellular bases of the T-cell-mediated antitumor response. However, due to the highly complex regulatory mechanisms that control both cell growth and the immune system, this task can be hardly achieved without the use of mathematical models. From a theoretical point of view, these models provide an analytical framework in which fundamental questions concerning cancer dynamics can be addressed in a rigorous fashion. The practical reason for their development is to make quantitative predictions that permit the refinement

of the existing therapies, or even the design of new ones.

Mathematical models of tumor growth and its interaction with the immune system [1] have demonstrated their potential to explain different properties of tumor-immune system interactions, as for example tumor dormancy and sneaking through. As pointed out in Chapter 2, it was precisely with the aim of giving insight into these two phenomena, that a continuous ODE model was engineered in Ref. [2]. Just to recall, such model consists of two cell populations, the tumor cells and the immune effector cells. It was inspired by enzymatic kinetics and developed in conformity with experimental results. However, in their original model, the rate at which a tumor is lysed, *i.e.*, the fractional cell kill, increased linearly with the number of immune cells, just as in an ordinary Lotka-Volterra model [3, 4]. Simply put, the velocity at which a tumor is destroyed can be increased unboundedly by simply adding more immune cells. In the hands of De Pillis and Radunskaya [5], the model evolved to include an interaction with the host healthy tissue. Years later, such inclusion was dropped in favor of a more specialized model, in which two interacting immune cell populations were considered: the NK cells and the $CD8^+$ lymphocytes. This model was validated [6] using experiments in mice [7] and humans [8], and to reproduce the experimental data a new fractional cell kill law was presented. These authors noticed that the lysis curves seen in experimental settings exhibited *saturation*. Briefly, the fraction of lysed tumor cells after a certain time (usually a few hours in chromium release assays) versus different values of the initial effector-to-target ratio saturates for increasing values of the later. Therefore, they proposed a Hill function [9] depending on the effector-to-target ratio as the mathematical function describing the rate at which a tumor is lysed. Their brilliant achievement notwithstanding, little theoretical explanation was given to this function and the original proposal of Ref. [2] was partly forgotten.

In the previous chapter, several hypotheses concerning the significance of this fractional cell kill were made, and its limitations for weak immune responses were debated. The following lines thoroughly inspect this mathematical function. In order to give insight into the significance of the parameters appearing in such law, a hybrid cellular automaton model describing the spatio-temporal evolution of tumor growth and its interaction with the cell-mediated immune response is used. When the CTLs eradicate efficiently the tumor cells, the model predicts a correlation between the morphology of the tumors and the rate at which they are lysed. As the effectiveness of the effector cells is decreased, a failure of the law at reproducing the CA is detected. We derive a new fractional cell kill capable of reproducing the results more accurately, and also having a clear interpretation.

## 4.2 Models

In the present chapter two models are utilized: a cellular automaton (CA) and an ordinary differential equation model. We make use of the CA to test the fractional cell kill that governs the lysis of solid tumors.

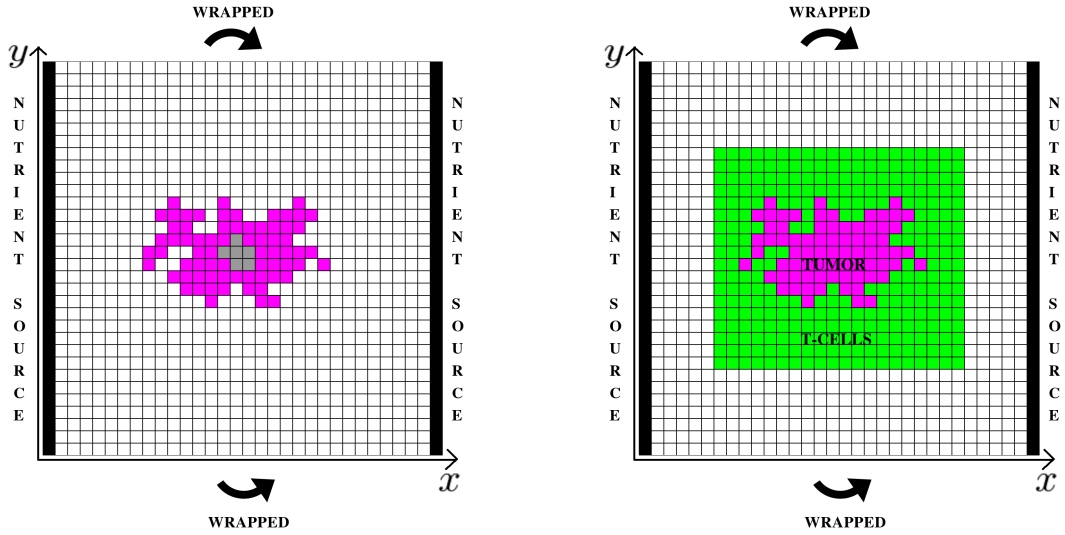


**Figure 4.1. Schematic representation of the cellular automaton**. (a) A grid in a square domain, with some tumor cells (pink) growing from its center, and some necrotic cells (gray) at its core. Two vertical vessels on the boundary supply the nutrients required for cell division and other cellular activities. The upper and lower bounds are identified, forming a cylinder. (b) To study the lysis of tumor cells, the cell co-cultures (initial conditions) are prepared by randomly placing effector cells in a rectangular region around the tumor. The size of this domain is selected so that for the maximum values of the effector-to-target ratio the region is almost filled with effector cells.

### 4.2.1 A hybrid cellular automaton model

The simulations are accomplished by means of a cellular automaton (CA) model developed in Ref. [10] to study the interactions between tumor and immune effector cells. An schematic representation of the CA can be seen in see Fig. 4.1. This model was built on a previously CA model designed to study the effects of *competition* for nutrients and growth factors in avascular tumors [11]. It is hybrid because the cells are treated discretely, allowing them to occupy diverse grid points in a particular spatial domain, and evolve according to probabilistic and direct rules. On the contrary, the diffusion of nutrients required for growth (such as glucose, oxygen and other types of nutrients) from the vessels into such spatial region is represented through linear *reaction-diffusion equations*, which are continuous and deterministic. Two types of nutrients are utilized in this model, making a distinction between those which are specific for cell division $N(x, y, t)$, and others $M(x, y, t)$ that are related to the remaining cellular activities. The partial differential equations for the diffusion

of nutrients are

$$\frac{\partial N}{\partial t} = D_N \nabla^2 N - k_1 T N - k_2 H N - k_3 E N \tag{4.1}$$

$$\frac{\partial M}{\partial t} = D_M \nabla^2 M - k_4 T M - k_5 H M - k_6 E M, \tag{4.2}$$

where $T(x, y, t)$, $H(x, y, t)$ and $E(x, y, t)$ are functions representing the number of tumor, healthy and immune cells at time $t$ and position $(x, y)$. For simplicity, we assume that both type of nutrients have the same diffusion coefficient $D_N = D_M = D$. Following Ref. [10], we consider that the competition parameters are equal $k_2 = k_3 = k_5 = k_6 = k$, except for the tumor cells, which compete more aggressively. We set $k_1 = \lambda_N k$ and $k_4 = \lambda_M k$, with $\lambda_M$ and $\lambda_N$ greater than one. An adiabatic limit is considered, assuming that the solutions are stationary. This approximation holds because the time it takes a tumor cell to complete its cell cycle, which is of the order of days [13], is much longer than that of the diffusion of nutrients, which is of the order of minutes. A quadrilateral domain $\Omega = [0, L] \times [0, L]$ is considered and Dirichlet boundary conditions are imposed on the vertical sides of the domain, where the vessels are placed, assigning $N(0, y) = N(L, y) = N_0$ and $= M(0, y) = M(L, y) = M_0$. For simplicity, the horizontal upper and lower bounds of the domain obey periodic boundary conditions $N(x, 0) = N(x, L)$ and $M(x, 0) = M(x, L)$, wrapping them together to form a cylinder.

The reaction-diffusion equations can be non-dimensionalized [11] by redefining the nutrients and the spatial and temporal coordinates in the form

$$\begin{aligned} \tilde{t} &= \frac{Dnt}{L^2}, (\tilde{x}, \tilde{y}) = \left(\frac{nx}{L}, \frac{ny}{L}\right), \\ \tilde{N} &= \frac{N}{N_0}, \tilde{M} = \frac{M}{M_0}. \end{aligned} \tag{4.3}$$

Dropping the tildes and considering that the solutions are stationary, we obtain the equations

$$\nabla^2 N - \alpha^2 (H + I + \lambda_N T) N = 0 \tag{4.4}$$

$$\nabla^2 M - \alpha^2 (H + I + \lambda_M T) M = 0, \tag{4.5}$$

where $\alpha^2 = kL^2/Dn^2$ is the dimensionless rate of consumption of nutrients by host and immune cells, while $\lambda_N \alpha^2$ is the rate of consumption of the nutrient $N$ by the tumor cells. The boundary conditions are now $N(0, y) = N(L, y) = 1$ and $= M(0, y) = M(L, y) = 1$. From a physical point of view, these elliptic partial differential equations represent the "scattering" of nutrients from the boundary of a tissue and their diffusion in it. The role of the cells at a particular point in space is to act as a "potential barrier", consuming nutrients and, therefore, attenuating their concentration at such position. The size of such "barrier" varies in space, depending on the number of cells at each position and the rate at which they consume nutrients.

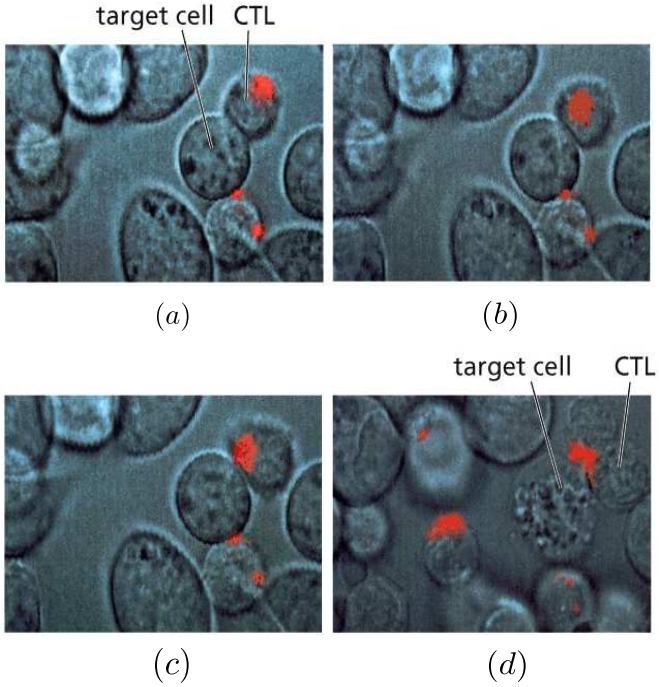


**Figure 4.2. An interaction between a T cell and a tumor cell.** (a) A cytotoxic T-cell detecting a tumor cell a particular moment through antigen recognition. The red spot represents the lytic granules of the T-cell. (b-c) During the next five minutes, then the cell polarizes (capping) through the reorganization of the cytoskeleton, with its Golgi apparatus aligned close to the receptor zone. Subsequent polymerization of perforins creates a hole in the membrane, and the enzymes are secreted. (d) Approximately forty minutes later, a tumor cell experiencing apoptosis is observed. From Ref. [12].

Since $\lambda_N \geq 1$ and $\lambda_M \geq 1$, tumor cells compete equally or more aggressively for nutrients.

We now briefly explain how the experiments are carried out, and also give a qualitative description of the CA rules. The experiments here presented are carried out in two successive steps. The first (1) is devoted to the growth of the tumors, while the second (2) focuses on the lysis of tumor cells by CTLs.

1. We generate distinct solid tumors as monoclonal growths, arising after many iterations of the cellular automaton. At each CA iteration the tumor cells can *divide, move or die* attending to certain probabilistic rules that depend on the nutrient concentration per tumor cell and some specific parameters. Each of these parameters $\theta_a$ represent the intrinsic capacity of the tumor cells to carry out a particular action $a$. The precise probabilistic laws and the corresponding actions are described in detail in the next section. Attending to morphology, diverse types of tumors can be generated, depending on the nutrient competition parameters among tumor cells $\alpha, \lambda_N$. We simulate four types of geometries (spherical, papillary, filamentary and disconnected), and inspect four tumors of different sizes for each shape.

2. The *lysis* of tumor cells is a hand-to-hand struggle comprising several processes. After recognition of these cells through antigen presentation via MHC class I molecules, the $CD8^+$ T cells proceed to induce apoptosis (see Fig. 4.3). The principal mechanism involves the injection of proteases through pores on the cell membrane, that have been previously opened by polymerization of perforins. Even though death may take about an hour to become evident, it takes minutes for a T cell to program antigen-specific target cells to die [14]. We assign a time of ten minutes for each iteration of the CA, and other choices can be made. Therefore, twenty four iterations of the CA equal the four hours after which the lysis of tumor cells is measured in the experiments [7]. Since the cell cycle time of a tumor cell is generally a few times longer, we assume a second adiabatic approximation and freeze the tumor cell dynamics during T cell lysis. The rules governing the effector cells evolution are as follows. At each iteration, those immune cells that are in contact with at least one tumor cell, might lyse them with certain probability. The intrinsic cytotoxic capability, which in the model also accounts for the capacity of T cells to recognize tumor cells [15], is related to the parameter $\theta_{lys}$. If a T cell destroys a tumor cell, recruitment might be induced in its neighboring CA elements. When immune cells are not in direct contact with a tumor cell, they can either move or become inactivated. We consider that a single T cell can not lyse more than three times, leaving the region of interest when this occurs [10]. Again, the precise probabilistic laws and the corresponding actions are thoroughly described in the next section. Each of the sixteen solid tumors is co-cultivated with different effector-to-target ratios as initial conditions and the lysis is computed four hours later.

Because our study mainly focuses on how fast lymphocytes lyse a tumor, two important simplifications between our cellular automaton and the one presented in Ref. [10] deserve notification. We have excluded the NK cells from the model, together with a constant source of immune cells.

### 4.2.2 Cellular automaton rules

In this section the CA rules are described quantitatively for the two mentioned steps, the first corresponding to the development of the tumors, and the other related to the lysis of the tumor cells by the cytotoxic T cells. They are almost the same as those used in Ref. [10], and any difference will be explicitly remarked. In what follows, $T(\vec{x})$ and $E(\vec{x})$ are the tumor and immune cells at position $\vec{x}$, while $N(\vec{x})$ and $M(\vec{x})$ are the concentration of nutrients in nondimensional variables at position $\vec{x}$. $N(\vec{x})$ represents those nutrients required for cell division, and $M(\vec{x})$ those required for other cellular activities. The paramters $\theta_a$ represent the *intrinsic capacity* of a cell to carry out a particular action $a$.

### First step

As in previous works, the role of the healthy cells is simplified to passive competitors for nutrients that allow the tumor cells to freely divide or migrate. At each CA iteration the tumor cells are randomly selected one by one, and a dice is rolled to choose whether each of these cell divides (1), migrates (2) or dies (3).

1. A tumor cell divides with probability

$$P_{div} = 1 - \exp\left(-\frac{(N/T)^2}{\theta_{div}^2}\right). \tag{4.6}$$

   This probability is compared to a similar randomly generated number using a normal distribution and the same standard deviation. If the former is greater than the last, division takes place. The higher the value of $\theta_{div}$, the more metabolic requirements for a cell to proliferate. When a cell at position $\vec{x} = (x, y)$ divides, if there are neighbouring CA elements that are not currently occupied by tumor cells, we randomly select one $\vec{x'} = (x', y')$ and place there the newborn cell, thus making $T(\vec{x'}) = 1$ and $H(\vec{x'}) = 0$ or $D(\vec{x'}) = 0$, where $D(\vec{x})$ is the function representing the necrotic cells at position $\vec{x}$. However, if all the neighbouring elements are occupied, we let the cells pile up, making $T(\vec{x}) \to T(\vec{x}) + 1$.

2. A tumor cell migrates with probability

$$P_{mig} = 1 - \exp\left(-\frac{(\sqrt{T}M)^2}{\theta_{mig}^2}\right). \tag{4.7}$$

   If $P_{mig}$ is greater than the probability of a randomly generated number, migration proceeds, otherwise it does not. The higher the value of $\theta_{mig}$, the more metabolic requirements for a cell to migrate, unless there are too many tumor cells. When a cell at position $\vec{x}$ moves, if there are neighbouring CA elements that are not currently occupied by tumor cells, we randomly select one at $\vec{x'}$ and place the cell there. If there is more than one cell in the original position, the moving cell simply replaces the healthy or the necrotic cell, thus making the transformation $T(\vec{x}) \to T(\vec{x}) - 1$, $T(\vec{x'}) = 1$ and $H(\vec{x'}) = 0$ or $D(\vec{x'}) = 0$.

3. On the other hand, if there is only one tumor cell at $\vec{x}$, then it interchanges its position with the healthy or necrotic cell at $\vec{x'}$. If all the neighbouring elements are occupied, we displace the cell to a randomly selected neighbouring element.

4. A tumor cell dies with probability

$$P_{nec} = \exp\left(-\frac{(M/T)^2}{\theta_{nec}^2}\right). \tag{4.8}$$

If $P_{nec}$ is higher than the probability of a randomly generated number, necrosis proceeds, otherwise it does not. The higher the value of $\theta_{nec}$, the greater the probability for a cell to die. When a cell at position $\vec{x}$ dies, we make $T(\vec{x}) \to T(\vec{x}) - 1$. If this is the only cell at $\vec{x}$, then $D(\vec{x}) = 1$.

### Second step

At each CA iteration the immune cells that have one or more tumor cells as first neighbours, carry out an attempt to lyse a randomly chosen surrounding tumor cell. This process occurs with probability

$$P_{lys} = 1 - \exp\left(-\frac{1}{\theta_{lys}^2}\left(\sum_{i\in\eta_1} E_i\right)^2\right), \tag{4.9}$$

where $\eta_n$ indicates summation up to the $n$-th nearest neighbors. If $P_{lys}$ is higher than the probability of a randomly generated number, then the selected tumor cell dies. Therefore $T(\vec{x'}) = 0$, $D(\vec{x'}) = 1$ and the immune cell counter decreases by a unit. If the counter reaches a value of zero, it dies and it is replaced by a healthy cell. The smaller the value of $\theta_{lys}$, the greater the probability for an effector cell to lyse a tumor cell. This parameter was not present in Ref.[10] and is introduced here to model the intrinsic cytotoxicity of T cells. When a tumor cell is destroyed by an immune cell, the first neighbouring cells are flagged for recruitment. For each CA element without tumor cells a new immune cell is born with probability

$$P_{rec} = \exp\left(-\frac{1}{\theta_{rec}^2}\left(\sum_{i\in\eta_1} T_i\right)^{-2}\right). \tag{4.10}$$

If $P_{rec}$ is higher than the probability of a randomly generated number, recruitment proceeds. The higher the value of $\theta_{rec}$, the less surrounding tumor cells that are required for T cell recruitment to succeed. When a cell is recruited at position $\vec{x'}$, we make $D(\vec{x'}) = 0$ or $H(\vec{x'}) = 0$, and $E(\vec{x'}) = 1$.

Those effector cells whose immediate neighbourhood is not occupied by tumor cells, either migrate or become inactivated. To decide which of these two processes is carried out, a coin is flipped. If the output is migration, it occurs for sure. In the opposite case, inactivation occurs with probability

$$P_{inc} = 1 - \exp\left(-\frac{1}{\theta_{inc}^2}\left(\sum_{i\in\eta_3} T_i\right)^{-2}\right). \tag{4.11}$$

If $P_{inc}$ is higher than the probability of a randomly generated number, inactivation proceeds. The smaller the value of $\theta_{inc}$, the less surrounding tumor cells that are required for a T cell to become inactivated. When a cell disappears from position $\vec{x}$, we simply make $H(\vec{x}) = 1$ and $E(\vec{x}) = 0$.

Note that the probability distributions are normal type distributions, which are very common in biological processes [16].

### 4.2.3 The algorithm

First, we let the tumors grow until they have reached some specific size. A variety of sizes will be used to inspect the fractional cell kill. The algorithm starts with a domain full of healthy cells, except for a single tumor cell placed at the centre of the domain. During this period of growth each CA step corresponds to one day. Each iteration begins with the integration of the reaction-diffusion equations, using a finite-difference scheme and a successive overrelaxation method. Then all the tumor cells are randomly selected with equal probability, and the CA rules are applied. As in previous works [11], every time an action takes place, the reaction-diffusion equations are locally solved in a neighbourhood with size $20 \times 20$ grid points. Once the tumors are grown, we freeze their dynamics, and only the immune cells are computed. This approximation holds because the experiments last four hours and it takes a tumor cell approximately one day to divide. The initial conditions are set by randomly placing the immune cells in the neighbourhood of the tumor, in a similar manner as co-cultures are prepared in immunological studies. Then the reaction-diffusion equations are solved at each step and then all the immune cells are randomly selected. For each immune cell, after applying the CA rules, the nutrients are computed in a local region, in exactly the same manner as before. The algorithm stops after 24 iterations of the cellular automaton. Each of these steps correspond to 10 minutes, which accounts for a total time of four hours.

### 4.2.4 An ordinary differential equation model

The results of the simulations performed with the cellular automaton model are fitted by means of a least-squares fitting method to the simplified Lotka-Volterra type model validated in the previous chapter. Our study focus mainly on $CD8^+$ T lymphocytes, but the model can be easily modified to reproduce NK cell dynamics. In the present chapter only those parameters appearing in the fractional cell kill law ($d$, $\lambda$ and $s$) are inspected. Accordingly to the CA model, we set $\sigma = 0$ in the ODE model since the CA does not include a constant input of effector cells. We have also selected a value $g = 0.15$, which is very close to one of the values appearing in Table 3.2. Importantly the CA model and the ODE model include the same type of processes. The logistic growth of tumor cells in the CA model arises as a consequence of competition for nutrients [11]. There is also competition among healthy cells and tumor cells for nutrients, which in the ODE model is represented by the competing Lotka-Volterra terms between healthy and tumor cells. T cell lysis, inactivation and recruitment are also present in both models. Only the competition term between tumor and immune cells $a_{31}$ is different. Although we keep this parameter as shown in Table 3.2, if desired, it can be made equal to zero. As far as we have investigated, reducing the value of this parameter produces no appreciable consequences in our study. Notwithstanding this correspondence, we recall that during the second step of our CA simulations, the tumor dynamics is freezed. Accordingly, the parameter $r_1$ should be made equal to zero. Again, we keep this parameter as shown in Table 3.2.

Reducing the value of this parameter produces no significant consequences in our study when the T cells are effective. For immunodeficient scenarios the effects are more sensitive, but still small. In other words, the dynamics of the model during the first four hours is dominated by T cell lysis, recruitment and inactivation.

## 4.3 Results

In this section we expose the CA results and fit the parameters of the fractional cell kill to the results. From an immunological point of view, two scenarios are studied. The first corresponds to immunocompetent hosts, while the second corresponds to the immunodeficient case.

### 4.3.1 Tumors

In Fig. 4.4 we depict the simulated solid tumors with four distinct morphologies, depending on the nutrient competition among tumor cells. The apparent three-dimensionality is an artefact resulting from the fact that we let cells pile up at the CA grid points. This piling mechanism was assumed in Ref. [11] for computational simplicity, and does not have any consequence in our study, since once the tumors are grown, we project them to study their lysis. High values of $\alpha$ and $\lambda_N$ lead to more branchy tumors, gradually changing from spherical to filamentary. This phenomenon is explained if we consider that when some nearby neoplastic cells on the boundary of a tumor compete aggressively for nutrients, those cells that divide and take ahead at some step, preserve this advantage at the next step, stealing the nutrients to those cells left behind. This positive feedback mechanism provokes a rupture of the spherical symmetry of the tumors. The resulting geometries are comparable to a variety of histologies (see Fig. 4.3).

Note that the necrosis of tumor cells due to the scarcity of nutrients in the core of the masses has been neglected, since it has no relevance in our study. In the CA this is achieved by setting $\theta_{nec} = 0$. Except for the disconnected patterns appearing in the last row in Fig. 4.4, motility has been also disregarded, considering sufficiently high values of $\theta_{mig}$.

### 4.3.2 Effective immune response

In the model given by Eq. (3.5), the fractional cell kill of tumor cells by CTLs is given by the function $K(E,T)$. In the previous chapter we took the decision of expressing this function in the form

$$K(E,T) = d\frac{E^\lambda}{h(T)+E^\lambda}, \tag{4.12}$$

with $h(T) = sT^\lambda$. Written this way, the fractional cell kill clearly states that the more effector cells, the greater the fractional cell kill, but bearing in mind the saturation of antigen-mediated immune response, which depends on the tumor burden.

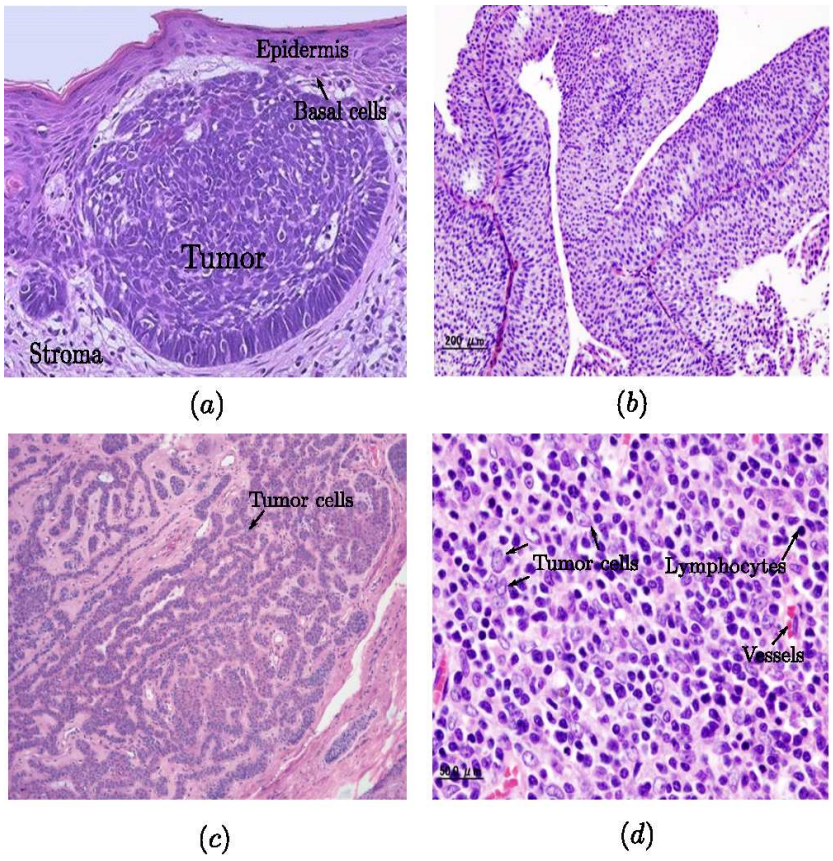


**Figure 4.3. Histological samples of tumors**. (a) A basal cell carcinoma (tumor of the basal cell of the epidermis) invading its underlying stroma. This tumor represents a connected spherical tumor. From `www.mrcophth.com/pathology/skin/basalcellcarcinoma.html` (b) An urothelial carcinoma, exhibiting papillary geometry. Distributed under license CC BY-SA 3.0. (c) A cancer of the hair follicle (trichoblastoma), were tumor cells acquire a filamentary disposition. From Ref. [17]. (d) A disconnected tumor in the thymus (thymoma), with tumor cells scattered in the tissue, among healthy cells. The healthy cells that separate them are T-cells, which mature in the thymus. Therefore their name. Distributed under license CC BY-SA 3.0.

We propose that the saturation is due to the crowding of immune effector cells, which is evident if we recall that these cells need to be in contact with tumor cells to exterminate them. In a solid tumor, once all the tumor cells on its surface are in contact with a first line of immune cells, the remaining effector cells are not lysing, although the adjacent lines behind probably contribute to immune stimulation through several feedback mechanisms. Therefore, at a certain point, no matter how many more immune cells are present in the region of interest, the rate at which the tumor is lysed remains practically unaltered. Before saturation appears, if two tumors of the same nature and different size at a certain time instant are lysed at the same rate by the immune system, the bigger tumor will require more effector cells. Put more simply, if two tumors of different size are reduced to a particular

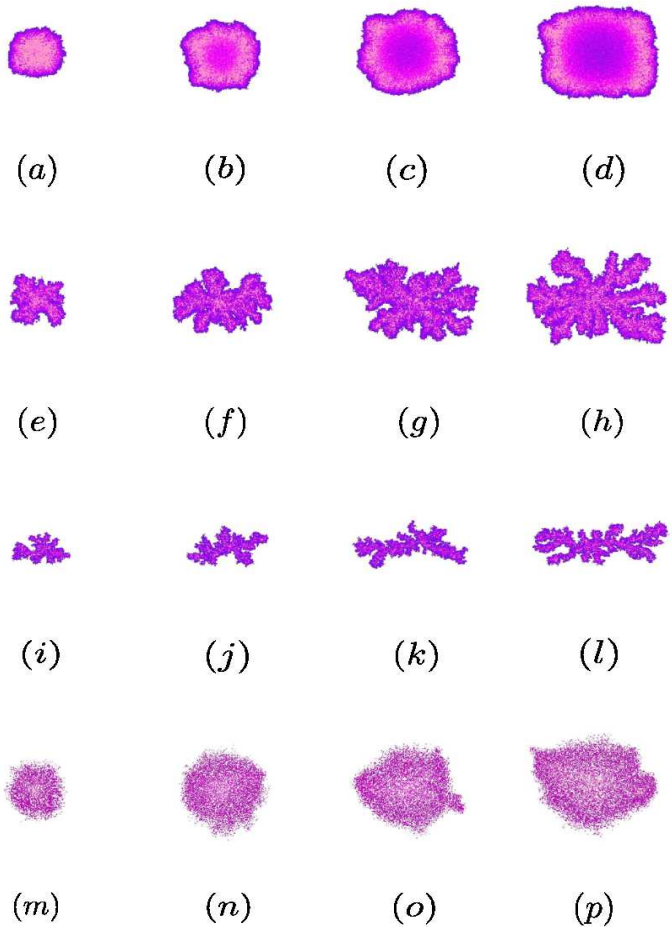


**Figure 4.4. Tumors generated using the cellular automaton model**. Tumors become increasingly branchy as the competition for nutrients increases. Colors go from dark purple (one cell) to light pink (highest number of cells in a grid point for each tumor). We set the parameters $\lambda_M = 10$ and $\theta_{nec} = 0$ in all the cases, disregarding necrosis. (a-d) Spherical tumors with increasing size and parameters $\alpha = 2/n$, $\lambda_N = 25$, $\theta_{div} = 0.3$ and $\theta_{mig} = \infty$. (e-h) Papillary tumors with increasing size and parameters $\alpha = 4/n$, $\lambda_N = 200$, $\theta_{div} = 0.3$ and $\theta_{mig} = \infty$. (i-l) Filamentary tumors with increasing size and parameters $\alpha = 8/n$, $\lambda_N = 270$, $\theta_{div} = 0.3$ and $\theta_{mig} = \infty$. (m-p) Disconnected tumors with increasing size and parameters $\alpha = 3/n$, $\lambda_N = 200$, $\theta_{div} = 0.75$ and $\theta_{mig} = 0.02$.

fraction of its size after a certain period of time, the bigger tumor will require more effector cells. The number of effector cells $E$ for which the fractional tumor cell kill is half of its maximum $d$, increases monotonically with the tumor size $h(T)$.

We use simulations to demonstrate that these assertions are sufficient to explain the fractional cell kill law, even though there might be others. With this purpose, for every tumor pictured in the previous section, we prepare co-cultures with different effector-to-target ratios. Then, we let the CA evolve and measure the lysis four hours later (see Fig. 4.7). As previouly explained, the tumors have been projected

| Parameter | Units | Value | Description |
|---|---|---|---|
| $d$(s) | day$^{-1}$ | $9 \pm 4$ | Saturation level of fractional tumor cell kill |
| $d$(p) | | $20 \pm 1$ | |
| $d$(f) | | $32 \pm 2$ | |
| $d$(d) | | $13 \pm 3$ | |
| $\lambda$(s) | None | $0.61 \pm 0.07$ | Exponent of of fractional tumor cell kill |
| $\lambda$(p) | | $0.87 \pm 0.04$ | |
| $\lambda$(f) | | $0.89 \pm 0.03$ | |
| $\lambda$(d) | | $0.63 \pm 0.03$ | |
| $s$ | None | 0.15 | Steepness coefficient of fractional tumor cell kill |
| $D_F$(s) | None | $1.09 \pm 0.02$ | Box counting dimension of the boundary before the lysis starts |
| $D_F$(p) | | $1.21 \pm 0.04$ | |
| $D_F$(f) | | $1.36 \pm 0.02$ | |
| $D_F$(d) | | $1.72 \pm 0.04$ | |

**Table 4.1. The parameters of the fractional cell kill**. The parameter values modified in the equation shown in Eq. (4.12) corresponding to an effective immune response. The parameters $\lambda$ and $d$ are obtained through a least-square fitting of the lysis of tumor cells between the CA simulations and the ODE model. The mean value and standard deviations is computed for each morphology using four different tumors sizes: spherical (s), papillary (p), filamentary (f) and disconnected (d).

before the lysis starts, to better correlate the geometry and the parameters in the fractional cell kill. Otherwise, we would have two-dimensionally distributed lymphocytes fighting three-dimensional-like tumors, as in Ref. [10]. Finally, the results are fitted to the ODE model using a least-squares fitting method. We recall that such model was validated using as initial conditions typical cell populations of $10^6$ cells, while the CA automaton grid used can harbor at most $9 \times 10^4$ cells. However, this is not a hurdle at all, since if desired, the cell populations in the ODE model can be renormalized and its parameters redefined so as the cell numbers coincide.

The resulting lysis curves are depicted in Fig. 4.5 and the values of the parameters $d$, $\lambda$ and $s$ in Eq. (4.12) are listed in Table 4.1, together with the fractal dimension $D_F$ of the contour of the initial tumors. Satellitosis is clearly appreciated as a consequence of T cell recruitment, and the resulting clusters of cells act like wave fronts that advance lysing the tumor. There is a correlation between the box counting dimension and the parameters $d$ and $\lambda$ for the connected tumors examined, but this is not the case for the disconnected one. In fact, the fractal dimension of the boundary of a solid tumor, is not generally a good measure concerning the cell mediated immune response. A counterexample suffices to convince ourselves, preventing us to search for power laws relating the parameters $d$ and $\lambda$ and the fractal dimension. For example, the disconnected tumors shown in Fig. 4.4 have the highest dimensions, but this is because these tumors are very drilled, so most of the tumor cells are on its boundary. However, they are rather spherical, so that the part of the boundary that is in the center of the mass is not initially accessible to the immune system. On the other hand, a tumor with a similar distribution of cells, but none making contact among them, will have fractal dimension smaller than one, but close lytic rates. These facts explain the low values of $d$ and $\lambda$ for such tumors, which are comparable to the spherical ones. Indeed, what matters to the cytotoxic cells is the

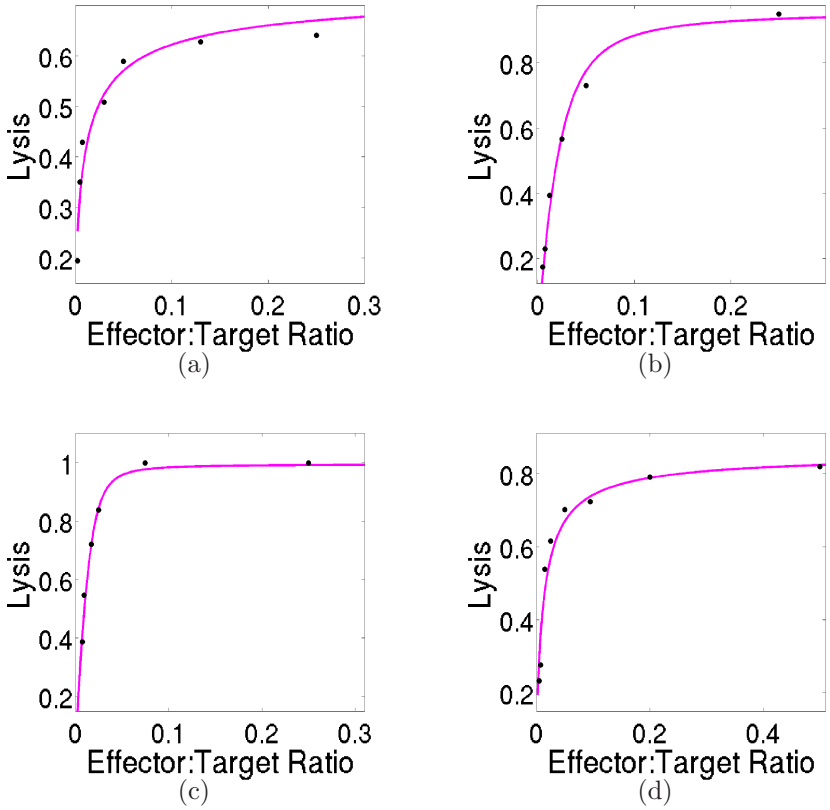


**Figure 4.5. The lysis curves**. The lysis of tumor cells after four hours versus the effector-to-target ratio $E_0/T_0$ in immunocompetent environments. The parameter values of the CA related to the lysis, recruitment and inactivation are $\theta_{lys} = 0.3$, $\theta_{rec} = 1.0$ and $\theta_{inc} = 0.5$, respectively. The solid curve corresponds to the ODE model, while the points correspond to the cellular automaton results. Here we show the results for four tumors. (a) The spherical tumor in Fig. 4.4(b). (b) The papillary tumor in Fig. 4.4(f). (c) The filamentary tumor in Fig. 4.4(l). (d) The disconnected tumor in Fig. 4.4(n).

accessibility to their enemies. The more tumor cells there are between an immune cell and a tumor cell, the lower the rate at which the effector cells kill their victims. This is starkly evident for the spherical tumors, which correspond to the smallest values of $d$ and $\lambda$.

Thus, according to our model, Eq. (4.12) is an emergent property of the tumor-immune interaction depending on the spatial distribution of the tumor cells. It reflects the tumor size dependent saturation of an effective immune system, fruit of the crowding of the effector cells and the arduousness to establish contact with their adversaries. Nevertheless, it takes hours for the effector cells to fully lyse the tumors so far investigated, what denotes that this extrinsic limitation to the lytic capacity of the immune system is barely important compared to the immunoevasive maneuvers that tumor cells commonly orchestrate [18].

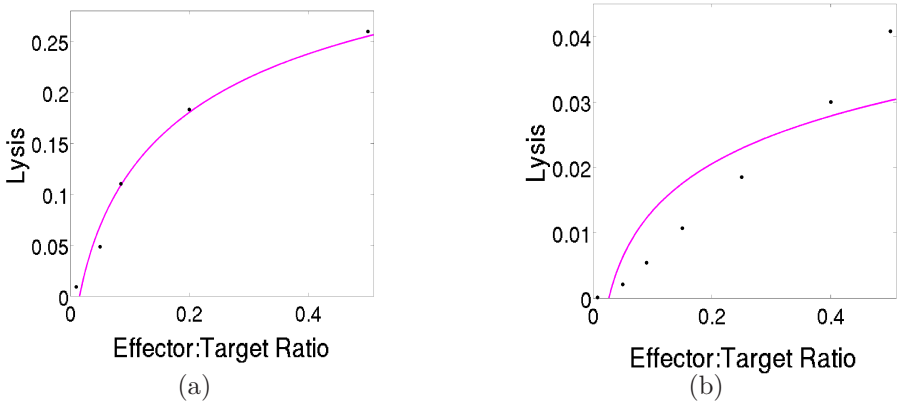


**Figure 4.6. The lysis curves**. The lysis of tumor cells after four hours versus the effector-to-target ratio $E_0/T_0$ in immunosuppressed environments. The spherical tumor represented in Fig. 4.4(b) is studied, with recruitment and inactivation CA parameters $\theta_{rec} = 1.0$ and $\theta_{inc} = 0.5$. The solid curve corresponds to the ODE model, while the points correspond to the cellular automaton results. (a) A more ineffective, but still effective, adaptive response is here represented, with $\theta_{lys} = 10$. (b) A value of the intrinsic cytotoxic capacity $\theta_{lys} = 100$ is set for the most ineffective immune system.

### 4.3.3 Ineffective immune response

Tumor cells find ways to evade the immune surveillance through a broad range of mechanisms [12]. They can acquire the ability to repress tumor antigens, MHC class I proteins or NKG2D ligands. They may also learn to destroy receptors or to saturate them, induce suppressor T cells formation, launch counterattacks against immunocytes by releasing cytokines, avoid apoptosis, etc. It is therefore pertinent to ask ourselves if the law can cover situations in which the tumor microenvironment is immunodeficient.

In Ref. [6] the authors show that the lysis curves corresponding to NK cells in the experiments borrowed from Ref. [7] do not show saturation, and that a fractional cell kill given by a simple power law $cE^\nu$ works to fit such data. Because much higher values of the effector-to-target ratio are required to obtain similar values for the lysis compared to the CTLs curves, it was suggested that when the effector cells are less effective, saturation is not observed.

Mathematical arguments have been given in previous chapters to explain this lack of saturation. Briefly, when the cytotoxic cells are less effective, only a fraction $f$ of the effector cells are interacting with the tumor. Thus we can replace $E$ by $fE$ in the fractional cell kill. Now, defining $\tilde{s} = s/f^\lambda$, the fractional cell kill law remains unchanged. This suggests that the parameter $s$ is related to the effectiveness of the cytotoxic cells, being this parameter inversely proportional to the effectiveness of such cells. On the other hand, if the effectiveness is small enough ($f \ll 1$), then $h(T)$ dominates over $E^\lambda$ in Eq. (4.12), as long as $E$ is not too high. The resulting lysis term becomes $df^\lambda E^\lambda T^{1-\lambda}/s$. This legitimates the estimation $cE^\nu T$ that has

| Parameter | Units | Value | Description |
|---|---|---|---|
| $d$(s) | day$^{-1}$ | 3.80 | Saturation level of the fractional tumor cell kill |
| $d$(i) | | 1.56 | |
| $\lambda$(s) | None | 0.62 | Exponent of the fractional tumor cell kill |
| $\lambda$(i) | | 0.17 | |
| $s$(s) | None | 0.50 | Steepness coefficient of the fractional tumor cell kill |
| $s$(i) | | 1.10 | |

**Table 4.2. The parameter values of the fractional cell kill law given by Eq.** (4.12). These parameters are obtained through a least-square fitting of the lysis of tumor cells between the CA simulations and the ODE model (see Fig. 4.6. Two cases are represented: a very ineffective (i) and a semi-effective (s) immune responses.

been used in other works [6, 19] to reproduce the fractional cell kill of tumor cells. Nevertheless, now we do not want to introduce phenomenological laws of this type, but rather concentrate our efforts on the significance of the parameter $s$. To this end, we diminish the intrinsic cytotoxic capacity of the immune cells, which is encoded in the parameter $\theta_{lys}$ in our cellular automaton. Higher values of this parameter represent more ineffective T cells. The results can be seen in Fig. 4.6 and the values of the parameters are listed in Table 4.2. As we increase the parameter $\theta_{lys}$, the lysis curves become progressively less convex, and at a certain point they look concave.

When $\theta_{lys} = 10$, the ODE model can be adjusted to the CA results. However, increasing $s$ is not sufficient to reproduce this data, and considerable variations of the remaining parameters $d$ and $\lambda$ is required. A much more dramatic case arises when $\theta_{lys} = 100$. In this case we have not been able to find any values of the parameters that represents faithfully the CA results. The best fitting provided by the ODE model exhibits strong saturation. The conclusion is that the fractional cell kill law represented by Eq. (4.12) works bad for immunodefficient environments and also confuses the geometrical effects and the intrinsic cytotoxic capacity of the immune cells. In the next section, we propose a new fractional cell kill law that allows to fit the results more accurately by simply reducing the value of $s$.

### 4.3.4 Modification of the fractional cell kill

In the previous chapter, the particular nature of the function $h(T)$ appearing in Eq. (4.12) was discussed, proving that if instead of $h(T) = sT^{\lambda}$, $h(T) = sT^{\lambda+\Delta\lambda}$ is used, the empirical results can also be validated by simply decreasing the value of $s$, even for values $\Delta\lambda/\lambda$ greater than one. This means that the original proposal of a saturating fractional cell kill depending on the quotient $E/T$ can not be guaranteed.

Furthermore, from a theoretical point of view, the function $h(T) = sT^{\lambda}$ makes the model ill-defined in the limit of very big tumors ($T \to \infty$) facing a comparably small fixed number of immune cells. The reason is that in this limit we get unbounded velocity for the lysis ($K(E,T)T \to \infty$). We demonstrate that $h(T) = sT$ is a much better choice. It has been shown [15, 20] that for a fixed number of effector cells

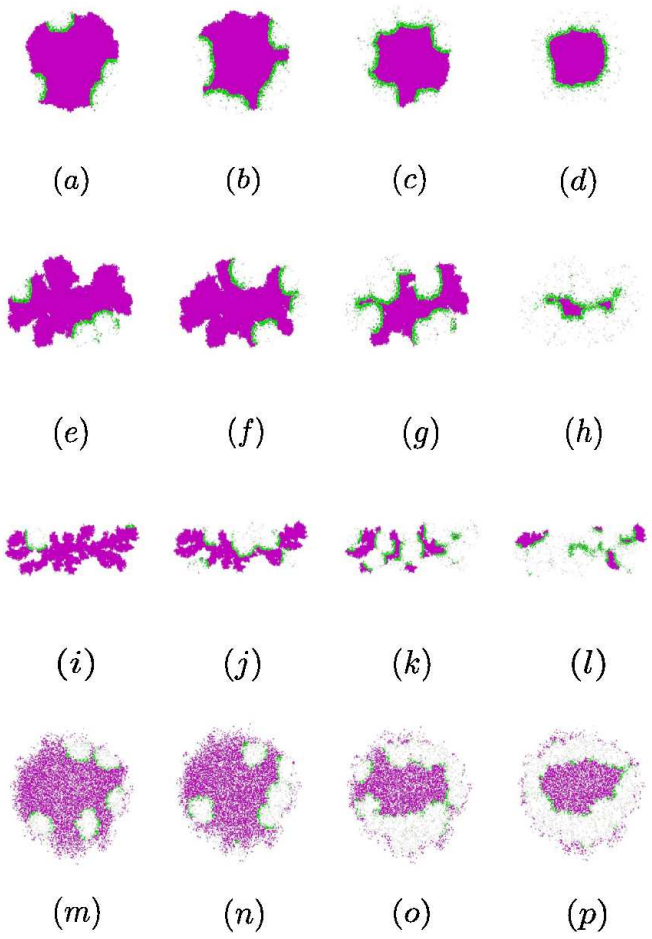


**Figure 4.7. Lysed tumors after four hours for different effector-to-target ratios**. The effector cells (green) form satellites that advance destroying their neoplastic enemies (violet) and leave apoptotic bodies (light gray) behind them, ready to be phagocytosed. The parameter values of the CA are $\theta_{lys} = 0.3$, $\theta_{rec} = 1.0$, $\theta_{inc} = 0.5$, $\lambda_M = 10$, $\lambda_N = 25$ and $\alpha = 2/L$. (a-d) Spherical tumor in Fig. 4.4(b) with $E_0/T_0$ taking values on the set $\{0.0025, 0.005, 0.05, 0.75\}$, respectively. (e-h) Papillary tumor in Fig. 4.4(f) with $E_0/T_0$ taking values on the set $\{0.005, 0.0075, 0.025, 0.25\}$, respectively. (i-l) Filamentary tumor in Fig. 4.4(l) with $E_0/T_0$ taking values on the set $\{0.0025, 0.0075, 0.025, 0.017\}$, respectively. (m-p) Disconnected tumor in Fig. 4.4(n) with $E_0/T_0$ taking values on the set $\{0.005, 0.0075, 0.015, 0.025\}$, respectively.

$E_0$, the Michaelis-Menten kinetics govern the lysis of tumor cells. The value of the lytic velocity at tumor saturation, *i.e.*, when $T \to \infty$, is reported in such works as a measure of the intrinsic cytotoxic capability of a particular number of effector cells. A Michaelis-Menten decay in Eq. (4.12) is obtained for a constant value of effector cells as long as $h(T) = sT$ in used. The value at saturation for a fixed number of effector cells is then $dE_0^{\lambda}/s$. An argument supporting saturation comes from the following fact. If the number of tumor cells is much higher than a fixed number of

effector cells, the velocity at which the tumor cells are lysed can not be enhanced by increasing the number of the neoplastic cells. This occurs because T cells kill tumor cells one by one, and for such ratios all the effector cells are already busy fighting other cells. In a similar fashion, for an enzymatic reaction, one can not increase arbitrarily the velocity at which the products are formed by simply adding more substrate. Precisely, this reasoning is reminiscent of the original formulation proposed in Ref. [2], in which the cell populations are regarded as chemical species obeying enzymatic kinetics in the quasi-steady state regime. In such work, the tumor cells are the substrate, the effector cells are the enzyme and the products are the dead cells. Indeed, it can be analitically demonstrated that such kinetics governs the lysis of tumor cells in the cited model for a constant number of effector cells (see Appendix 4.4). A fractional cell kill law that yields bounded velocity for the lysis of tumor cells when any of these two cell populations is sufficiently high compared to the other is represented by

$$K(E,T) = d\frac{E^{\lambda}}{sT + E^{\lambda}}. \tag{4.13}$$

Following the point of view of Ref. [2], this law can be regarded as a *Michaelis-Menten kinetics* where the rate constants of the formation of the "enzyme-substrate" conjugates, their dissociation and their conversion to product depend nonlinearly (as power laws) on the enzyme concentration. It establishes the saturation of the velocity of the lysis of tumor cells for both the tumor and the immune cell populations. In Fig. 4.8(a) we first reproduce the experiments of the spherical tumor shown in Fig. 4.4(b) for $\theta_{lys} = 0.3$. This allows us to obtain the parameter values of the modified fractional cell kill law shown in Eq. (4.13). Then we carry out the simulations of the preeceding section for immunodeficient evironments and see how, mainly by increasing the value of $s$, the CA results are reproduced (see Figs. 4.8(b) and 4.8(c)). The parameter values are listed in Table. 4.3. This sheds light into the significance of this parameter, which is now manifestly related to the intrinsic cytotoxic potential of the T cells. Moreover, this implies that the limit $T \to \infty$, for which the quantity $dE^{\lambda}/s$ is obtained, is not a good measure of lymphocyte cytotoxicity, as suggested in Refs. [15, 20]. This limit, which for a constant value of the T cells implies a linear decay of the tumor, involves geometry as well. Ideally, if we consider that there is just one immune cell, and it takes this cell an hour to lyse a tumor cell, then a spherical tumor would be reduced at approximately one cell per hour (assuming that this immune cell does not become inactivated at some step). However, the geometry of the tumor, which is coded in the parameters $d$ and $\lambda$, clearly affects how fast this single cell can erase it.

Even though the reduction of saturation for ordinary values of the effector-to-target ratio can be justified mathematically and numerically, the change in curvature for the CA results appearing in Fig. 4.8(c) is hard to put on a rational basis. Since $0 < \lambda < 1$, the quantity $dE^{\lambda}/s$, as a fucntion of $E$, will always have negative curvature. Therefore, a positive feedback mechanism is required to explain the change in curvature. A candidate mechanism responsible of this phenomenon is effector

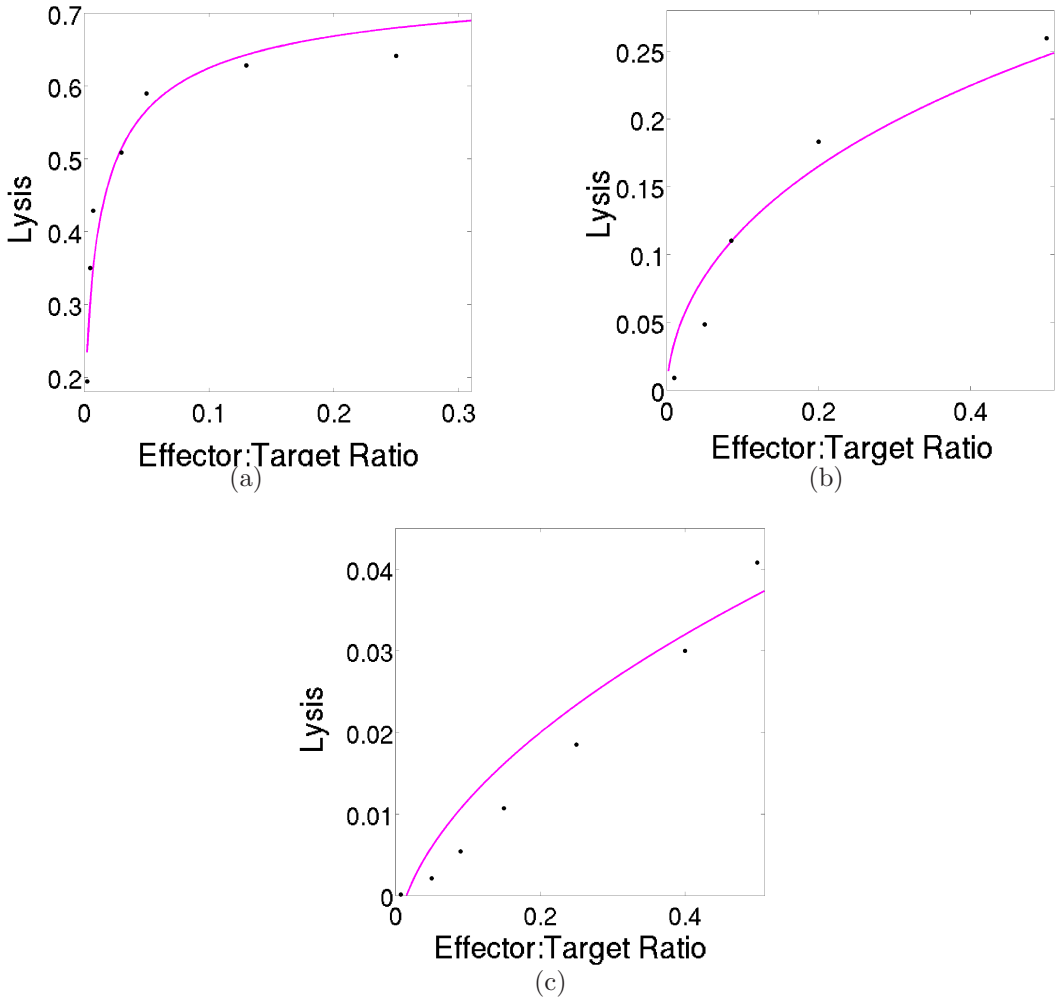


**Figure 4.8. The lysis curves**. The lysis of tumor cells after four hours versus the effector-to-target ratio $E_0/T_0$ for increasing inneffectiveness of the lymphocytes. The spherical tumor represented in Fig. 4.4(b) is studied, with recruitment and inactivation CA parameters $\theta_{rec} = 1.0$ and $\theta_{inc} = 0.5$. The solid curve corresponds to the ODE model, while the points correspond to the cellular automaton results. (a) An effecetive immune response for $\theta_{lys} = 0.3$. (b) A more ineffective, but still effective, adaptive response is here represented, with $\theta_{lys} = 10$. (b) A value of the intrinsic cytotoxic capacity $\theta_{lys} = 100$ is set for the most ineffective immune system. As shown in Table 4.3, the intrinsic cytotoxic potential of the T cells is chiefly represented by parameter $s$ in Eq. (4.13).

cell recruitment. As the effectiveness of the T cells decreases, this terms become increasingly important. Further research concerning this mathematical function is deserved.

| Parameter | Units | Value | Description |
|---|---|---|---|
| $d$(e) | day$^{-1}$ | 9.22 | Saturation level of the fractional tumor cell kill |
| $d$(s) | | 9.62 | |
| $d$(i) | | 9.52 | |
| $\lambda$(e) | None | 0.50 | Exponent of the fractional tumor cell kill |
| $\lambda$(s) | | 0.51 | |
| $\lambda$(i) | | 0.55 | |
| $s$(e) | cells$^{\lambda-1}$ | $1.0 \times 10^{-5}$ | Steepness coefficient of the fractional tumor cell kill |
| $s$(s) | | $1.4 \times 10^{-4}$ | |
| $s$(i) | | $9.5 \times 10^{-4}$ | |

**Table 4.3. The parameter values of the fractional cell kill appearing in Eq.** (4.13). These parameters are obtained through a least-square fitting of the lysis of tumor cells between the CA simulations and the ODE model (see Fig. 4.8). Three cases are represented: an effective (e), a semi-effective (s) and inneffective immune responses (i). Note that it is only the parameter $s$, which is related to the intrinsic cytotoxic capacity, that varies substantially. It increases as the immune cells become less effective.

## 4.4 The fractional cell kill as a Michaelis-Menten kinetics

The fractional cell kill represented by Eq. (4.13) can be derived from the Michaelis-Menten kinetics [21, 22] assuming that the rate constants of the reaction depend on the enzyme concentration. During the process of lysis, the effector cells $E$ bound to the tumor cells $T$ forming complexes $C$, and dead tumor cells $T^*$ result from this interaction. Therefore, the tumor cells play the role of the substrate and the effector cells act as the enzyme. This cellular reaction can be written in the form

$$E + T \underset{k_{-1}}{\overset{k_1}{\rightleftharpoons}} C \underset{k_{-2}}{\overset{k_2}{\rightleftharpoons}} T^* + E. \tag{4.14}$$

Once a tumor cell is induced to apoptosis it can not resurrect, so we must set $k_{-2} = 0$. Generally, also the backward reaction represented by $k_{-1}$ should be disregarded, since after tumor cell recognition and complex formation, destruction proceeds. However, we keep this term for reasons explained bellow.

Assuming that the *law of mass action* holds, the system of differential equations governing the reactions is

$$\frac{d[E]}{dt} = -k_1[E][T] + (k_{-1} + k_2)[C] \tag{4.15}$$

$$\frac{d[T]}{dt} = -k_1[E][T] + k_{-1}[C] \tag{4.16}$$

$$\frac{d[C]}{dt} = k_1[E][T] - (k_{-1} + k_2)[C] \tag{4.17}$$

$$\frac{d[T^*]}{dt} = k_2[C]. \tag{4.18}$$

The Briggs-Haldane [23] quasi-steady state approximation $[\dot{C}] = 0$ was assumed

in [2]. This approximation requires

$$\frac{[E_0]}{[T_0]+K_M} \ll 1, \tag{4.19}$$

where $K_M = (k_{-1}+k_2)/k_1$ is the Michaelis constant, and $[E_0]$ and $[T_0]$ are the initial concentrations of the effector and the tumor cells respectively.

Because we are dealing with situations in which the substrate concentration can be smaller than the enzyme, the quasi-steady state approximation implies $K_M \gg [E_0]$. Since this condition can not be generally guaranteed, instead, we consider Michaelis and Menten original formulation, and suppose that the substrate is in instantaneous equilibrium with the complex. We believe this is more reasonable, beacuse it takes about an hour for a cytotoxic T cell to fully lyse a tumor cell and, if the cells are effective, the recognition and complex formation should occur quite fast when brought together. In this manner, we have $k_1[E][T] = k_{-1}[C]$. From Eqs. (4.15) and (4.17) we get the conservation law $[E] + [C] = [E_0]$. These two equations put together and substituted in Eq. (4.18) yield

$$\frac{d[T^*]}{dt} = k_2 k_1 [E_0] \frac{[T]}{k_1[T]+k_{-1}}. \tag{4.20}$$

So far, this is nothing else but the Michaelis-Menten kinetics. It is at this point that we have to consider a dependence of the rate constants of the reaction on the concentration of the effector cells. The mathematical relations are derived heuristically, based on the idea that for higher concentrations of the immune cells the rate constants vary in a such a manner that the reaction is pushed backwards. Since saturation is due to crowding of T cells, and this depends on the geometry of the tumor, it seems a natural choice to use power laws.

Once the first lines of effector cells cover the surface of a solid tumor, the remaining immune cells are not in contact with it. Alternatively, an equivalent argument is attained if we suppose that the non-interacting effector cells do interact with some tumor cells unsuccesfully (say ghost tumor cells), so that the complexes are dissociated without lysis. The more effector cells, the higher the rate of dissociation, and when the number of effector cells is small compared to the number of tumor cells, the dissociation should vanish. Therefore, we consider a power law dependence $k_{-1}([E_0]) = \kappa_{-1}[E_0]^\alpha$, with $0 < \alpha < 1$, as suggested from the experiments. Substitution in Eq. (4.20) yields

$$\frac{d[T^*]}{dt} = k_2 k_1 \frac{[E_0]}{k_1[T]+\kappa_{-1}[E_0]^\alpha}[T]. \tag{4.21}$$

The fractional cell production of dead cells in this equation already resembles very much to Eq. (4.13). To obtain the exact result we have to consider dependence of $k_1$ and $k_2$ on the effector concentration as well. Note that for the inverse reaction to take place complexes have to be formed first, and this requires some time. Therefore, saying that complexes dissociate without lysis is not exactly equivalent to stating that the complexes are not formed. These rates should decay for

increasing concentrations of the effector cells, diminishing the rate of formation of complexes and products. Once again, we postulate power law relations in the form $k_1([E_0]) = \kappa_1[E_0]^{-\beta}$ and $k_2([E_0]) = \kappa_2[E_0]^{-\gamma}$ where again $0 < \beta < 1$ and $0 < \gamma < 1$. It might result surprising that in the limit $[E_0] \to \infty$ these functional relations tend to zero, suggesting that the reaction stops. However, this is not the case, because when subsituted in Eqs. (4.15), (4.16), (4.17) and (4.18), $k_1([E])[E]$ and $k_2([E])[C]$ both increase with the number of effector cells. Replacing the rate functions in Eq. (4.21) we obtain

$$\frac{d[T^*]}{dt} = \frac{\kappa_1\kappa_2}{\kappa_{-1}} \frac{[E_0]^{1-\gamma}}{\frac{\kappa_1}{\kappa_{-1}}[T] + [E_0]^{\alpha+\beta}}[T]. \tag{4.22}$$

We now rename the constants $\lambda = \alpha + \beta$, $s = \kappa_1/\kappa_{-1}$, $d = \kappa_1\kappa_2/\kappa_{-1}$, and remember that the velocity for the lysis must remain bounded for $[E_0] \to \infty$, what imposes the constraint $\alpha + \beta + \gamma = 1$. Thus, the result is

$$\frac{d[T^*]}{dt} = d\frac{[E_0]^{\lambda}}{s[T] + [E_0]^{\lambda}}[T]. \tag{4.23}$$

## 4.5 Discussion

Our study demonstrates that the saturation of the fractional cell kill of tumor cells by their cytotoxic opponents is a consequence of cell crowding. This limitation depends on the morphology of the tumor, insofar as geometry restricts the access of effector cells to tumor cells. In theory, those tumor growing with "spherical symmetry" will be the harder to lyse, because many layers of tumor cells have to be erased to reach the cells at the center. In the next chapter a rigorous mathematical proof of this fact will be provided. We recall that the process of T cell recruitment from circulation to the tumor site is complex, involving several steps [24]. This implies that the crowding might happen before contact with the tumor occurs, as for example, during adhesion to the endothelium. In such a case, a relation between the parameters in the fractional cell kill and the shape of the tumor can not be established. At all events, mathematically, this extrinsic barrier to the lytic capacity of the effector cells is reflected in the parameters $d$ and $\lambda$. The more accessible the tumor cells are, the higher both of these parameters. Interestingly, the values of $\lambda$ are expected to be between zero and one, as suggested by the experiments and the simulations. From the enzymatic kinetics point of view, if we think of Eq. (4.13) as a Hill function depending on the effector cells, this can be interpreted as *non-cooperative binding*. Certainly, if we pay attention to the process of lysis only, the best that an immune cell can do to another is not to interpose between itself and their adversaries. Of course, cooperative effects exist, as the recruitment term exemplifies. Quite the opposite, as the intrinsic lytic capacity of cytotoxic cells is decreased, saturation gradually vanishes. This capability is inversely proportional to the parameter $s$. It is not surprising that the limit $dE^{\lambda}/s$ dictates the lysis when the immune response

is ineffective. As argued in the previous chapter, this occurs because saying that a small fraction of a cytotoxic cell population $fE$ interacts with a tumor is, to what the tumor concerns, equivalent to considering a small number of effector cells confronting a big tumor. These limits are more thoroughly studied in the following chapter.

# References

[1] N. Bellomo and L. Preziosi, "Modelling and mathematical problems related to tumor evolution and its interaction with the immune system", *Math. Comput. Modelling* **32**, 413-452 (2000).

[2] V.A. Kuznetsov, I.A. Makalkin, M.A. Taylor, and A.S. Perelson, "Nonlinear dynamics of immunogenic tumors: parameter estimation and global bifurcation analysis", *Bull. Math. Biol.* **56**, 295-321 (1994).

[3] A.J. Lotka, "Analytical note on certain rhythmic relations in organic systems", *Proc. Natl. Acad. Sci. U.S.* **6**, 410-415 (1920).

[4] V. Volterra, "Variazioni e fluttuazioni del numero d´ individui in specie animali conviventi, *Mem. Acad. Lincei Roma* **2**, 31-113 (1926).

[5] L.G. De Pillis and A. Radunskaya, "The dynamics of an optimally controlled tumor model: a case study", *Math. Comput. Modelling* **37**, 1221-1244 (2003).

[6] L.G. De Pillis, A.E. Radunskaya, and C.L. Wiseman, "A validated mathematical model of cell-mediated immune response to tumor growth", *Cancer Res.* **65**, 235-252 (2005).

[7] A. Diefenbach, E.R. Jensen, A.M. Jamieson, and D.G. Rauelt, "Rae1 and H60 ligands of the NKG2D receptor stimulate tumor immunity", *Nature* **413**, 165-171 (2001).

[8] M.E. Dudley, J.R. Wunderlich, P.F. Robbins, J.C. Yang, P. Hwu, J. Schwartzentruber, S.L. Topalian, R. Sherry, N.P. Restifo, A.M. Hubicki, M.R. Robinson, M. Raffeld, P. Duray, C.A. Seipp, L. Rogers-Freezer, K.E. Morton, S.A. Mavroukakis, D.E. White, and S.A. Rosenberg, "Cancer regression and autoimmunity in patients after clonal repopulation with antitumor lymphocytes", *Science* **298**, 850-854 (2002).

[9] A.V. Hill, "The possible effects of the aggregation of the molecules of haemoglobin on its dissociation curves", *J. Physiol.* **40**, 4-7 (1910).

[10] D.G. Mallet and L.G. De Pillis, "A cellular automata model of tumor-immune system interactions", *J. Theor. Biol.* **239**, 334-350 (2006).

[11] S.C. Ferreira Jr., M.L. Martins, and M.J. Vilela, "Reaction-diffusion model for the growth of avascular tumors", *Phys. Rev. E* **67**, 051914 (2002).

[12] R.A. Weinberg, *The Biology of Cancer*, (Garland Science, New York) (2013).

[13] C.M. Cooper and R.E. Hausman, *The cell: a molecular approach*, (ASM. Washington, DC) (2004).

[14] C.A. Janeway, P. Travers, M. Walport, and M.J. Shlomchik, *Immunobiology*, (Garland Science, New York) (2012).

[15] E.C. Holmes, "Immunology of tumor infiltrating lymphocytes", *Ann. Surg.* **201**, 158-163 (1985).

[16] P. Érdi, *Complexity explained*, (Springer-Verlag, Berlin) 2007.

[17] V. Morillo, P. Manrique, S. Vildsola, A. Saiz, JL. Artola, and I. Bilbao, "Tricoblastoma gigante", *Actas Dermosifiliogr.* **97**, 467-469 (2006).

[18] D. Hanahan and R.A. Weinberg, "Hallmarks of Cancer: the next generation", *Cell* **144**, 646-673 (2011).

[19] A.G. Lopez, J.M. Seoane, and M.A.F. Sanjuan, "A validated mathematical model of tumor growth including tumor-host interaction, cell-mediated immune response and chemotherapy", *Bull. Math. Biol.* **76**, 2884-2906 (2014).

[20] M. Ulberg, J. Merril, and M. Jondal, "Interferon induced NK augmentation in humans: an analysis of target recognition, effector cell recruitment and effector cell recycling", *Scand. J. Immunol.* **14**, 285-292 (1981).

[21] L. Michaelis and M.L. Menten, "Die Kinetik der Invertinwirkun", *Biochem. Z.* **49**, 333-369 (1913).

[22] K.A. Johnson and R.S. Goody, "The original Michaelis constant: translation of the 1913 Michaelis-Menten paper", *Biochemistry* **50**, 8264-8269 (2011).

[23] G.E. Briggs and J.B.S. Haldane, "A note on the kinematics of enzyme action", *Biochem. J.* **19**, 338-339 (1925).

[24] C.Y. Slaney, M.H. Kershaw, and P.K. Darcy, "Trafficking of T cells into tumors", *Cancer Res.* **74**, 7168-7174 (2014).

# Chapter 5
# The kinetics of tumor lysis

*"It has been observed that missiles and projectiles describe a curved path of some sort; however, no one has pointed out the fact that this path is a parabola."*

-Galileo Galilei (1564-1642)

In the previous chapter we saw the usefulness of the enzymatic conceptual framework to describe the interactions of cells. We modified the fractional cell kill of tumor cells by T cells, imposing the condition that the velocity of tumor cell lysis must remain bounded for an increasing tumor cell population. Using the chemical kinetics framework as a metalanguage, we derived the mathematical function analytically, so that now the parameters have a clear biological significance. In the present chapter, we further explore this mathematical expression by examining the different limits that it provides. To reproduce also the time series as well as the lysis curves, we introduce one last rearrangement, which we believe makes it theoretically more conspicuous.

## 5.1 Introduction

The oversimplification of cancer as the growth of an independent subset of rebel mutated cells within a tissue presents great difficulties explaining tumor development [1, 2]. The relative importance of the dynamics at the tissue level, represented by the interactions of the tumor cells with their environment, compared to the role played by mutations, is still a subject of intense debate [3, 4]. The tumor microenvironment includes stromal cells (*e.g.* immune cells, fibroblasts or endothelial cells), the

extracellular matrix, and signalling molecules such as cytokines or growth factors. The particular cellular and molecular mechanisms, as well as their role in tumor development, are complex and not sufficiently well understood [5]. Even though all of them might prove to be important in the fight against cancer, immunotherapy is lately focusing great attention. Probably, this is because the immune system is better known and has evolved for centuries to neatly destroy threatening foreign organisms in our body. Therefore, there is evidence and hope that it can be trained to effectively destroy tumor cells, which originate in the body, as well. However, given the complexity of biological systems and the ubiquity of nonlinearity at all scales, it is hardly believable that this task can be rigorously achieved without the guidance of mathematical models. Positively, these models, together with the experimental ones, might provide the guiding principles that biologists precise to unveil the counter-intuitive nature of the complex interactions among cancer cells and their environment during the evolution of tumors. This, in turn, might permit clinicians to design better treatments for the vast variety of cancers [6].

In the context of tumor-immune interactions, it is worth and interesting to analyse the potential that enzyme kinetics offers [7, 8]. Enzymatic reactions can be viewed in an abstract manner as an asymmetric interaction between two entities, one being rather passive (the substrate) and the other being rather active (the enzyme). When these two entities make contact, the latter affects the former transforming it into some other entity (the product). Thus, an enzymatic reaction can be casted in three steps: the formation of a complex from the two parts, a subsequent transformation of the passive part by its active counterpart and their final dissociation. As long as these conditions are fulfilled, there is no general reason preventing us to use this conceptual framework not only at the chemical scale, but also at the cellular scale and, perhaps, even at higher scales. For example, the growth of microorganisms in the presence of a limited substrate obeys the Michaelis-Menten kinetics [9]. In ecology, the intake rate of a consumer as a function of the density of preys is also a kinetics of this type [10]. In all these cases, whenever there is a considerable imbalance between the number of active and passive elements, saturation occurs. This is due to the limited capacity of the active part to interact with a sufficiently high number of elements of the passive counterpart. Note that this is also true in the reverse direction, since the passive elements can not interact with an enormous number of active elements for short times. In other words, interactions occur locally and require some time.

## 5.2 Tumor lysis kinetics

A mathematical expression describing the velocity at which a population of cytotoxic cells lyse a tumor was derived in the previous chapter using the Michaelis-Menten kinetics as the modelling framework describing tumor-immune interactions at the cellular scale [11]. According to this model, the process of tumor cell lysis is equivalent to an enzymatic reaction where the tumor cells correspond to the substrate and the immune cells correspond to the enzyme. An schematic representation of

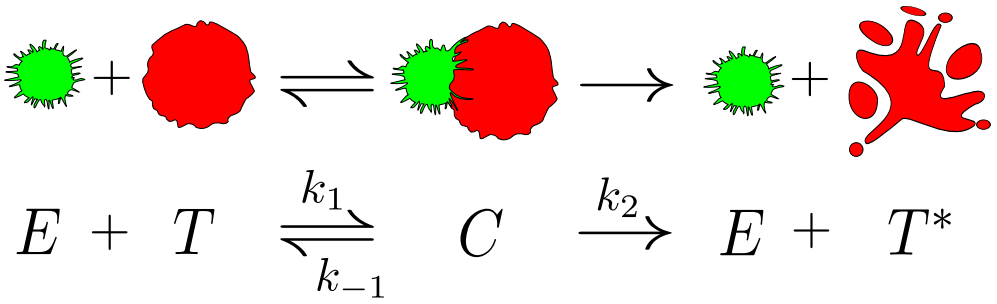


**Figure 5.1. The cell-mediated immune response as an enzymatic reaction**. An interaction between an activated lymphocyte $E$, colored in green, and a tumor cell $T$, painted in red. When the lymphocyte identifies the tumor cell these two cells form a complex. The result of the interaction is the initial T-cell and an apoptotic tumor cell $T^*$. This cellular interaction is similar to an enzymatic chemical reaction, where the tumor cell plays the role of the substrate and the T-cell acts as an enzyme.

such a cellular reaction can be seen in Fig. 5.1. When a T-cell identifies a tumor cell through the recognition of antigens, these two cells form complexes. As a result, apoptosis is induced and a dead tumor cell is produced. However, some of the assumptions that lead to the Michaelis-Menten kinetics, such as a high substrate concentration compared to the enzyme concentration, or high values of the Michaelis constant compared to the enzyme concentration, are not met in the present case. To reproduce experiments, the constant rates of the reaction require dependence on the number of effector cells, in such a manner that saturation of the velocity is also found for increasing numbers of the effector cells. As previously stated, saturation occurs in both directions. The differential equation [12] describing the velocity at which the tumor cells are destroyed is $\dot{T} = -K(E,T)T$, with $K(E,T)$ the fractional cell kill, which can be written as

$$K(E,T) = d\frac{E^\lambda}{sT + E^\lambda}, \tag{5.1}$$

where $T$ and $E$ represent the number of tumor cells and immune cells respectively. The parameters $d$ and $\lambda$ depend on the tumor geometry. Less spherical tumors lead to higher values of these parameters. On the other hand, the parameter $s$ is related to the intrinsic ability of the cytotoxic cells to recognize and destroy their adversaries. Smaller values of this parameter are related to more effective immune cells. Thus, the velocity at which a tumor is lysed is given by

$$\dot{T} = -d\frac{E^\lambda}{sT + E^\lambda}T. \tag{5.2}$$

This equation states that the velocity at which a tumor is lysed by a population of cytotoxic cells becomes faster as this immune cell population increases. However, once the vicinity of the tumor is vastly occupied with several layers of immune cells, the remaining immune cells are not in contact with their tumor adversaries, and

saturation is attained. Even in a situation in which the tumor cells are considerably bigger than the immune cell, and several immune cells are in contact with a single tumor cell, the velocity at which the tumor is lysed is not substantially enhanced. Accordingly, the saturation process depends on the size of the tumor. The number of immune cells for which the fractional cell kill $K(E,T)$ is half of its maximum $d$ increases monotonically with the tumor burden. Concerning the tumor cell population, also faster lytic velocity occurs for bigger tumors, but again saturation befalls. Now the reason is that for a big tumor cell population compared to the immune cell population, at some point the addition of tumor cells can not increase the velocity at which the tumor is lysed, since these added tumor cells are not in contact with immune cells, which are already busy lysing some of the initial tumor cells.

It is worth and interesting to carefully examine the different limits that this equation possesses (see Fig. 5.2). For a fixed number of immune cells $E_0$, when the immune cell population is small compared to the tumor size ($E_0^\lambda \ll sT$), the tumor cell population is reduced at a constant velocity

$$\dot{T} = -dE_0^\lambda/s. \tag{5.3}$$

This *linear decay* makes perfect sense if we bear in mind the extreme situation in which there is only one lymphocyte fighting a tumor of a certain size. Ideally, if it takes the immune cell approximately one hour to lyse a tumor cell, then the velocity of the decay is simply one tumor cell per hour. Even though this is fairly obvious, in Fig. 5.3 we show the random walk of a lymphocyte lysing a tumor that occupies a square domain, at one cell per hour. In practice, the velocity clearly depends on the intrinsic ability of the cytotoxic cell $s$ to lyse the tumor cells and also on the tumor morphology $\lambda$ and $d$. On the other hand, when the immune cell population is high enough compared to the tumor cell population ($E_0^\lambda \gg sT$), Eq. (5.2) yields an *exponential decay*

$$\dot{T} = -dT. \tag{5.4}$$

Now, the scenario corresponds to the case in which the tumor is totally covered with effector cells. For the sake of simplicity, we consider a tumor spheroid [13]. At each step the immune cells lyse a layer of tumor cells, and the radius of the spheroid decreases. In the next round another layer is eliminated but, since the tumor has smaller radius, so it does the length of this second layer. Therefore, the velocity decreases as the tumor is gradually erased. Nevertheless, note that for a three-dimensional solid tumor the reduction occurs in surface while the tumor is distributed in volume, suggesting that the decay should be slower than exponential.

In Ref. [12] it was demonstrated that Eq. (5.2) reproduces accurately the values of the lysis after some fixed time versus different values of the effector-to-target ratio as initial conditions. However, here we show that it is unable to reproduce the time series of the tumor decay faithfully. A mathematical function which is good at reproducing the time series of the tumor decay can be derived in the following manner. Assume that a two-dimensional tumor with the shape of a disk is plainly

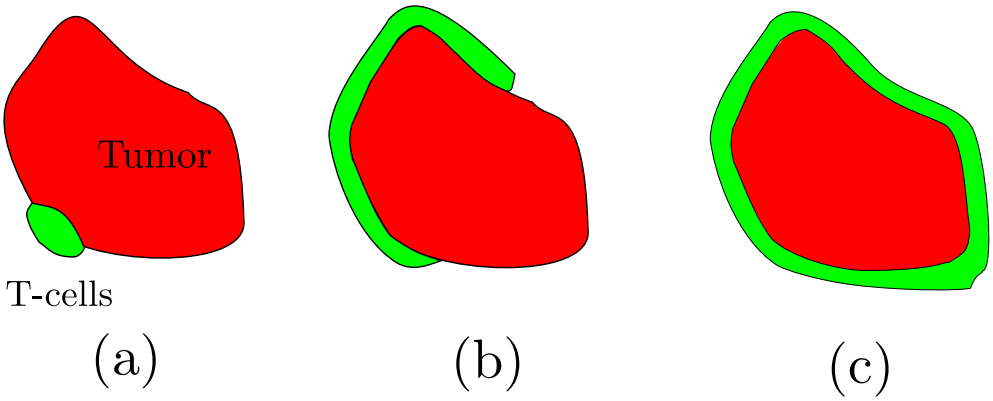


**Figure 5.2. The limits of the fractional cell kill**. (a) A small immune cell population facing a big tumor. In this limiting situation the decay of the tumor is rather linear, as shown in Eq. (5.3). (b) The intermediate case in which a considerable part of the tumor is covered with immune cells. (c) A tumor which surface is totally covered with immune cells. In this extreme case the velocity of the decay can be approximated by a power-law decay, as shown in Eq. (5.6).

covered with immune cells. As shown in Fig. 5.4(a), a layer of tumor cells is erased by the immune cells at each step, like peeling an onion. If we write the radius of the disk at the $n$-th step as $R_n$, and the diameter of a cell as $\Delta R$, the dynamics of the tumor can be represented by a very simple map in the form $R_{n+1} = R_n - \Delta R$. Since the area of a disk is related to the radius through $A = \pi R^2$, a direct substitution yields the map $A_{n+1} = A_n + \pi \Delta R^2 - 2\pi^{1/2} \Delta R A_n^{1/2}$. If we consider that the immune cells lyse at a constant rate, then $\Delta R = c\Delta t$, and we obtain

$$\frac{\Delta A_n}{\Delta t} = \pi c^2 \Delta t - 2\pi^{1/2} c A_n^{1/2}. \tag{5.5}$$

Finally, assuming that the cell density of the tumor is approximately constant, that the tumor is big enough so that the time intervals can be considered infinitesimal and defining a decay constant as $d = 2\pi^{1/2} c$, we obtain the differential equation

$$\dot{T} = -dT^{1/2}. \tag{5.6}$$

More simply, if we consider a disk of area $A = \pi R^2$ and assume that the velocity at which the radius decreases is constant $\dot{R} = -c$, with $c > 0$, we can write

$$\frac{dA}{dt} = 2\pi R \frac{dR}{dt} = -2\pi^{1/2} c A^{1/2}. \tag{5.7}$$

If the tumor has a more sophisticated geometry, we can still apply Eq. (5.6) under appropriate assumptions. Suppose that a layer of a tumor with complex geometry is erased by the immune system. At every step along the tumor decay, we can associate to the tumor mass a disk of equal area. Thus, the decay of the tumor is again equivalent to a sequence of disks with decreasing radii. Now, however, we can

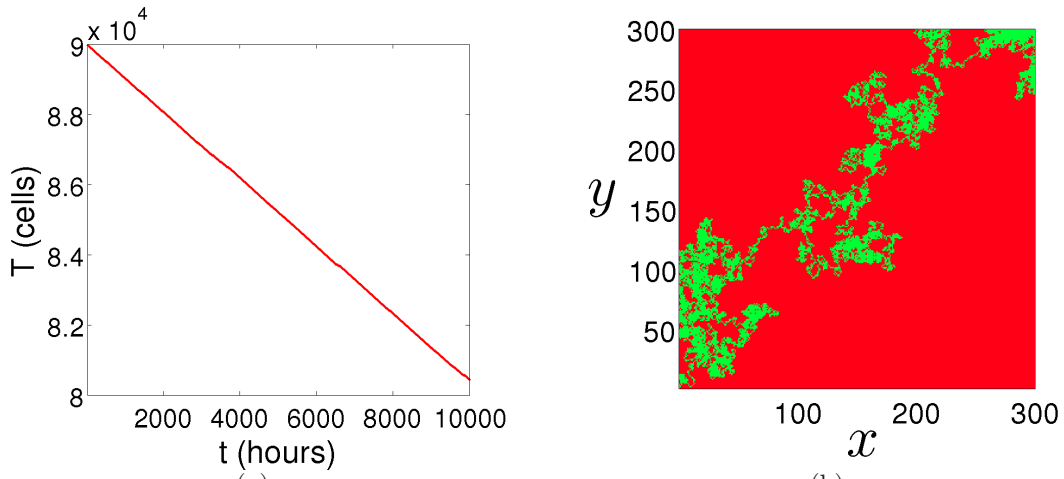


(a) (b)

**Figure 5.3. A single T-cell wandering inside a tumor, destroying one tumor cell per hour**. (a) The linear decay of the tumor. (b) The random walk described by a lymphocyte (green) inside a quadrilateral domain occupied by tumor cells (red). The green path are lysed cells.

not guarantee that the radius decreases a fixed value at each step. To demonstrate this statement, it suffices to consider a pair of counterexamples. A very simple one arises if we consider a tumor with the shape of an ellipse. Assuming that the semi-major axis $a$ and the semi-minor axis $b$ both decrease at a constant rate $\dot{a} = \dot{b} = -c$, we find

$$\frac{dA}{dt} = \pi \frac{da}{dt} b + \pi a \frac{db}{dt} = -\pi^{1/2} c[(1-e^2)^{1/4} + (1-e^2)^{-1/4}] A^{1/2}, \tag{5.8}$$

where $e = e(t)$ is the eccentricity of the ellipse, which changes over time. Note that for $e = 0$ we recover Eq. (5.7).

Things get even more complicated if we take an initial tumor which is not a convex set, as the one depicted in Fig. 5.4(b). Even in the case in which all the immune cells act synchronously and are equally effective, the topology of the tumor might change during the process of lysis, becoming disconnected. Assuming equal decay rates $d$ and using Eq. (5.6), it is straightforward to verify that the total area of two tumors with the shape of a disk does not decay as a whole with the same velocity than that of a single tumor with such shape and equal total area. The two small tumors decay faster, because the ratio between the perimeter and the enclosed area is larger. Analytically, this is simply a consequence of the nonlinear nature of Eq. (5.6). Therefore, we designate the mean value of the variations of the radius of such sequence of disks as $\Delta R$. Then, we write the variation of the radius as $\delta_n \Delta R$, where $\delta_n$ accounts for the deviations with respect to the mean value, that must be bounded. The map is now $R_{n+1} = R_n - \delta_n \Delta R$ and the area goes as $A_{n+1} = A_n + \pi \delta_n^2 \Delta R^2 - 2\pi^{1/2} \delta_n \Delta R A_n^{1/2}$. Making the same assumptions as

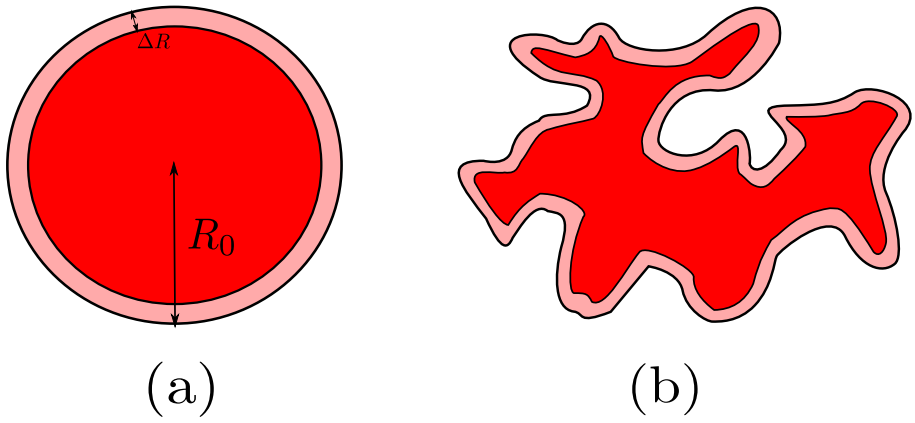


**Figure 5.4. Two tumors with a destroyed layer.** (a) A tumor with the shape of a disk and initial radius $R_0$. At each step the immune system erases a layer (light red), reducing its radius by an amount $\Delta R$. (b) Again a tumor with a destroyed layer, but exhibiting a more complex geometry.

in the previous case, the final result is

$$\dot{T} = -d(t)T^{1/2}, \tag{5.9}$$

where $d(t) = 2\pi^{1/2}c\delta(t)$, and $\delta(t)$ a function which takes into account the deviations from Eq. (5.6) due to the change in morphology and connectedness at each step. In Sec. 5.4 we show that these deviations due to a complex morphology are small for the connected tumors here examined. Therefore, the *parabolic decay* represented in Eq. (5.6) works well at reproducing the decay of the tumors in the limit in which they are completely surrounded by immune cells, as long as they are not formed by disconnected pieces and their shape does not differ too much from a spherical shape. In Sec. 5.5 we derive an explicit relation between $\delta(t)$ and the geometrical properties of the tumor. Also a more general differential equation representing the decay of a two-dimensional surface with a non-trivial shape and topology is developed.

## 5.3 The cellular automaton model

The cellular automaton model previously described is now used to study the velocity at which the tumors decay. As a reminder, an schematic representation of the CA is once more depicted in Fig. 5.5.

As in the previous chapter, the simulations are carried out in two successive steps. The first is devoted to the growth of the tumors. Then the immune cells are placed in the immediate domain of the tumor and we let the system evolve. We are only interested in the dynamics of the lysis of the tumor. Thus, during this second step, we freeze the tumor growth, as if the tumor cells had been irradiated. Since now we focus only on the lysis of the tumor, some restrictions in the use of the cellular automaton deserve notification. The decay laws here investigated, given by Eq. (5.4) and Eq. (5.6), are deterministic and valid in the limit in which the tumor

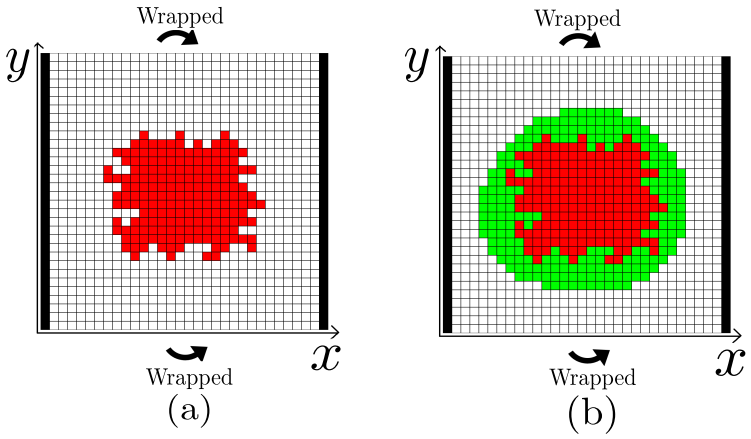


**Figure 5.5. The cellular automaton.** (a) A grid representing the cellular automaton during the growth of a tumor. The tumor cells are shown in red, while the remaining spots are occupied by healthy cells. The vertical black stripes in the boundary of the square domain represent the vessels from which nutrients diffuse, and periodic boundary conditions are considered in the remaining part of the boundary. (b) Once a tumor is grown up to a certain size, immune cells are placed around the tumor (green) and the lysis of the tumor is registered until it is totally eradicated. During this second step, the dynamics of the tumor is freezed, since we are only interested in the lysis.

is totally covered by immune cells. Therefore, we assume that, as the successive layers of the tumor are lysed, the immune cells advance quickly towards the tumor. In our cellular automaton this can be guaranteed when the immune cells are placed isotropically covering the whole tumor through the mechanism of recruitment. We insist that it is only in this limiting situation that we can make use of the cellular automaton for comparison with Eq. (5.6).

After placing the cells as shown in Fig. 5.5(b), those immune cells that are far from the tumor become inactivated (disappear from the region). As a result, what we see are several outer layers of immune cells lysing the tumor. However, when a few immune cells are placed at a particular location in the boundary of the tumor, stochastic effects associated to T-cell inactivation and recruitment impose an appreciable deviation from the expected linear decay. Nevertheless, the tendency to linearity is observed as the initial number of effector cells becomes smaller.

## 5.4 The effect of morphology

We use the cellular automaton model to inspect three different morphologies of two-dimensional tumors: a spherical tumor, a papillary tumor and a filamentary tumor. The tumors generated with the cellular automaton are shown in Fig. 5.6. We place these three tumors inside a circumference and, for each of them, we repeat the experiments for several initial conditions. To this end, we fill with immune cells the remaining space of the circumference for increasing angles, as depicted in Fig. 5.7.

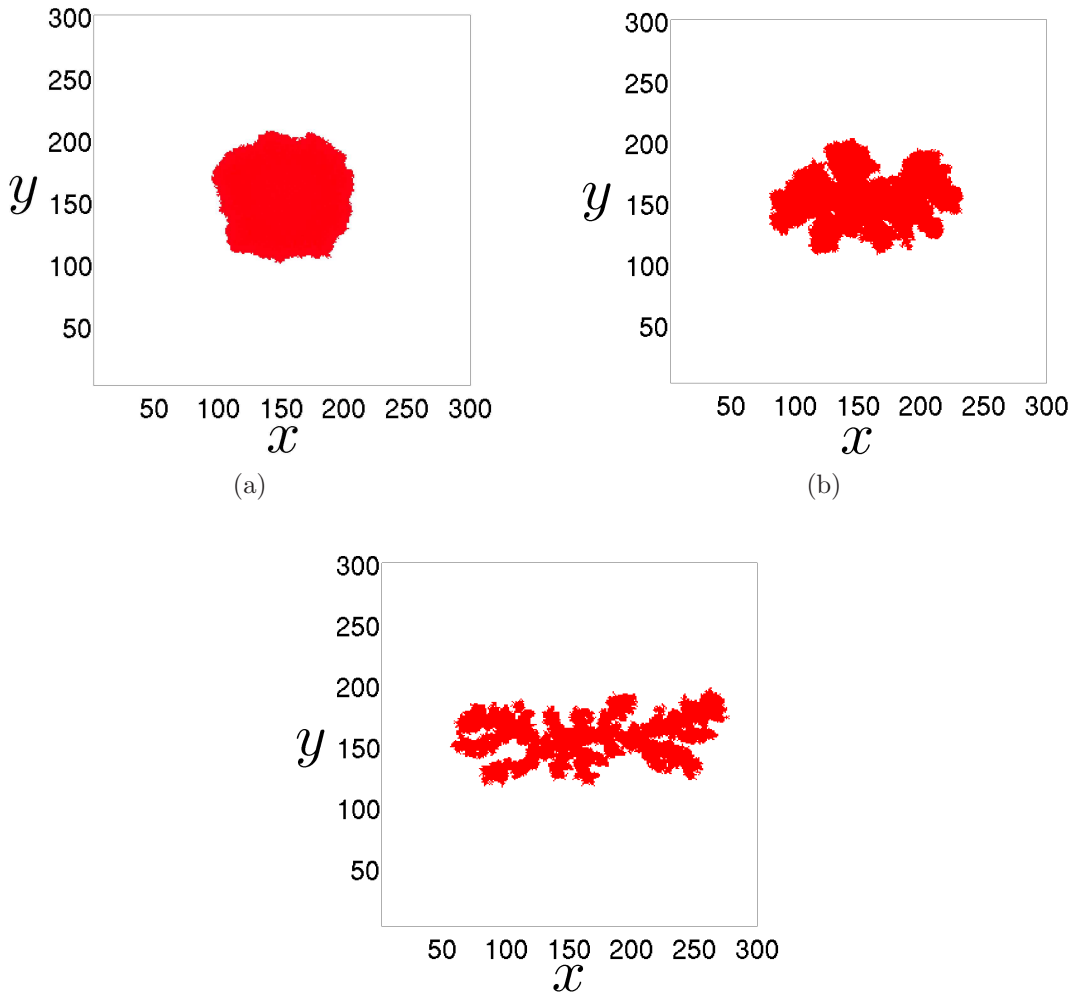


**Figure 5.6. Three tumors grown by iteration of the cellular automaton.** A grid of $n \times n$ cells, with $n = 300$ has been used. We disregard necrosis and motility of tumor cells by setting the parameters, $\theta_{nec} = 0$ and $\theta_{mig} = \infty$. In all the three cases $\lambda_M = 10$. (a) A spherical tumor obtained for parameter values $\alpha = 2/n$, $\lambda_N = 25$ and $\theta_{div} = 0.3$. (b) A papillary tumor obtained for parameter values $\alpha = 4/n$, $\lambda_N = 200$ and $\theta_{div} = 0.3$. (c) A filamentary tumor obtained for parameter values $\alpha = 8/n$, $\lambda_N = 270$ and $\theta_{div} = 0.3$. These three tumors have grown up to approximately 9100 cells.

The time series representing the decay of the tumors are shown in Fig. 5.8. As explained in Sec. 5.2, we see a tendency towards linearity as the tumor is initially less covered with immune cells. Even the curvature is inverted for such small values of the initial angle, but this is surely a consequence of recruitment in the cellular automaton. Note also that the stochastic effects are more noticeable when the number of initial effector cells is low.

The cases in which the tumors are totally covered with immune cells as initial

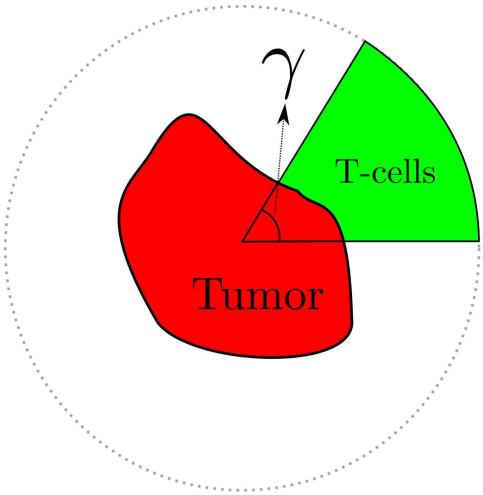


**Figure 5.7. How the initial conditions are set to investigate the lysis of the different tumors.** The tumors are inscribed in a circumference and immune cells are placed in the surroundings for different angles $\gamma$. Since those cells that are not close to the tumor outest layer become inactivated during the first steps of the CA, small values of the angle correspond to the case shown in Fig. 5.2(a), while the case $\gamma = 2\pi$ is related to Fig. 5.2(c).

conditions ($\gamma = 2\pi$) are fitted to the equation $\dot{T} = -dT^{\nu}$ and also to $\dot{T} = -dT$, to elucidate which type of decay represents better the tumor cell lysis. The parameters are obtained through a least square fitting method, and are listed in Table 5.1. As can be seen in Fig. 5.9, the exponential decay is much worse at describing the time evolution of this dynamical system. Moreover, the value of $\nu$ that gives the best fit to the power-law decay is equal to one half for the papillary and the filamentary tumors, and practically one half for the spherical case. The agreement is striking and, as previously predicted, the fluctuations are higher when the tumors exhibit a more complex geometry. Concerning the parameter $d$, we see that more branchy tumors display higher values. The explanation for this behavior is evident, since the higher it is the contact surface of a tumor, the more cells that can interact with it and the faster the speed at which it is lysed. This is in conformity with results obtained in Ref. [12], where it was claimed that tumors with an spherical symmetry are harder to lyse. For a rigorous mathematical demonstration of this statement we refer the reader to Sec. 5.5. The crucial concept here is the accessibility that the immune cells have to the tumor cells.

Thus, we have demonstrated that in the limit in which a solid tumor is totally covered with immune cells, the velocity at which it decays is slower than exponential. This fact requires modifying Eq. (5.2) so that such limit is attained. The arguments employed in Sec. 5.2 can be perfectly applied to tumors that live in a three-dimensional space. If we recall that saturation of the velocity must be attained in the limit of infinitely big tumors, we propose that the kinetics of tumor lysis in

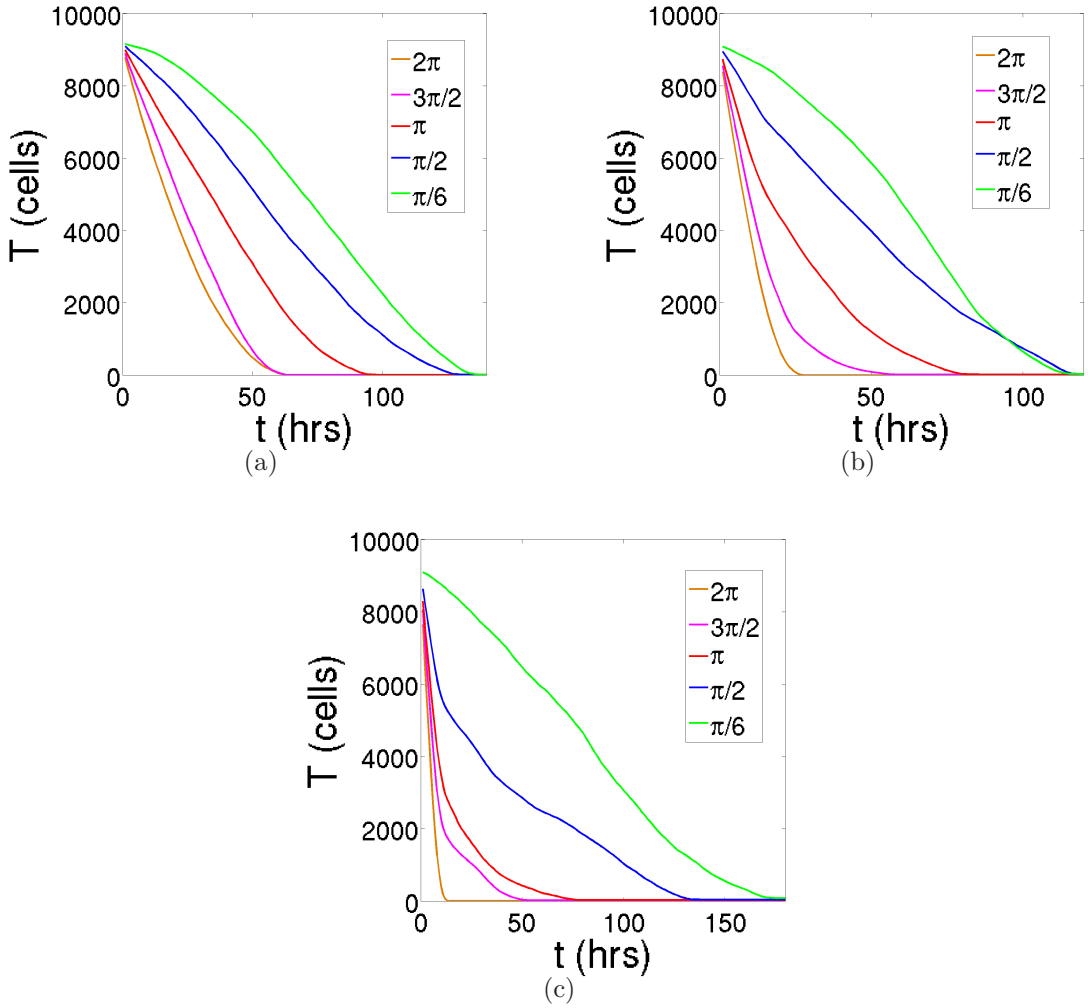


**Figure 5.8. The decay of the three tumors for different initial conditions.** The immune cells are placed in the neighbourhood of the tumors for values of the angles $\gamma = \{\pi/6, \pi/2, \pi, 3\pi/2, 2\pi\}$ and we iterate the CA. The CA actions corresponding to the lymphocytes have parameter values $\theta_{lys} = 0.3$, $\theta_{rec} = 0.5$ and $\theta_{inc} = 0.5$. The tumor cells dynamics has been frozen, and the parameters related to the diffusion of nutrients are the same as those appearing in previous figures. (a) The decay of the spherical tumor for the different initial conditions. (b) The decay of the papillary tumor for the different initial conditions. (c) The decay of the filamentary tumor for the different initial conditions. As less immune cells are placed in the vicinity of the tumors as initial conditions (from $\gamma = 2\pi$ to $\gamma = \pi/6$), the power-law decay transforms into a more or less linear type of decay.

the cell-mediated immune response to tumor growth is given by

$$\dot{T} = -d\frac{E^{\lambda}}{sT^{\nu} + E^{\lambda}}T^{\nu}, \tag{5.10}$$

where the exponent $\nu$ depends on the dimension of the space, the morphology of the tumor and its connectedness. For realistic, connected and rather spherical solid

| Power-law decay | | | |
|---|---|---|---|
| Parameter | Units | Value | Description |
| $d$(s) | cell$^{1/2}$ hr$^{-1}$ | 1.34 | Rate of decay |
| $d$(p) | cell$^{1/2}$ hr$^{-1}$ | 3.36 | Rate of decay |
| $d$(f) | cell$^{1/2}$ hr$^{-1}$ | 7.31 | Rate of decay |
| $\nu$(s) | | 0.49 | Exponent |
| $\nu$(p) | | 0.50 | Exponent |
| $\nu$(f) | | 0.50 | Exponent |
| Exponential decay | | | |
| Parameter | Units | Value | Description |
| $d$(s) | hr$^{-1}$ | 0.04 | Rate of decay |
| $d$(p) | hr$^{-1}$ | 0.10 | Rate of decay |
| $d$(f) | hr$^{-1}$ | 0.21 | Rate of decay |

**Table 5.1. The parameter values of the decay**. The parameter values of the power-law decay $\dot{T} = -dT^{\nu}$ and the exponential decay $\dot{T} = -dT$, to which the data of the cellular automaton are fitted by means of a least-squares fitting method. We see that as the geometry of the tumor changes from spherical (s) through papillary (p) to filamentary (f), the parameter $d$ increases. However, the value of $\nu$ is almost the same for the three geometries.

tumors we have $\nu = 2/3$, with the 2 standing for surface, and the 3 for volume. However, in those cases in which the tumor is very disconnected and the immune cells are well mixed with the tumor cells, as for instance in haematological cancers or solid tumors profusely infiltrated with lymphocytes, $\nu = 1$ should be used. The exponential decay arising in the limit $E_0^{\lambda} \gg sT$ would be then interpreted from a stochastic point of view, regarding the process as a Poisson process. Indeed, not all the immune cells have the same capacity to recognize a tumor cell, neither they act synchronously. In this case, the decay of a tumor does not differ substantially from other types of decay phenomena, as for example one-decay processes in radioactivity. For intermediate situations, the exponent $\nu$ will take a value between 2/3 and 1.

## 5.5 The decay of an arbitrary tumor

We start with a convex set in $\mathbb{R}^2$, and assume that the boundary of such set is differentiable. We consider a solid tumor that is plainly covered with activated lymphocytes, in such a manner that the outmost layer of the tumor is erased at each step. Given a tumor with a particular boundary, we can approximate the T cells by small disks of diameter $\Delta R$ placed on such boundary. Then, perhaps, the most reasonable assumption is to consider that these cells reduce the surface in the normal direction to the boundary of the tumor, as depicted in Fig. 5.10.

At each step $n$ of the process of lysis, the boundary can be represented by a parametric curve in the form $\gamma_n(\lambda) = (x_n(\lambda), y_n(\lambda))$, being $\lambda$ the parameter used in such representation. Then, the decay can be mathematically expressed as a sequence

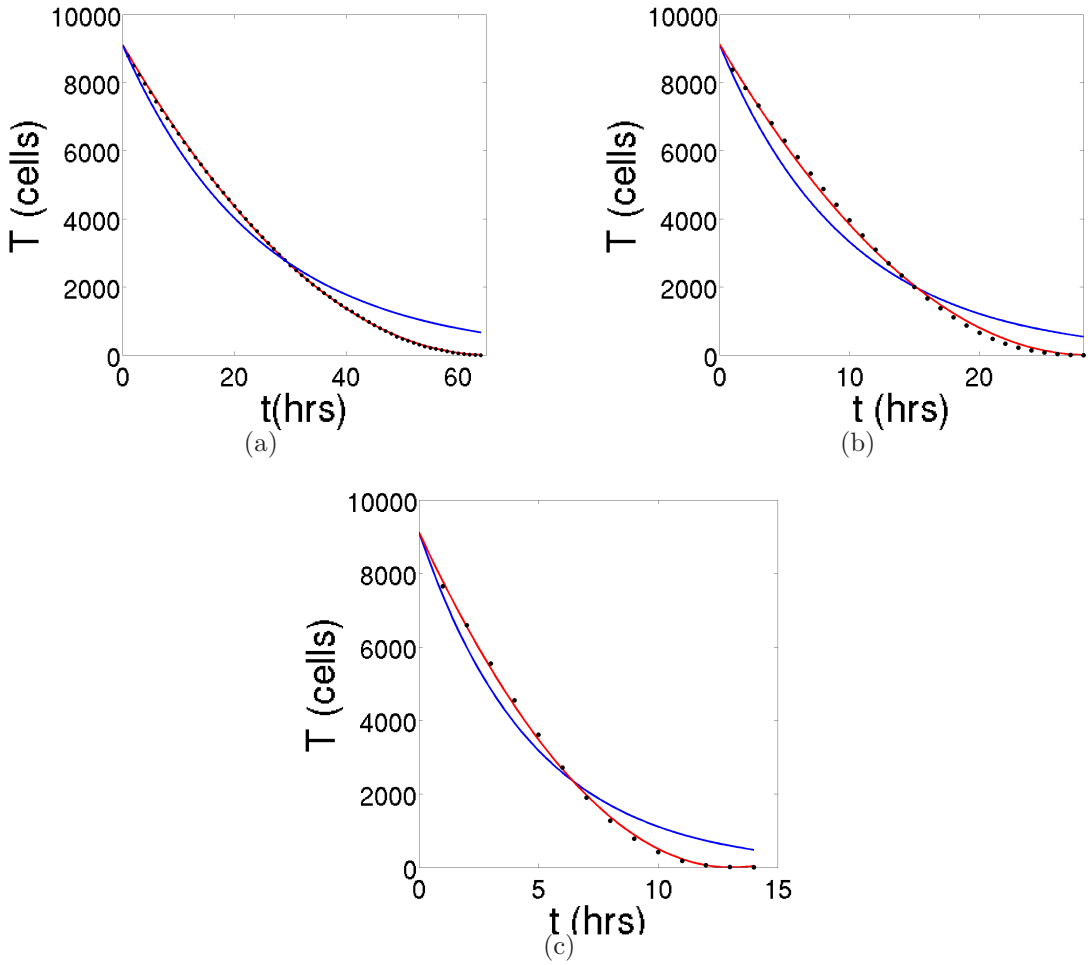


**Figure 5.9. The decay of the three tumors for $\gamma = 2\pi$.** We have iterated the cellular automaton in the limit in which the tumors are totally covered with immune cells. The results are fitted to a power-law decay $\dot{T} = -dT^{\nu}$, shown in red, and an exponential decay $\dot{T} = -dT$, shown in blue, to elucidate which type of decay represents better the velocity with wich the tumors shrink. (a) The decay of the spherical tumor. (b) The decay of the papillary tumor. (c) The decay of the filamentary tumor. In all the cases a power-law decay with an approximate value of $\nu = 1/2$ fits much better the results of the CA. The exact values are listed in Table 5.1.

of planar curves

$$\gamma_{n+1}(\lambda) = \gamma_n(\lambda) + \Delta R p_n(\lambda), \tag{5.11}$$

where $p_n(\lambda)$ is the normal unitary vector to $\gamma_n(\lambda)$. Recursive relations for the tangent and the normal vectors have to be found using the Frenet-Serret formulas, and a sequence of planar surfaces enclosed by these curves has to be defined. Finally, the element of area can be derived from the metric, its integral computed to obtain an equation for the variations of the area at each step, and a continuum limit worked out. These computations are very extensive, involve complicated integrals depending

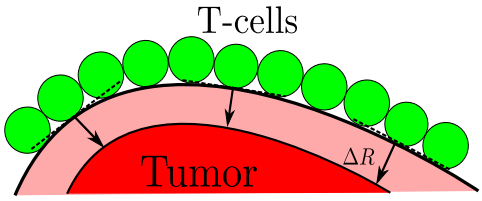


**Figure 5.10. Lymphocytes on the surface of a tumor.** Assuming that the tumor (red) has a smooth boundary, the lymphocytes (green) erase a layer of the tumor (light red) in the normal direction to its boundary, at each step.

on the curvature at each step, and do not allow to draw clear conclusions.

Another possibility is to use polar coordinates, and consider that the initial boundary of the set can be represented through the curve $R_0(\theta)$. The area enclosed by this initial curve is computed as

$$A_0 = \frac{1}{2}\int_0^{2\pi} R_0^2(\theta)d\theta. \tag{5.12}$$

Now, we introduce the dependence on time, so that the initial area decreases in all directions at constant velocity. Mathematically, we have

$$A(t) = \frac{1}{2}\int_0^{2\pi} R^2(\theta,t)d\theta, \tag{5.13}$$

with the radius of the set decreasing with constant velocity in every direction, *i.e.*,

$$\frac{\partial R}{\partial t} = -c. \tag{5.14}$$

Note that now the surface is reduced in the radial direction, which is not normal to the boundary, except for a spherical tumor. Therefore, this approximation is worse than the first suggested. Nevertheless, it allows to derive continuous equations and draw neat conclusions in a very simpler manner. Generally, it takes a T cell around fourty minutes to lyse a tumor cell. If we approximate the diameter of a cell to $10\mu$m, the value of $c$ is around $10\mu$m/hr. Integrating Eq. (5.14) we can obtain the equation of motion representing the decay of the radius, which can be written in a simple manner as $R(\theta,t) = R_0(\theta) - ct$. This equation is only valid as long as the radius does not vary too much in different directions, compared to its size. Otherwise, the radius in a particular direction $R(\theta,t)$ could become zero (even negative) as other directions are still being erased. Thus, we assume that the condition $R_0(\theta) \gg |R_0'(\theta)|$ holds. Differentiating Eq. (5.13) with respect to the time yields

$$\dot{A}(t) = -c\int_0^{2\pi} R(\theta,t)d\theta. \tag{5.15}$$

Substituting the equation of the radius in Eq. (5.15) leads to

$$\dot{A}(t) = -c\int_0^{2\pi} R_0(\theta)d\theta + 2\pi c^2 t. \tag{5.16}$$

Under the condition previously imposed, the integral appearing in Eq. 5.16 is approximately the length of the boundary of the initial set $L_0$. Thus, the differential equation governing the decrease of a convex set with a non-spherical shape can be approximated by

$$\dot{A}(t) = -cL_0 + 2\pi c^2 t. \tag{5.17}$$

It is straightforward to integrate this equation, if we consider the initial condition given by $A(0) = A_0$. The result is

$$A(t) = A_0 - cL_0 t + \pi c^2 t^2. \tag{5.18}$$

This equation represents a uniformly accelerated motion [14], where the initial velocity is $v_0 = -cL_0$, while the acceleration is $a = 2\pi c^2$. In other words, the decay is *parabolic*. Intuitively, if the radius decays linearly, the area does it quadratically. The time $\tau$ at which the tumor is totally erradicated can be computed by setting $A = 0$, which yields

$$\tau = \frac{L_0}{2\pi c}\left(1 - \sqrt{1 - 4\pi\frac{A_0}{L_0^2}}\right). \tag{5.19}$$

Note that the isoperimetric inequality [15] imposes $4\pi A_0 \leq L_0^2$ for any planar surface, with the inequality saturating for a disk. Thus, tumors with a spherical shape are the hardest to lyse. Since for a disk we have $L_0 = 2\pi^{1/2} A_0^{1/2}$, substitution in Eq. (5.18) yields

$$A(t) = \left(A_0^{1/2} - \frac{1}{2}(2\pi^{1/2}c)t\right)^2. \tag{5.20}$$

This function is the solution to the differential equation $\dot{A} = -(2\pi^{1/2}c)A^{1/2}$, obtained in Sec. 5.2. However, for more complex morphologies this power-law function does not rigorously hold. We can obtain the deviation from this type of decay for a complex morphology. As shown in Sec. 5.2, the Eq. (5.15) can be written as

$$\dot{A}(t) = -d(t)A^{1/2}, \tag{5.21}$$

where

$$d(t) = \sqrt{2}c\frac{\int_0^{2\pi} R(\theta,t)d\theta}{\sqrt{\int_0^{2\pi} R^2(\theta,t)d\theta}} = 2\pi^{1/2}c\sqrt{\frac{L^2(t)}{4\pi A(t)}}. \tag{5.22}$$

Again, we have assumed that the variations of the radius with respect to the angle are small compared to the size of the radius for all times. Therefore, the function $\delta(t)$ presented in Sec. 5.2 is approximated as

$$\delta(t) = \sqrt{\frac{L^2(t)}{4\pi A(t)}}. \tag{5.23}$$

A three-dimensional version of the inverse of this parameter has been called the sphericity [16]. For a planar set, the sphericity measures the deviations of a geometrical objet from the spherical shape, in terms of the ratio between the area $A$

enclosed by a curve and the length of its squared perimeter $L$[1]. It takes a maximum value of one for a disk, and it would take a value of zero for a fractal closed curve, as for example the Koch snowflake, which is made out of three Koch curves [17] placed on the sides of an equilateral triangle. However, we have assumed differentiability.

If the tumor is not convex, then it might occur that during the process of lysis it becomes disconnected. For a disconnected tumor the decay law can also be obtained following the same recipe. But now we have to be more careful, since once a piece has been eliminated, this piece does not contribute anymore to the decay. This difficulty can be circumvented by introducing Heavyside step functions. The decay of a disconnected tumor formed by $N$ pieces can be approximated by

$$A(t) = \sum_{i=1}^{N} \left(1 - \Theta(t - \tau_i)\right) A_i(t), \tag{5.24}$$

where each function $A_i(t)$ is like Eq. (5.18) and $\tau_i$ can be computed from equation Eq. (5.19). The time it takes a disconnected tumor to decay is $\tau = \max \tau_i$.

Finally, it may well happen that the velocity with which the radius decreases is not isotropic, varying for different angles. Or that the velocity at which the radius decreases is not constant in time. In such a case, the best we can do is to provide a partial differential equation relating the variations of the area in time and angle and those of the radius in time

$$\frac{\partial^2 A}{\partial t \partial \theta} = R \frac{\partial R}{\partial t}. \tag{5.25}$$

Given $R(\theta, t)$, this inhomogeneous second order linear PDE can be integrated to obtain the variations of the area in space and time. For example, we can consider that the velocity with which the radius decreases is anisotropic but constant in time. Then $R(\theta, t) = R_0(\theta) - c(\theta)t$, and again a parabolic decay results, but with a velocity and an acceleration averaged over the different angles.

## 5.6 Discussion

This chapter demonstrates that the kinetics governing the lysis of a two-dimensional solid tumor that is not infiltrated with lymphocytes ranges from a linear decay to a parabolic decay. When infiltration occurs the decay ranges from linear to exponential. The linear decay corresponds to small values of the effector-to-target ratio as initial conditions, while the parabolic decay represents a tumor that is widely surrounded by immune cells. Intermediate situations are governed by Eq. (5.10), which is a crossed Hill function for both the tumor and the immune cell populations. The two exponents in this function are both smaller or equal than one, representing the non-cooperative effects among tumor cells and immune cells that arise in the

[1] We prevent the reader from trying to relate the Eq. (5.7) to Eq. (5.23) to obtain the perimeter of an ellipse in a closed form, which, as it is well known, does not exist and must be given in terms of elliptic integrals. These equations are rough approximations.

interaction as a consequence of geometry and cell crowding. To conclude this work, we also want to recall that when the immune cells are not effective recognizing the tumor cells ($s \to \infty$), a linear decay results once again. As reasoned in other works [12], a large number of immune cells that "interact" ineffectively with a tumor can be considered equivalent to a small number of immune cells interacting effectively. To demonstrate this assert mathematically, we recall that when a population of cytotoxic cells is ineffective lysing a tumor, only a fraction $f$ of such cell population interacts with it. By inserting $fE$ in Eq. (5.10), we can redefine $s/f^{\lambda}$ to be $s$ and obtain the same equation.

# References

[1] D. Hanahan and R. A. Weinberg, "Hallmarks of Cancer", *Cell* **100**, 57-70 (2000).

[2] D. Hanahan and R. A. Weinberg, "Hallmarks of Cancer: the next generation", *Cell* **144**, 646-673 (2011).

[3] C. Sonneschein and A.M. Soto, "The dead of the cancer cell", *Cancer Res.* **71**, 4334-4337 (2011).

[4] C. Sonneschein and A.M. Soto, "The aging of the 2000 and 2011 Hallmarks of Cancer reviews: A critique", *J. Biosci.* **38**, 651-666 (2013).

[5] I.P. Witz and O. Levy-Nissenbaum, "The tumor microenvironment in the post-PAGET era", *Cancer Lett.* **242**, 1-10 (2006).

[6] L. Norton, "Conceptual and practical implications of breast tissue geometry: towards a more effective, less toxic therapy", *The Oncologist* **10**, 370-381 (2005).

[7] L. Michaelis and M.L. Menten, "Die Kinetik der Invertinwirkun", *Biochem. Z.* **49**, 333-369 (1913).

[8] K.A. Johnson and R.S. Goody, "The original Michaelis constant: translation of the 1913 Michaelis-Menten paper", *Biochemistry* **50**, 8264-8269 (2011).

[9] J. Monod, "The growth of bacterial cultures", *Annu. Rev. Microbiol.* **3**, 371-393 (1949).

[10] C.S. Holling, "Some characteristics of simple types of predation and parasitism", *Can. Entomol.* **91**, 385-398 (1959).

[11] V.A. Kuznetsov, I.A. Makalkin, M.A. Taylor, and A.S. Perelson, "Nonlinear dynamics of immunogenic tumors: parameter estimation and global bifurcation analysis", *Bull. Math. Biol.* **56**, 295-321 (1994).

[12] A.G. López, J.M. Seoane, and M.A.F. Sanjuán, "On the fractional cell kill governing the lysis of solid tumors", *Commun. Nonlinear Sci. Numer. Simul.* (Submitted) (2016).

[13] G.C. Schaller, M. Meyer-Hermann, "Continuum versus discrete model: a comparison for multicellular tumour spheroids", *Phil. Trans. R. Soc. A* **364**, 1443-1464 (2006).

[14] G. Galilei, *Discorsi e dimostrazioni matematiche, intorno à due nuove scienze attenenti alla mecanica & i movimenti locali*, (Elsevier, Leiden) (1904).

[15] R. Osserman, "The isoperimetric inequality", *Bull. Amer. Math. Soc.* **84**, 1182-1238 (1978).

[16] H. Wadell, "Volume, shape and roundness of quartz particles", *J. Geol.* **43**, 250-280 (1935).

[17] H. von Koch, "Sur une courbe continue sans tangente, obtenue par une construction géometrique élémentaire ", *Arkiv för Matematik Astronomi och Fysik* **1**, 681-704 (1904).

# Chapter 6
# Dynamics of tumor-immune interactions

*"It is by no means inconceivable that small accumulations of tumour cells may develop and, because of their possession of new antigenic potentialities, provoke an effective immunological reaction with regression of the tumor and no clinical hint of its existence."*

-Macfarlane Burnet (1899-1985)

In this last chapter we investigate the process of cancer immunoedition by means of an hybrid cellular automaton. Even though a very interesting and similar work has been carried out in this context [1], the present work includes new features, which we believe makes it more realistic, permitting a correlation between the results and the theory of immunoedition. Mainly, the time scale of the cytotoxic cell action (about an hour) differs from the time scale of tumor cell proliferation (about a day). Secondly, our cellular automaton includes a new parameter, which allows us to represent immunosupressed environments. The exploration of different immunological scenarios enables the discussion of a possible dynamical origin of tumor dormancy and the sneaking through of tumors, as originally proposed in Ref. [2].

## 6.1 Introduction

Cancer immunoediting can be described by three phases: elimination, equilibrium and escape [3]. The first of these three Es corresponds to what has traditionally been termed immunosurveillance [4], and involves the innate and adaptive immune responses. During this phase, the immune system keeps in check the tumor cell population, whose majority of cells are successfully recognized and destroyed. However,

some residual tumor cells might remain unnoticed and asymptomatic for long periods of time, ranging from 5 years to more than 20 years. This leads to a second stage, in which a small cell population is kept at equilibrium. The mechanisms through which the immune system upholds the tumor at low cell numbers (*i.e.*, dormant) are diverse. In a first approach, cancer dormancy can be generally classified into two categories: *tumor mass dormancy* and *cellular dormancy* [5]. In the former case, the equilibrium of the tumor is the result of a balance between cell growth and cell death. In the latter, the cells arrest and survive in a quiescent state until more benevolent conditions are provided by their environment. This work only deals with tumor mass dormancy, whose occurrence is commonly associated again to two different mechanisms [6]. The first is angiogenic dormancy, which occurs when the cells are unable to induce angiogenesis, and therefore to recruit oxygen and other nutrients to their location. In this manner, the proliferation rate is counterweighted by elevated rates of apoptosis. The second mechanism is the immune system response. This response is very complex and involves many types of cells and molecules [7]. There is evidence that the cell-mediated immune response collaborates with the humoral immune response promoting the dormancy of tumors, and that $CD8^+$ lymphocytes and IFN-$\gamma$ play a transcendental function in its maintenance [8]. Here, we focus on the cell-mediated immune response. Finally, the phase of escape is led by some tumor cells that might present *a priori*, or have acquired along their evolutionary process, a non-immunogenic phenotype.

## 6.2 The model

We consider a model of limited nutrient growth of an immunogenic tumor consisting on a hybrid cellular automaton (CA) very similar to those presented in the previous chapters. For an schematic representation of the model see Fig. 6.1. The present model extends the prior CA models in two ways. First, we introduce a constant input of immune cells, as those appearing in the ODE models previously described. Importantly, now we let the tumors grow as the immune systems tries to reduce them. So, in a loose sense, both systems co-evolve. Two competing forces guide the dynamics of the model: those contributing to the reproduction of the tumor cells and those stimulating the immune system surveillance, which tries to destroy it. Since the reader might have forgotten some aspects of the CA model, in the following lines, and for the last time, we summarize its fundamental features.

The role of the healthy cells is reduced to passive competitors for nutrients that allow the tumor cells to freely divide or migrate. The dead cells play no significant role in the model, and they can be replaced by the tumor and the immune cells, just as if they were phagocytized by wandering macrophages.

At each CA iteration, the tumor cells can carry out different actions attending to certain probabilistic rules. These rules depend on the nutrient concentration per tumor cell and some specific parameters. Each of these parameters $\theta_a$ represent the intrinsic capacity of the tumor cells to carry out a particular action $a$. The tumor cells can divide $\theta_{div}$, move $\theta_{mig}$ or die $\theta_{nec}$. Attending to morphology, diverse types of

tumors can be generated, depending on the nutrient competition parameters among tumor cells $\alpha, \lambda_N$. Here, we consider parameter values that, in the absence of an immune response, generate rather spherical tumors [9, 10].

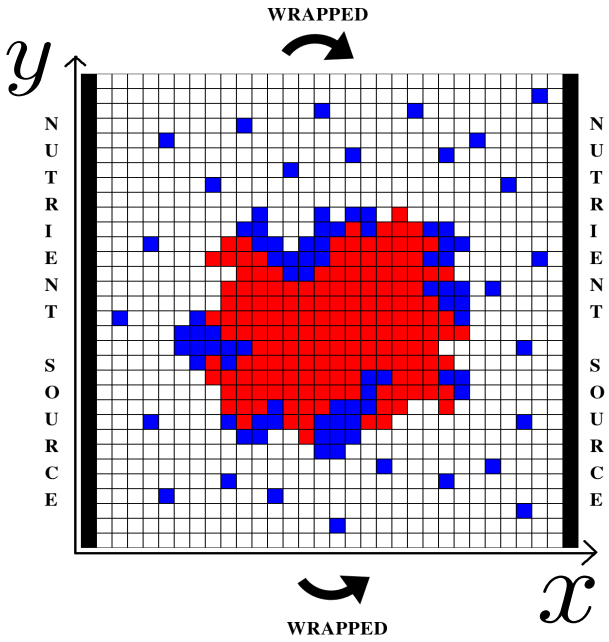


**Figure 6.1. The cellular automaton.** A grid representing the cellular automaton during the growth of a tumor in the presence of immune effector cells. The tumor cells are shown in red and the immune cells appear in blue. The remaining spots are occupied by healthy or dead cells. The vertical black stripes in the boundary of the square domain represent the vessels from which nutrients diffuse. Periodic boundary conditions are considered in the remaining part of the boundary. Some immune cells are scattered in the region, and some other form clusters that advance reducing the tumor.

Concerning the immune cells, we assume a constant input of cytotoxic cells into the region. When these cells are in contact with at least one tumor cell, they attempt to lyse it. The fate of this tumor cell depends on the intrinsic cytotoxic ability of the immune cells, which is coded in the parameter $\theta_{lys}$. We outline the importance of this parameter, which allows us to represent immunosuppressed tumor microenvironments. Following Refs. [2, 11], we assume that when a cytotoxic cell interacts with a tumor cell, several citokines are secreted by the immune cells, which induce the recruitment of other immune cells to the domain. We note that the constant input of immune cells can, to some extent, be regarded as a mechanism of recruitment as well. Commonly, cytokines are secreted by other types of immune cells, as for example T helper cells, which are not explicitly modelled here. When immune cells are not in direct contact with a tumor cell, they can either move or become inactivated $\theta_{inc}$. As in previous chapters, we assume that a single immune cell can not lyse more than three times, leaving the region of interest when this

occurs [1].

Concerning the natural input of immune cells into the domain, we let them appear with certain probability and place them at random in the domain, at points that are not occupied by tumor cells. Every grid point is examined and, if the probabilistic condition holds, the healthy or dead cells that might occupy it are replaced with an immune cell. An immune cell is placed in the background with probability

$$P_{bkg} = f - \frac{1}{n^2} \sum_{i \in \mathrm{CA}} E_i, \tag{6.1}$$

where $f$ is a number between 0 and 1, that represents the intensity of the input of immune cells into the tissue. If $P_{bkg}$ is greater than a randomly generated number between zero and one, then an immune cell appears in the corresponding grid point. This probability condition is designed in such a manner that the total number of immune cells is approximately a fraction $f$ of the CA grid points.

The modifications explained right above, imply changes in the algorithm. Therefore, we briefly describe the new algorithm. The algorithm starts with a domain full of healthy cells, except for a single tumor cell placed at the centre of the domain. First, we let the tumor growth until it is detected by the immune system, when it has reached some specific size $T_{det}$. During this period of growth each CA step corresponds to one day. Each iteration begins with the integration of the reaction-diffusion equations, using a finite-difference scheme and a successive overrelaxation method. Then all the tumor cells are randomly selected with equal probability, and the CA rules are applied. As in previous works [12], every time an action takes place, the reaction-diffusion equations are locally solved in a neighbourhood with size $20 \times 20$ grid points. When the time of detection is reached, the immune cells start to evolve. Now the CA step corresponds to one hour, and during the next twenty-three steps, only the immune cells are computed. First, the background source of immune cells is executed. Then the reaction-diffusion equations are solved and all the immune cells are randomly selected. For each immune cell, after applying the CA rules, the nutrients are computed in a local region, in exactly the same manner as before. Every twenty-three iterations, the tumor cells are checked and the tumor cell rules applied as previously described, before immune detection. The algorithm stops when a maximum number of steps after the elapse of the immune response has been reached, or when a tumor cell is at a distance of two grid points from its boundary.

## 6.3 Simulations and results

We study the evolution of the tumor and the immune system for three different scenarios. The first scenario is used as a reference, and it is characterized by high levels of immune cell recruitment and negligible necrosis due to the scarcity of nutrients in the core of the tumor masses. In the second scenario, the recruitment levels are reduced, while the necrosis of tumor cells is enhanced in the third. Unless specified, the remaining parameters are all the same in every case. Beginning with one tumor

cell, the tumors grow up to $5 \times 10^3$ cells, and at this moment the immune response triggers. In order to elucidate the effects of tumor immunogenicity, we devise what shall be called a *transient bifurcation diagram*. Given a dynamical system, an ordinary bifurcation diagram is a plot of the asymptotic values of a particular variable against a set of values of some relevant parameter. However, in many situations there might exist very long transients before the asymptotic state is established. These transients are of great importance in our context, since tumors may exhibit long periods of latency before the development of recurrence. Therefore, we compute the number of tumor cells for the last 100 iterations of a trajectory comprising 24000 iterations of the CA from immune detection. Then, these 100 points are represented on the vertical axis for different values of the $\theta_{lys}$ parameter, which lies on the horizontal axis. Since each of these iterations corresponds to one hour, we are registering the size of the tumor for approximately the last 4 days of a period of 33 months from immune detection. We recall that the parameter $\theta_{lys}$ codes the intrinsic ability of the immune cells to recognize and lyse their adversaries. Higher values of this parameter correspond to more immunodeficient environments.

### 6.3.1 Reference scenario

The set of parameters for this scenario is $\theta_{div} = 0.3$, $\theta_{nec} = 0.05$, $\theta_{mig} = \infty$, $\theta_{rec} = 1.0$, $\theta_{inc} = 0.1$, $\lambda_M = 10$, $\lambda_N = 25$ and $\alpha = 2/n$. Regarding the natural flow of immune cells into the tissue, two situations are inspected for each scenario. The first corresponds to a high input of immune cells into the tumor area. In this case a value $f = 0.10$ is set, what means that approximately 10% of the background is occupied by immune cells. The other has a lower input of 5%, thus $f = 0.05$. In the absence of immune response, the tumors display a rather spherical shape, as those appearing in Refs. [9, 10]. As we can see from the transition bifurcation diagrams shown in Fig. 6.2, three different regions are clearly distinguished. In the first region, when the immune system is effective, the tumors are completely eliminated. The second is related to an equilibrium phase, for which tumors spend very long transients oscillating at low cell numbers. Finally, tumors with increasing size, eventually leaving the domain through the vessels, appear in the third region. Thus, here we see how immunogenicity affects the fate of tumors, in accordance with the theory of immunoedition.

To give insight into the second and the third regions, time series have been computed (see Figs. 6.3 and 6.4), until the tumor escapes. Initially, the tumors grow in the absence of immune response, and then the immune cells start to reduce them or, in the worst case, delay their growth. Depending on how effective the immune cells are, longer or shorter transients follow this reduction phase. The asymptotic dynamics is always the same: if the tumors are not totally eliminated by an efficient immune system, they eventually escape from the region. These two attractors are reminiscent of those appearing in Ref. [2]. As shown in Fig. 6.3(a), the length of the transients in the second region, which are of around twelve years, clearly indicate a phase of prolonged tumor mass dormancy. During the period of dormancy the

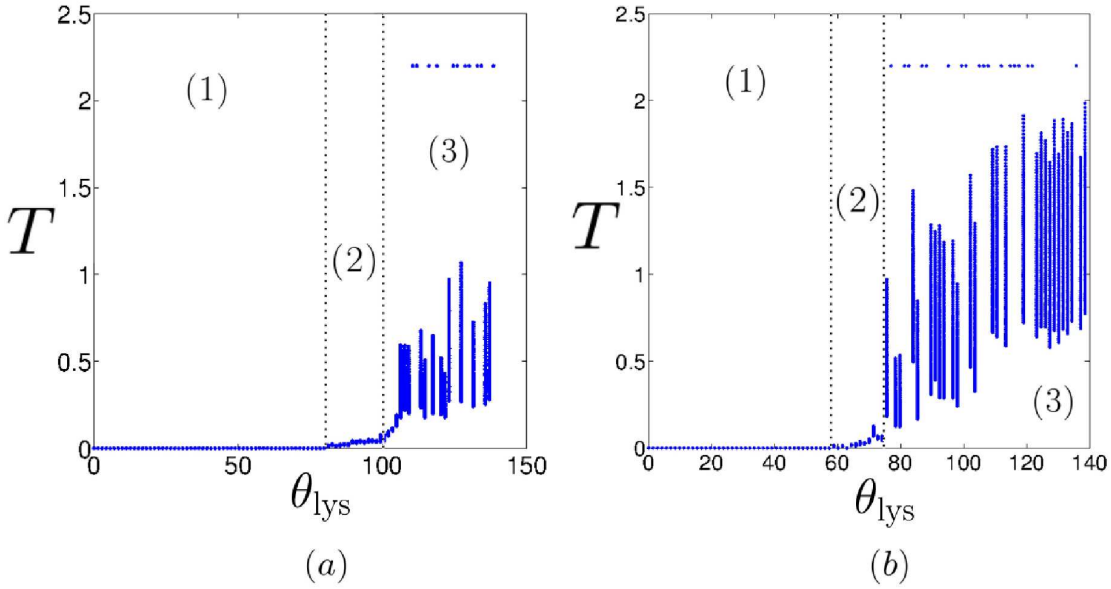


**Figure 6.2. Transient bifurcation diagrams**. Two transient bifurcation diagrams for the reference scenario. The size of the tumor $T$ for the last 100 hours of a trajectory comprising 1000 days is plotted against the parameter that models the immunogenicity of the tumor $\theta_{lys}$. The size of the tumor has been renormalized, dividing it by the number of total grid points $n^2$. Tumors having escaped the region are assigned a value of $T = 2.2$, which is over the maximum obtained in all simulations. (a) A transient bifurcation diagram for a constant input of tumor cells into the domain given by $f = 0.1$. (b) A transient bifurcation diagram for a constant input of tumor cells into the domain given by $f = 0.05$. Three different regimes are clearly discerned. The first (1) corresponds to the elimination of the tumors, the second (2) to abiding small tumors kept in equilibrium by the immune cells and the third (3) to fast growing tumors that eventually escape. The distances between the escape points in the third region clearly suggest that the time it takes a tumor to escape is stochastic.

immune system keeps the tumor at low cell numbers and randomly displaces its disconnected pieces until one of them reaches the vessels. In the third region again transients are found, but they are shorter (less than four years) and the tumors escape with bigger sizes. As predicted in Ref. [2], the duration of the transients is stochastic. This randomness is evident from the transient bifurcation diagrams, since after 33 months of tumor-immune struggle, some tumors have escaped and some others have not, disregarding how immunogenic they are. When the immune system barely responds to the tumor, we see very big tumors occupying the domain and escaping rapidly, as depicted in Fig. 6.3(e).

Interestingly, the equilibrium region shrinks as the normal input of cells into the tissue reduces from $f = 0.1$ to $f = 0.05$. As it is shown in Fig. 6.4, the oscillations during the equilibrium phase are more pronounced. This makes the equilibrium more unstable and suggests that having cells scattered all over the domain is important for the maintenance of dormancy. Probably, the reason is that these spread immune

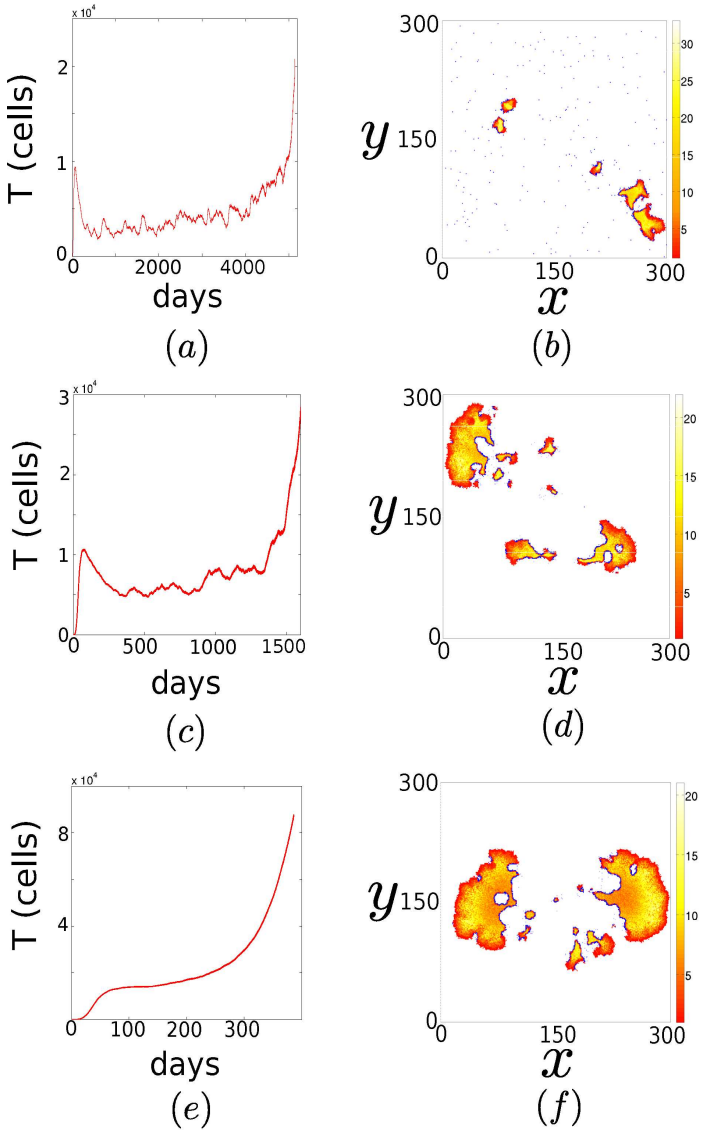


**Figure 6.3. Asymptotic dynamics and tumor escape**. Three time series of the tumor size for the reference scenario are plotted. The constant input of immune cells to the domain is $f = 0.1$. The size of the tumors is registered until they escape the domain through the vessels. The tumors at escape are shown beside. The immune cells appear in dark blue, while the tumor cells range from red to white. The color bar represents the number of tumor cells at a grid point. The dead cells are represented in light blue. (a) A long-lived tumor is kept at equilibrium for $\theta_{lys} = 90$. This is an example of immune-mediated tumor mass dormancy. (b) The corresponding small tumor at escape. (c) A less immunogenic tumor $\theta_{lys} = 106$ is kept at equilibrium, but for a considerably shorter time. (d) The corresponding tumor at escape, which is noticeably bigger compared to the previous case. (e) A tumor that is barely immunogenic for $\theta_{lys} = 140$. Now the tumor escapes very rapidly and exhibits the largest size, although the immune system delays its growth. (f) The corresponding tumor at escape, which is the biggest of the three.

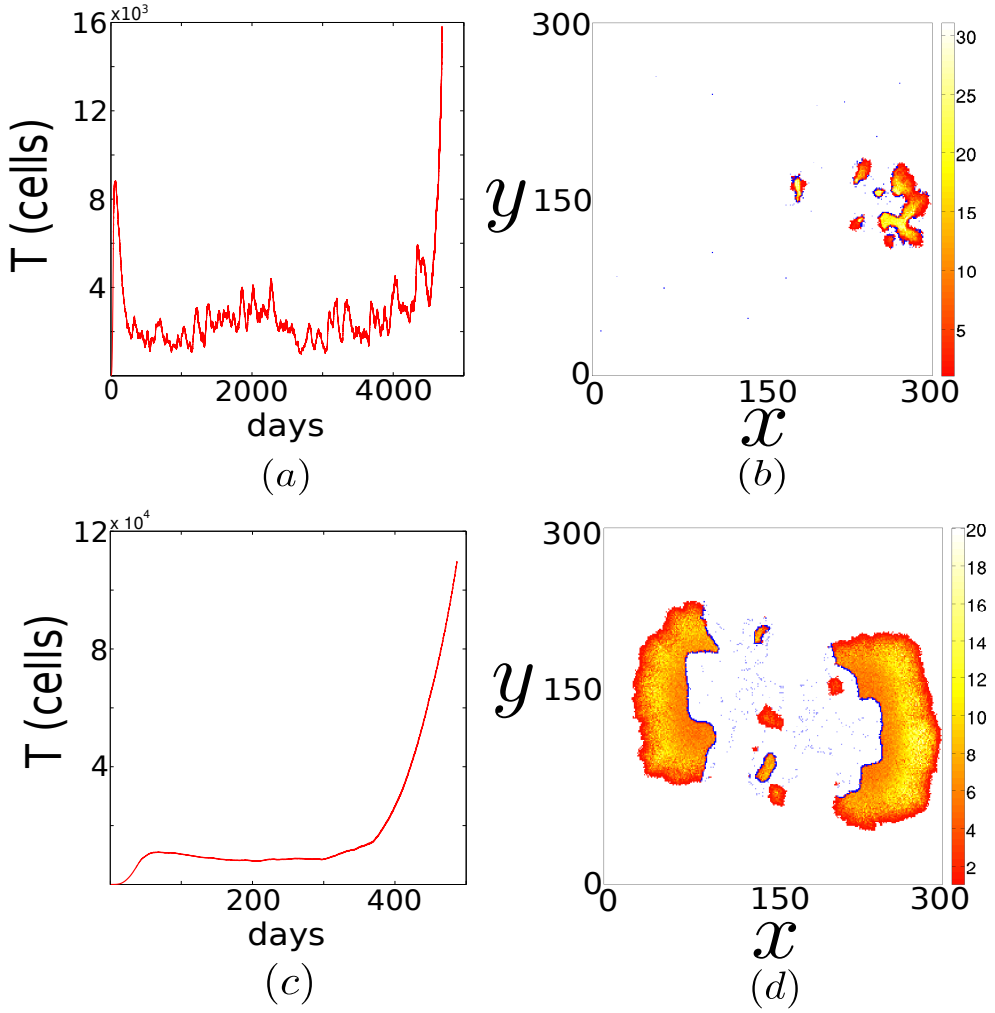


**Figure 6.4. Asymptotic dynamics and tumor escape**. Two time series of the tumor size for the reference scenario are plotted. The constant input of immune cells to the domain is now smaller $f = 0.05$. We register size of the tumors until they escape the domain, and the tumors at escape are shown beside. As before, the immune cells appear in dark blue, while the tumor cells range from red to white. The color bar represents the number of tumor cells at a grid point. The dead cells are represented in light blue. (a) A long-lived tumor is kept at equilibrium for $\theta_{lys} = 67$. Now the oscillations of the tumor size during the equilibrium are higher. (b) The corresponding tumor at escape. (c) Another tumor $\theta_{lys} = 89$ that is slightly reduced and kept at a constant size for a year, but that soon after escapes. (d) The corresponding tumor at escape.

cells keep the tumor at a small size, not allowing its overgrowth in any specific direction.

We have also explored the importance of the tumor size at detection by reducing this size to $5 \times 10^2$. The results are depicted in Fig. 6.5 and resemble very much those shown in Fig. 6.2. There is no hint of a sneaking through mechanism in our model. According to the definition given in Ref. [13], sneaking through is the preferential

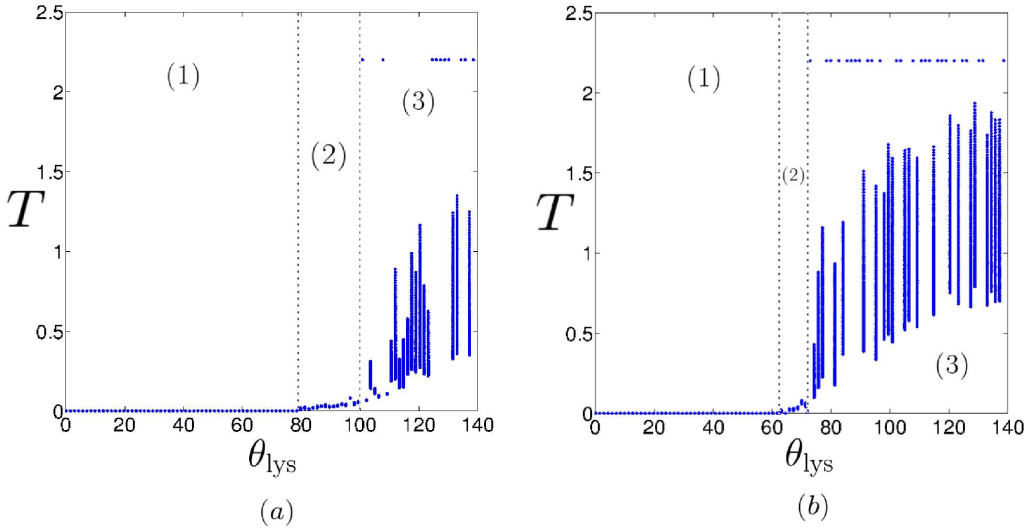


**Figure 6.5. Transient bifurcation diagrams**. Two transient bifurcation diagrams for the reference scenario, represented as previously explained. Now a smaller tumor size at detection $T_{det} = 500$ has been considered. (a) A transient bifurcation diagram for a constant input of tumor cells into the domain given by $f = 0.1$. (b) A transient bifurcation diagram for a constant input of tumor cells into the domain given by $f = 0.05$. The effects of tumor size at detection does not introduce significant changes in the dynamics.

take of tumors after small size inocula to a similar degree with that seen with large size inocula, compared to the rejection of medium sized inocula. More clearly put, small and big tumors escape immune surveillance, while intermediate do not. Such phenomenon has not been observed in the present case for other values of the tumor size at detection. However, we do not discard it, since motility of tumor cells has not been included in this first investigation, and might be crucial for these cells to escape.

Finally, even though the tumors here inspected are homogeneous and no evolutionary process is really taking place in our model, the transient bifurcation diagrams insinuate how the sculpting of the phenotype occurs, moving from the first region to the second, and then to the third. Thus, the present model is in accordance with the theory of immunoedition, which suggest that the immunosurveillance of tumors sculpts the phenotype of a tumor. In fact, a similar cellular automaton can be used to explore the impact of heterogeneity and how the immunoedition process takes place. It suffices to consider that the immune cells intrinsic cytotoxicity, represented by the parameter $\theta_{lys}$, varies for each tumor cell.

### 6.3.2 Low recruitment scenario

We now evaluate the impact of the recruitment of immune cells to the domain of the tumor. For this purpose, we reduce the value of $\theta_{rec}$ from 1 to 0.35. Our interest in this parameter is due to the fact that, in many occasions, the recruitment of cells to

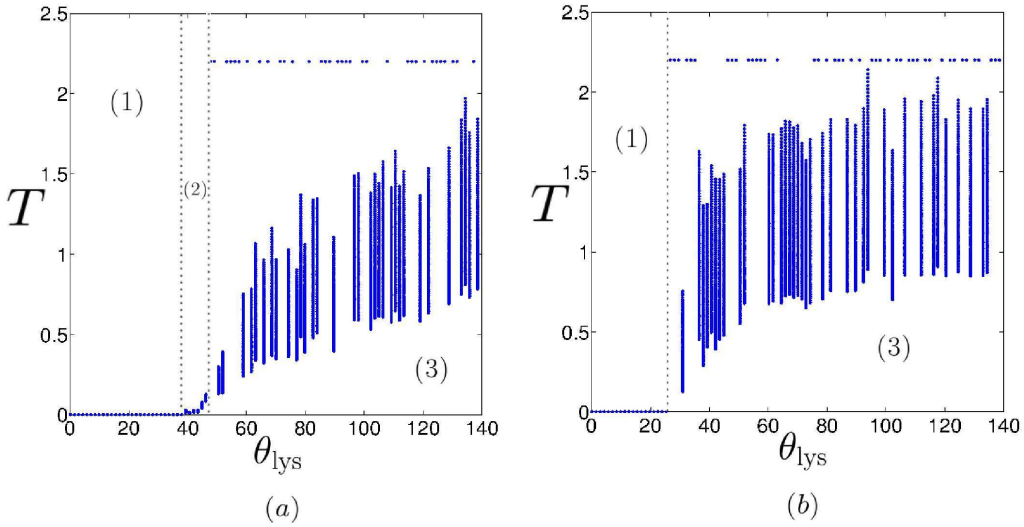


**Figure 6.6. Transient bifurcation diagrams**. Two transient bifurcation diagrams for the low recruitment scenario $\theta_{rec} = 0.35$, represented as previously explained. (a) A transient bifurcation diagram for a constant input of tumor cells into the domain given by $f = 0.1$. (b) A transient bifurcation diagram for a constant input of tumor cells into the domain given by $f = 0.05$. A decrease of the immune cell recruitment value reduces the window of equilibrium. Thus large periods of dormancy require significant levels of immune cell recruitment.

the site of the tumor might be very complicated. The recruitment of immune cells is a very complex process, at least from a physical point of view. The extravasation of leukocytes requires an initial contact between these cells and the endothelial cells, which depends on adhesion molecules. After adhesion to the walls of the vessels, the immune cells traverse them through diapedesis, which again relies on several cytokines. Finally, chemokines bias their random walks to the tumor location [14]. Thus we expect this parameter to exhibit great fluctuations, depending on the tissue location and other factors, as for instance the degree of inflammation.

The effects of decreasing the recruitment parameter are shown in Fig. 6.6. As expected, the elimination region shrinks, while the escape region widens. A dramatic reduction of the dormancy window is observed in both plots. When $f = 0.1$, the window still exists, but for $f = 0.05$ it has even disappeared. These results suggest that a relatively tight balance between lysis and growth is required to maintain the dynamical equilibrium of the tumor.

Note that, as previously proposed, the equilibrium of the tumor implies that reduction must occur in an isotropic manner. If a region of the tumor grows over the immune system capacity, then a soon overgrowth and a consequent escape would be expected. In the present model, this relies on a positive feedback mechanism between the natural input of immune cells and their recruitment. The more cells there are spread in the domain, the more chances for an immune cell to lethally hit a tumor cell. When this occurs, recruitment proceeds, favouring the local aggregation of

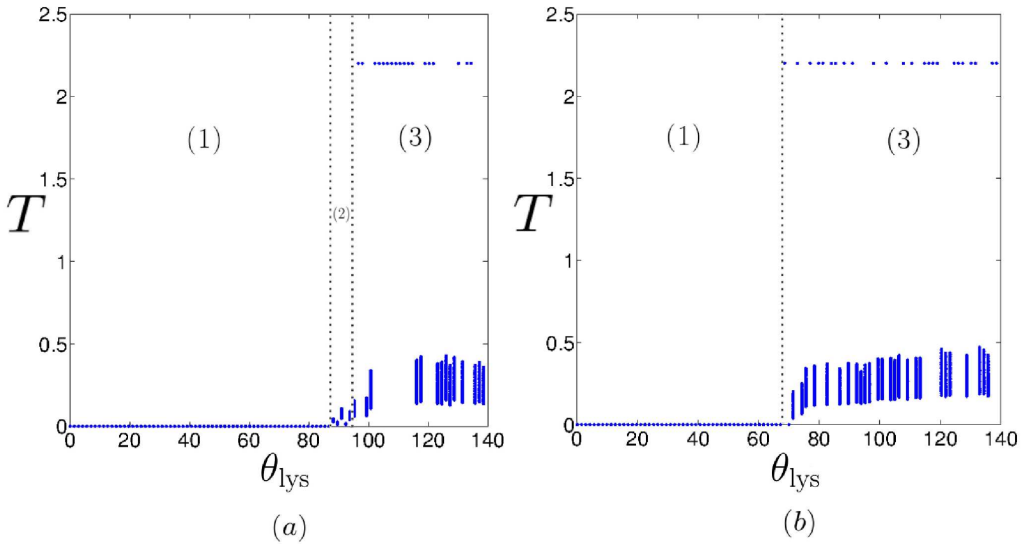


**Figure 6.7. Transient bifurcation diagrams**. Two transient bifurcation diagrams for the high necrosis scenario $\theta_{nec} = 1.0$, represented as previously explained. (a) A transient bifurcation diagram for a constant input of tumor cells into the domain given by $f = 0.1$. (b) A transient bifurcation diagram for a constant input of tumor cells into the domain given by $f = 0.05$. Obviously, an increase of tumor cell necrosis enlarges the elimination region and shrinks the remaining ones. Interestingly, the window of equilibrium has again reduced, what suggests that long-lived periods of dormancy are based on a delicate equilibrium between the proliferation rate of the tumor and its lysis by the immune system.

immune cells at this site of the tumor and giving rise to satellites [1]. This isotropy can be appreciated in the equilibrium represented in Figs. 6.3(b) and 6.4(b), as opposed to those situations that lie in the third region, represented in Figs. 6.3(d), 6.3(f) and 6.4(d).

### 6.3.3 High necrosis scenario

Solid tumors usually exhibit necrotic cores due to the scarcity of nutrients. Other chemical species can be represented with the present model (e.g. growth factors) and, if desired, necrosis can be regarded as apoptosis, at least to some extent [12]. Therefore, we now inspect the effects of cell death in the model. To this end, we increase the value of $\theta_{nec}$ from almost zero to 0.5. Obviously, the increase of necrosis facilitates the labour of the immune system. As shown in Fig. 6.7, the elimination region enlarges substantially, compared to the reference case. Also in the equilibrium region, lower tumor cell numbers are seen before the escape of the tumor. More importantly, the equilibrium window, which has been associated to large periods of tumor mass latency, is practically imperceptible for $f = 1.0$ and has completely vanished for $f = 0.05$. We have again computed time series, showing that transients occur in the equilibrium region, sometimes as long as those appearing before in the

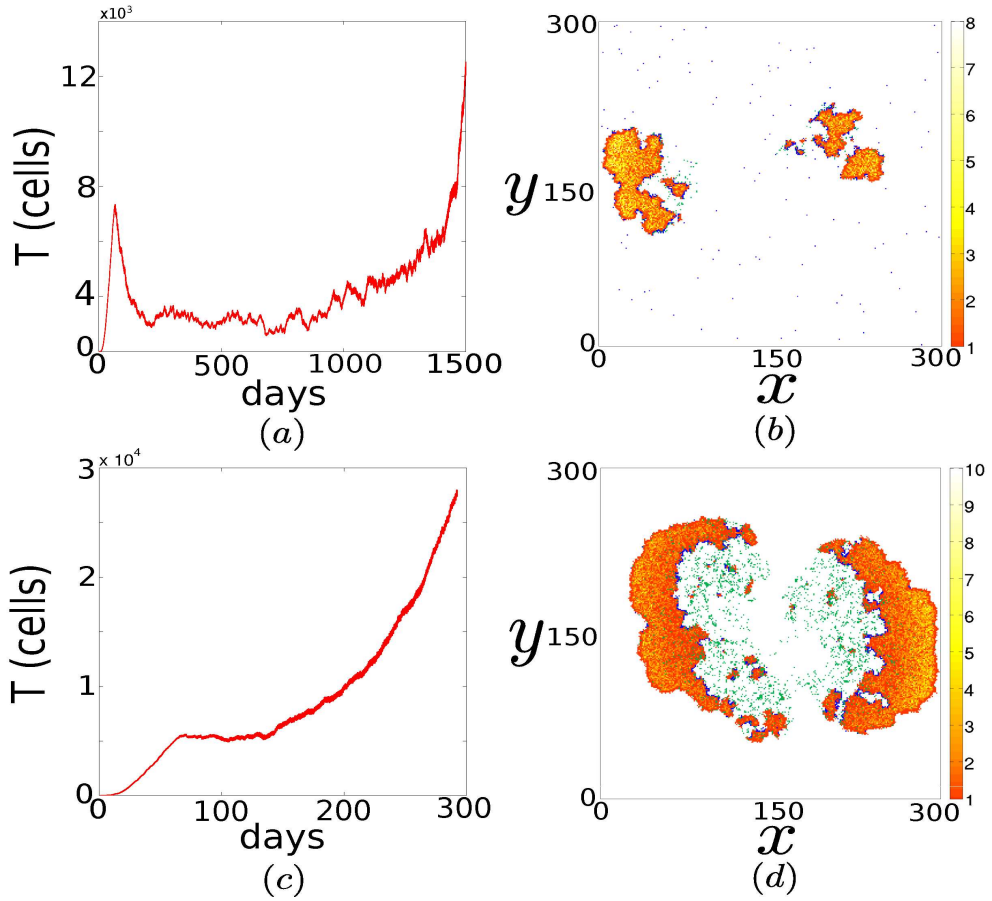


**Figure 6.8. Asymptotic dynamics and tumor escape**. Two time series of the tumor size for the reference scenario are plotted. The constant input of immune cells to the domain is now smaller $f = 0.05$. The size of the tumors are registered until they escape the domain. The tumors at escape are shown beside. The immune cells appear in dark blue, while the tumor cells range from red to white. The color bar represents the number of tumor cells at a grid point. The dead cells, which now also appear inside the tumor, are represented in green. (a) A quite long-lived tumor is kept at equilibrium for $\theta_{lys} = 92$. (b) The corresponding tumor at escape. (c) Another tumor $\theta_{lys} = 118$ that is barely reduced and kept at a constant size for less that half a year, and then escapes rapidly. (d) The corresponding tumor at escape.

equilibrium, but generally shorter (see Fig. 6.8). In fact, the equilibrium window and the escape zone drawn in Fig. 6.7(a) overlap.

It seems that the equilibrium region appearing in the reference scenarios has been swept under the elimination region. Once more, this confirms the requisite of a relatively delicate balance between the mechanisms that maintain the cytotoxic effects of the immune system and the growth of the tumor, in order to keep it at low cell numbers for very long periods of time.

## 6.4 Discussion

We have studied the transient and asymptotic dynamics of a cellular automaton model for tumor-immune interactions. We have shown that, depending on the immunogenicity of the tumor, the model furnishes three main types of dynamics, which are in accordance with the three Es of the theory of immunoedition. Importantly, we have shown that a dynamical equilibrium between the tumor can occur for long periods of time, as proposed in Ref. [2]. However, after inspection of the parameter space, our model suggests that this equilibrium is quite fragile, since it is based on an adjusted balance between the mechanisms that stimulate the immune response and tumor cell proliferation. It is worth asking if this also occurs in the model presented in Ref. [2]. We must bear in mind that such model is very sensitive to a parameter, there called $\mu$, which is related to the rate at which tumor cells are lysed. In their model, tumor cell lysis is represented by a simple Lotka-Volterra competition term. In the previous chapters it has been demonstrated that the rate at which a tumor is lysed should be represented by a more sophisticated function, that depends on the geometrical properties of the tumor and its immunogenicity. Finally, it was not assessed in their work the importance of the parameters that model the recruitment. Although their model is tested against experimental data, obtained from a $BCL_1$ lymphoma in chimeric mice, these tumors develop in the spleen of the mice. As explained in the introduction, the spleen is a secondary lymphoid organ through which T-cells are permanently trafficking, and the process of recruitment to other types of tissues might be more arduous. Interestingly, a reduction of the value of the parameter $\rho$ from 1.131 to 0.6300, which in their model is related to the rate at which T-cells are recruited, produces a saddle-node bifurcation through which the dormant state disappears. Just as in the present work, "high" levels of recruitment are required to sustain dormancy. Nevertheless, both models clearly demonstrate that a state of tumor mass dormancy mediated by the immune system is likely to occur. It is the length of this dormant period that it is being questioned here. Thus, we conclude that, even though tumor mass dormancy can result from the cell-mediated immune response to tumor growth, long periods of dormancy, as commonly found in recurrent metastatic tumors [5, 6], are not likely to arise by this single mechanism. It is therefore pertinent to ask ourselves if the role of the cell-mediated immune response in the promotion of the dormancy of tumors is rather to synergize with other types of mechanisms, as for example cellular dormancy.

# References

[1] D.G. Mallet and L.G. De Pillis, "A cellular automata model of tumor-immune system interactions", *J. Theor. Biol.* **239**, 334-350 (2006).

[2] V.A. Kuznetsov, I.A. Makalkin, M.A. Taylor, and A.S. Perelson, "Nonlinear dynamics of immunogenic tumors: parameter estimation and global bifurcation analysis", *Bull. Math. Biol.* **56**, 295-321 (1994).

[3] G.P. Dunn, L.J. Old, and R.D. Schreiber, "The three Es of cancer immunoediting", *Annu. Rev. Immunol.* **22**, 329-360 (2004).

[4] M.W.L. Teng, J.B. Swann, C.M. Kohebel, R.D. Schreiber, and M.J. Smyth, "Immune-mediated dormancy: an equilibrium with cancer", *J. Leukoc. Biol.* **18**, 645-653 (2008).

[5] J.A. Aguirre-Ghiso, "Models, mechanisms and clinical evidence for cancer dormancy", *Nat. Rev. Cancer 7*, 834-846 (2007).

[6] P. Paéz, M.J. Labonte, P. Bohanes, W. Zhang, L. Nebhamin, Y. Ning, T. Wakatsuki, F. Loupakis, and H. Lenz, "Cancer dormancy: a model of early dissemination and late cancer recurrence", *Clin. Cancer Res.* **18**, 645-653 (2012).

[7] C.A. Janeway, P. Travers, M. Walport, and M.J. Shlomchik, *Immunobiology*, (Garland Science, New York) (2012).

[8] J.D. Farrar, K.H. Katz, J. Windsor, G. Thrush, H.S. Richard, J.W. Uhr, and N.E. Street, "Cancer Dormancy. VII. A regulatory role for $CD8^+$ T Cells and IFN-$\gamma$ in establishing and maintaining the tumor-dormant state", *J. Immunol.* **162**, 2842-2849 (1999).

[9] A.G. López, J.M. Seoane, and M.A.F. Sanjuán, "On the fractional cell kill governing the lysis of solid tumors", *Commun. Nonlinear Sci. Numer. Simul.* (Submitted) (2016).

[10] A.G. López, J.M. Seoane, and M.A.F. Sanjuán, "Decay dynamics of tumors", *PLoS One* (Submitted) (2016).

[11] L.G. De Pillis, A.E. Radunskaya, and C.L. Wiseman, "A validated mathematical model of cell-mediated immune response to tumor growth", *Cancer Res.* **65**, 235-252 (2005).

[12] S.C. Ferreira Jr., M.L. Martins, and M.J. Vilela, "Reaction-diffusion model for the growth of avascular tumor", *Phys. Rev. E* **67**, 051914 (2002).

[13] P.A. Gatenby, A. Basten, and P. Creswick, "Sneaking through: a T-cell-dependent phenomenon", *Br. J. Cancer. 44*, 753-756 (1981).

[14] M.J. Miller, S.H. Wei, M.D. Cahalan, and I. Parker, "Autonomous T cell trafficking examined in vivo with intravital two-photon microscopy", *Proc. Natl. Acad. Sci. U. S. A.* **100**, 2604-2609 (2003).

# Chapter 7
# Conclusions

*"True laws of nature cannot be linear"*

-Albert Einstein, (1879-1955)

In this research work, the interactions between tumor cells and cytotoxic immune cells have been analysed from a dynamical point of view. Clearly, its nature is mostly numerical and theoretical. The experimental data required to validate our models have been borrowed from other works published in renowned scientific journals. We expose the main conclusions of our work in the three following sections.

## 7.1 Control of tumor growth

In the first part of this thesis, which comprises the second chapter, we have studied the possibility to control the chaotic oscillations in a model of tumor and immune cell interactions. The two most relevant conclusions of this work are:

- For an immune system which is very effective in the recruitment of cells and a very aggressive tumor, chaotic oscillations can be observed. Therefore, the use of immunotherapeutic protocols (and also other therapies) might induce the unpredictable oscillations of the size of a tumor.

- In spite of the practical limitations of the applied method, the work suggests an interesting alternative to deal with non metastatic cancers, in contrast to treat-

ment protocols aimed at destroying the tumor, as for instance in chemotherapy and immunotherapy. In many situations, such treatments lead to a subsequent regrowth of those resistant cells that have escaped the applied control (minimal residual disease). An alternative to destroy a tumor, is to keep it at non dangerous levels by performing a feedback control of its size, and taking advantage of the competition among tumor cells.

## 7.2 The velocity at which tumors are lysed

In the second part of this work, we have validated a mathematical model and established the mathematical function representing the velocity with which a population of immune cells destroys a tumor. The main contents of this function and its deep significance are itemized in the following lines:

- The velocity at which a tumor is lysed by a population of cytotoxic cells increases monotonically with the size of this population, but saturation is observed for sufficiently high numbers of the immune cells. This saturation is a consequence of cell crowding, and can be explained in a simple manner. When the outmost layer of a solid tumor is profusely covered with several lines of lymphocytes, the addition of cells can not enhance the rate at which the tumor is lysed, because these cells are not in contact with it. Consequently, the geometry of the tumors affects this velocity. The more spherical a tumor is, the smaller the surface-to-volume ratio, and the slower the speed at which it is erased. On the other hand, given a small number of immune cells in comparison to the tumor, the increase of the tumor also translates into higher speed, but again, saturation is found. Now the reason is that at some point, all the immune cells are busy lysing other tumor cells, and the addition of tumor cells can not enhance the speed. Therefore, the velocity depends nonlinearly on both cell populations.

- Two of the four parameters appearing in the mathematical function representing the rate at which a tumor is lysed are related to its geometry, one is related to its topology, while the fourth represents the intrinsic ability of the cytotoxic cells to recognize and destroy their adversaries. Importantly, the present work has provided, for the first time, a clear measure of the intrinsic cytotoxicity of lymphocytes.

- In the limit in which the immune cell population is very small compared to the tumor, the tumor decays at a constant velocity. When the tumor is plainly covered with immune cells, it decays with a power law decay, the exponent ranging from cubic to exponential. The former corresponds to connected tumors, while the latter corresponds to completely disconnected tumors, in which both cell populations are homogeneously distributed. Intermediate situations are represented by a crossed Hill function, with exponents representing non-cooperative binding.

- The process of lysis can be understood as an enzymatic process, where saturation is found for both, the substrate (the tumor) and the enzyme (the lymphocytes). Perhaps the most important conclusion of our results is that they query the general validity of the law of mass action, stating that the velocity at which the products of a reaction are originated, can not be increased without limits, by simply adding more of one of the two reactants. Unless the species are added homogeneously and in equal proportions, according to their stoichiometric coefficients, a point must be always reached for which saturation is observed. This is because interactions occur in a local manner and take some time, no matter how small this time is. Certainly, the effects of saturation are more sensible at higher scales, such as for cellular interactions and animal interactions, in comparison to chemical reactions. This is probably because interactions take longer at higher scales.

## 7.3 The dynamics of tumor-immune interactions

In the last part of this work, we have used a cellular automaton to inspect the transient and asymptotic dynamics of the interactions between neoplastic cells and cytotoxic cells. The main conclusions are itemized in the following two points:

- Asymptotically, the dynamics of the cell-mediated immune response can only lead to two outcomes: the destruction of the tumor, or its escape. Transiently, long periods of dormancy can be mediated by the immune system. If the immune cells are effective at recognizing the tumor cells, the tumor can be eliminated. If they are not effective, the tumor escapes. Intermediate situations can lead to latency periods in which the tumor is kept at low numbers in an asymptomatic equilibrium. These results are in conformity with the theory of immunoedition, and support its content.

- The equilibrium phase depends on a relatively fine tuning of the mechanisms that strengthen the immune response and the rate at which the tumor grows. Therefore, the equilibrium phase can be easily destabilized by the stochastic fluctuations and the movement of the tumor, leading to its escape. This implies that long periods of tumor mass dormancy uniquely mediated by the immune system are not likely to occur.

# Appendices

## Appendix: Basics of immunology

In this appendix we describe the role of the immune system, its components at different levels of hierarchy and the mechanisms through which these cells monitor the organism.

The first lines of defence of an organism against pathogens are the physical and chemical barriers. The physical barriers correspond to the skin and the mucous, which are supported by several enzymes capable of destroying dangerous intruders. When a pathogen overtakes these first obstacles, reaching aseptic tissues in the body and infecting them, the immune response is triggered. The immune system is a complex system that comprises many biological processes and cell interactions. It appears in most multicellular organisms (around 98 % have a more or less developed immune system) and evolved to protect such organisms against pathogens, such as viruses, bacteria or fungi. The immune system cells and molecules are distributed over a network of organs (bone marrow, thymus, lymph nodes, spleen, etc.). Broadly speaking, the immune system has developed two different mechanisms to fight infections. Depending on the requirement of previous knowledge of their enemies, and also on the molecular structures involved in the their recognition, the immune response is classified as *innate* or *adaptive* (see Fig. 1).

The innate immune response is based on the activation of preformed molecules, called complement proteins, and several types of cells, such as phagocytes or inflammatory cells. Cytolitic cells, like the *natural killer cell* (NK), play a key role in the context of tumor immunology. All these cells and proteins have the potential to recognize and interact with highly conserved molecular patterns, without prior exposition to them. Therefore their belonging to the innate arsenal of the immune system. Other proteins, which are not usually preformed, but rather synthesized and secreted by the immune cells as a consequence of the interaction with antigens, are indispensable for the self-regulation of both the adaptive and the innate response. These proteins are technically known as *cytokines*, and will be introduced at the end of this section. In the following lines, we briefly list and describe the constituents of the innate immune response.

**Complement:** a set of proteins circulating in the blood and the tissues. Its activation leads to a cascade reaction which ultimate result is the direct or indirect elimination of pathogens and the begin of inflammation. As an example of a direct elimination process we can think of the protein complement C9, which creates holes in the membrane of a target cell, producing their lysis. An indirect process is, for instance, the marking of pathogens that promotes phagocytosis. The complement is activated through three different pathways, which will not be discussed here.

**Phagocytes:** immune cells responsible for the ingestion and digestion of pathogens. Phagocytes can be classified by the morphology of their nucleus. Macrophages and monocytes are mononuclear phagocytes. The latter usually navigate through the circulatory system until they land in some particular tissue. Then

these cells mature and differentiate into macrophages. Macrophages mainly concentrate in the connective tissue underlying the epithelium and in the lymphoid organs. They posses membrane receptors that have been selected by evolution to recognize conserved antigenic structures. Apart from eating pathogens, they induce inflammation by secreting soluble proteins (cytokines) and unleash the adaptive immune response through antigen presentation. This task is also carried out by another type of cell of the innate immune response: the dendritic cell. Polynuclear phagocytes are also referred in the literature as granulocytes, since these cells present a multilobulated nucleus and a cytoplasm full of granules. They are shorter-lived (days) and spend most of their time in the circulatory system, until the emission of cytokines or complement proteins provokes their recruitment to the tissues. There are three types of granulocytes: neutrophils, eosinophils and basophils. Neutrophils are the most abundant among the granulocytes (approximately 90 %). They can phagocyte and destroy pathogens directly, but they can also dump the contain of its lytic granules through a process called exocytosis. However, it is eosinophils that are more specialized in this last procedure. These comprise about $3 - 5\%$ of the leukocytes, and are frequently found in tissues. Basophils represent a very small cell population and participate in inflammation. Together with the complement, phagocytes constitute the first line of defence of the immune system.

**Mastocytes:** theses cells are the most important mediators of the inflammatory response. They live close to the blood vessels and locally regulate their permeability. When they are activated by pathogens, mastocytes release high doses of preformed inflammatory mediators, such as histamine. The region is then flooded with blood carrying fresh leukocytes and the pathogens are destroyed by brute force.

**NK cells:** these are the innate *cytotoxic* cells, capable of recognizing molecular proteins without previous activation. After recognition, they proceed to *lyse* (destroy) their enemies by releasing proteins contained in their granules. These granules mainly contain a protein called perforin and granzymes. The former polymerizes in the membrane of the target cell, opening holes on it. The latter is responsible for triggering the apoptotic machinery of the cell, leading to its programmed death. NK-mediated cytotoxicity is based on the recognition of MHC-class I molecules and it is explained by a model of double receptor, that combines activatory and inhibitory signals. A *receptor* is a protein on the surface of a cell that binds to other proteins, allowing it to recognize other cells and substances. In the language of complex systems, cells communicate and process information through chemical signals, and receptors are responsible for the transduction of these signals. The receptors of the NK cells are classified into two groups: immunoglobuline-like receptors and lectine-like receptors. Two respective examples of receptors are the KIR receptor and the NKG2 receptors. Specifically, the NKG2D receptor appears in Chapter 3.

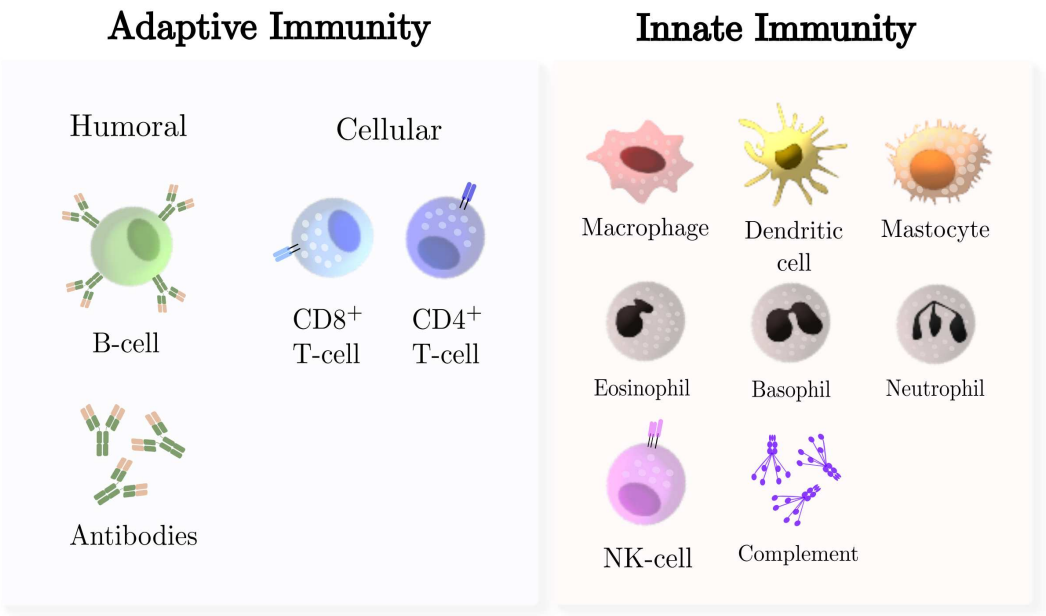


**Figure 1. The two arms of the immune response**. (a) The cells and proteins that mediate the adaptive immune response. (b) The cells and proteins that mediate the innate immune response.

Contrary to the innate immune response, adaptive immunity is constantly evolving through processes of genetic recombination and Darwinian selection. The cells that integrate this response exhibit a tremendous heterogeneity of receptors, which are randomly generated. This increases the chances of detecting new pathogens that can not be recognized by innate immune cells. When such detection takes place, the specific immune cell *activates* and begins to proliferate, creating a powerful army capable to counteract the infection. As a proof of the complexity of the immune adaptive response, it is interesting to see that part of the cells differentiate into memory cells, so that a faster and more efficient response is executed in later similar encounters. Two types of responses can be discerned in the adaptive immune response: the *humoral* response and the *cell-mediated* response.

The humoral arm of adaptive immunity is mediated by a set of specific proteins called *immunoglobulines*, and the B cells. These molecules are also called *antibodies*, since they bind to specific *antigens*. An antigen is a protein related to a foreign microorganism, that might appear linked to the surface of such agent, or free-floating in the serum and in tissue fluids. Antibodies are synthesised and secreted by plasma cells, which differentiate from B cells. Antibodies carry out different assignments. For example, IgM and IgG antibodies can activate the complement system. In fact, IgM levels are referred in Chapter 3, since they can be correlated to tumor size in plasmacytomas (a cancer of the plasma cells). Antibodies commonly attach to pathogens as well. This phenomenon is called *opsonization*, and has two important consequences. First, it neutralizes or blocks the infective agents, and second, by

marking these pathogens, it facilitates the labour of recognition and destruction of phagocytes. Antibodies are also important regulators of the process of inflammation, by stimulating basophils and mastocytes, and are also abundant in MALT tissues. Concerning B cells, these cells can use their receptor (BCR) to recognize antigens in native form and to secrete antibodies as well. However, it is precisely when these cells interact with specific antigens in the secondary lymphoid organs, that they are activated and the humoral adaptive response is triggered with intensity. After activation, they differentiate into plasma cells and memory B cells. The latter also act as antigen presenting cells, by means of their receptor.

The cell-mediated arm is mostly comprised by the T cells. The two most important types of T cells are the T helper cells (mostly $CD4^+$ cells) and the *cytotoxic T cells* (mainly $CD8^+$ cells). T helper cells interact with B cells and other T cells through their TCR receptor and through the emission of cytokines, helping them to activate, divide and differentiate. They can also help macrophages and NK cells to destroy pathogens. To some extent, T helper cells control and orchestrate the adaptive immune response by secreting cytokines and interacting with antigen presenting cells (dendritic cells and macrophages), which arrive to the lymphoid organs from the site of infection. Antigens are presented to T helper cells through MHC class II molecules and, under proper co-stimulation, these cells activate or differentiate to memory T cells. On the other hand, the cytotoxic T cell, as its name indicates, is specialized in destroying other types of cells. For example, they can lyse cells infected by viruses or tumor cells. Since they are very harmful, their prior activation requires higher co-stimulatory signals than T helper cells. Cytotoxic lymphocytes can be activated directly by antigen presenting cells or, when co-stimulatory signals are not abundant, by T helper cells. The particular mechanism of destruction is relevant to our study and operates in the following manner. When a cell is infected by some intracellular pathogens, it starts to present on its membrane fragments of antigenic proteins associated to the molecules of the major histocompatibility complex one (MHC I). These complexes are responsible for presenting on the cell surface fragments of proteins inside the cell, so that they can be checked. When an activated cytotoxic lymphocyte recognizes specific molecular patterns presented by their target cells, these cells polarize (capping) by reorienting their cytoskeleton. Then, they induce apopotosis in the target cells in the same manner as described before by NK cells. As it is explained in Chapter 4, the time duration of the lytic process lasts around an hour, and will be of great importance in our models.

In order to understand the process of recruitment, that plays an important role in our models, we now give a short summary on cytokines. Cytokines are proteins that allow the different constituents of the immune system to interact and communicate, leading to an unilateral response. Cytokines are commonly produced during the first moments of cellular activation and have a rather local effect, alerting other immune cells of the ongoing of an immune response. Thus, cytokines have three main effects:

- Regulate the duration and amplitude of the immune response
- Recruit other immune cells to the site of conflict

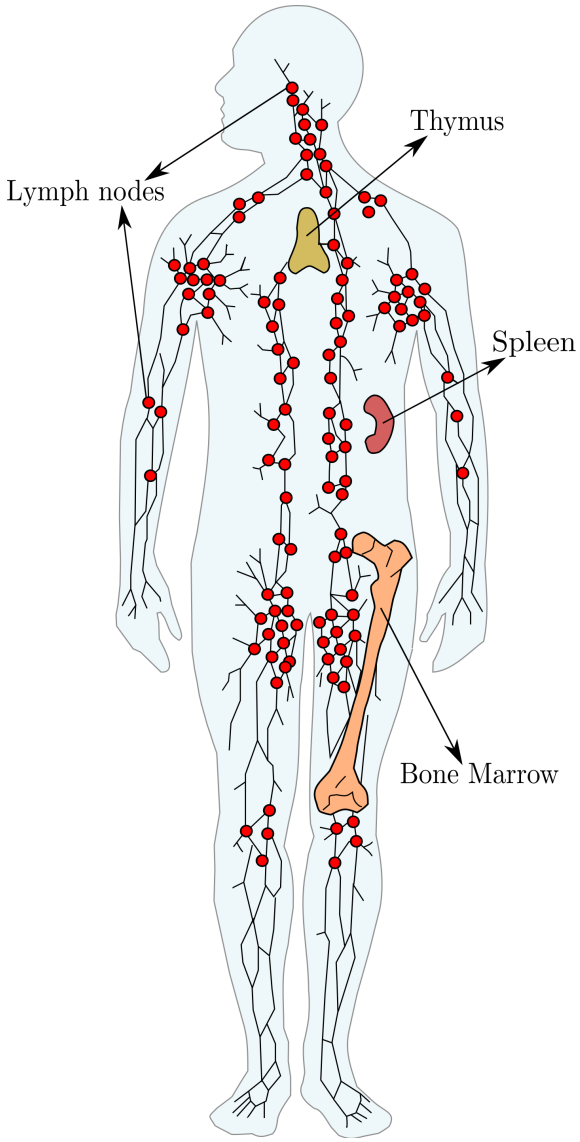


**Figure 2. The lymphatic system**. A network of lymph nodes (red) connected by lymphatic vessels. This network allows to process the substances circulating in the body to detect antigens. Other lymphoid organs, such as the spleen, the bone marrow and the thymus are shown.

- Induce the generation of immune cells from their hematopoietic precursors

Although many immune cells secrete cytokines, the major producers are the macrophages and T lymphocytes, which principally orchestrate the innate and adaptive immune response, respectively. Cytokines can be classified in six different groups, depending on the protean nature of their receptor. For brevity, we better describe a few examples that are relevant in the context of our investigations. The interleukin IL-2 increases the cytotoxic activity of NK cells and the proliferation of T-cells and macrophages. It is mainly secreted by T cells and monocytes. The

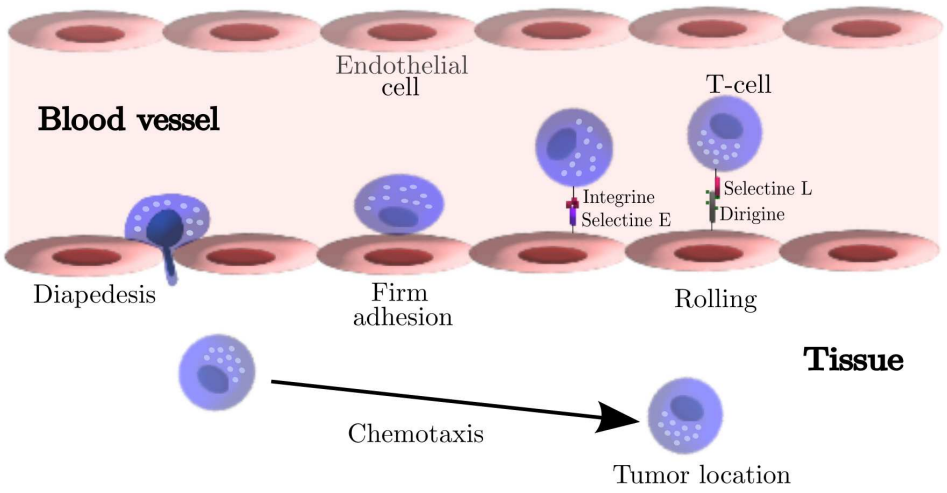


**Figure 3. The process of T cell recruitment**. A cell circulating attaches to the endothelium, rolls on it and transverses these walls of the vessel (diapedesis). Then, it directs to the tumor, following chemical gradients (chemotaxis).

tumor necrosis factor alpha TNF-$\alpha$ triggers the inflammatory response, producing the increase of the diameter of vessels and their permeability, and inducing the expression of adhesion molecules of the endothelium. The interleukins IL-1, IL-6 and IL-12 are important for increasing the temperature of the body, causing fever. T helper cells secrete IL-4, IL-10 and IL-12, which are potent activators of lymphocyte activation and differentiation. T cytotoxic lymphocytes secrete IL-16 which promotes chemotaxis. A very important cytokine is interferon gamma IFN-$\gamma$. It is secreted by T lymphocytes and NK cells, and induces MHC-class I and II molecules presentation. Finally, the transforming growing factor beta TGF-$\beta$ is secreted by macrophages and T helper cells, to inhibit the activation of T cells and macrophages themselves.

To end this succinct introduction to immunology, we describe the origin and trafficking of the immune cells repertoire, with the aim of showing the action of the immune system as a whole complex and coordinated system. The immune system cells are organized forming a network of organs and tissues, communicated by lymphatic vessels (see Fig. 2). Altogether, these structures are known as the lymphatic system. The organs of the lymphatic system are usually classified into primary lymphoid organs (the bone marrow and the thymus) and secondary lymphoid organs (the spleen, the lymph nodes and the mucosa-associated-lymphoid-tissue or simply MALT). The first are responsible for the maturation and differentiation of cells, while the second are sinks for antigenic molecules and cell multiplication.

**Bone marrow:** it is located inside the bones and formed by islets of of hematopoietic cells. All the immune cells are generated from these pluripotent stem cells, and then these precursors of immune cells migrate to other organs where they suffer differentiation. As an exception, immature B-cells both divide and differentiate in this organ.

**Thymus:** it is located in the thorax. Immature T cells migrate to this organ to divide and differentiate. During this process the lymphocytes experience somatic recombination and later suffer positive and negative selection processes. This mechanism ensures the generation of a very heterogeneous population of lymphocytes each with a different receptor, capable of recognizing specific surface proteins.

**Spleen:** it is a big node that drains antigens from the blood. All types of immune cells are found in this organ, that participates in the generation of immune responses against antigens coming from the blood.

**Lymph nodes:** they are located throughout the body including the armpit and the stomach, and are linked by the lymphatic vessels. B cells and T cells are abundant in this organ, which acts as a filter for foreign particles (antigens). Antigen presenting cells (dendrites and macrophages) usually travel to the lymph nodes and present their antigens to T cells, triggering the adaptive response through their activation.

**MALT:** a diffuse system of small concentrations of lymphoid tissue found in various mucosal sites of the body (gastrointestinal tract, thyroid, breast, lung, salivary glands, skin). It is populated by lymphocytes such as T cells, B cells, plasma cells and macrophages. Again, in this site these cells encounter antigens passing through its epithelium.

The bone marrow is constantly generating leukocytes that later on enter the circulatory system. Some of them extravasate in different tissues and wait for the appearance of pathogens, until they die after several weeks (macrophages, mastocytes, dendritic cells). Some other just live a few days in the circulatory system (granulocytes). T cells have to enter the thymus to mature and then, just like mature B cells, are daily recirculating. These cells have an average life of weeks. They abandon the blood vessels and enter the lymph nodes, then leave these nodes through the lymph vessels and close their loop by reentering the blood stream through the subclavian veins. This constant recirculation augments the probability of being activated by a specific antigen.

Things change dramatically when a tissue is infected. Then the inflammatory response triggers. The vessels become more permeable and selectively export immune cells, which are guided by chemotactic molecules. Some of these recruited cells stay in the zone lysing pathogens and secreting cytokines, to reinforce the *recruitment*. Others travel through the blood until they arrive to nearby lymph nodes, where they present antigens and trigger the adaptive immune response, which takes around a week to fully develop. Then, the activated effector T and B cells leave the lymph nodes, and the first travel to the site of infection while the second direct towards the bone marrow, where they secret antibodies. The entire process of recruitment and cell trafficking is accomplished by means of adhesion molecules, such dirigins, integrins and selectins (see Fig. 3).

# Curriculum Vitae

## Publicaciones

- A.G. López, J.M. Seoane and M.A.F. Sanjuán. Effective suppressibility of chaos. *Chaos* **23**, 023107 (2013).

- A.G. López, J. Sabuco, J.M. Seoane, J. Duarte, C. Januário, and M.A.F. Sanjuán. Avoiding healthy cells extinction in a cancer model. *J. Theor. Biol.* **349**, 74-81 (2014).

- A.G. López, J.M. Seoane and M.A.F. Sanjuán. A validated mathematical model of tumor growth including tumor-host interaction, cell-mediated immune response and chemotherapy. *Bull. Math. Biol.* **349**, 74-81 (2014).

- A.G. López, J.M. Seoane, and M.A.F. Sanjuán. On the fractional cell kill law governing the lysis of solid tumors. *Commun. Nonlinear Sci. Numer. Simul.* (Submitted). Available: arXiv:1601.07144v1[q-bio.TO].

- A.G. López, J.M. Seoane, and M.A.F. Sanjuán. Decay dynamics of tumors, *PLoS One* (Submitted).

- A.G. López, J.M. Seoane, and M.A.F. Sanjuán. Dynamics of the cell-mediated immune response to tumor growth. *Proc. R. Soc. A* (Submitted).

## Presentaciones en congresos y seminarios

- **Conferencia**: 6th International scientific conference on physics and control
  **Presentación oral**: Effective suppressibility of chaos
  **Autores**: Álvaro García López, Jesús M. Seoane, and Miguel A. F. Sanjuán
  **Lugar y Fecha**: San Luis de Potosí, Méjico, August, 2013

- **Conferencia**: 6th International scientific conference on physics and control
  **Presentación oral**: Avoiding healthy cells extinction in a cancer model
  **Autores**: Álvaro García López, Juan Sabuco, Cristina Januário, Jorge Duarte, Jesús M. Seoane, and Miguel A. F. Sanjuán
  **Lugar y Fecha**: San Luis de Potosí, Méjico, August, 2013

- **Conferencia**: I Jornadas RSEF / IFIMED de Física Médica
  **Presentación oral**: Cancer Dynamics: Tumor-Immune interactions
  **Autores**: Álvaro García López, Jesús M. Seoane, and Miguel A. F. Sanjuán
  **Lugar y Fecha**: IFIC, Valencia, Spain, March 09-11, 2016

- **Seminario**: Seminars Prof. Yorke's Doctor Honoris Causa
  **Presentación oral**: Avoiding healthy cells extinction in a cancer model
  **Autores**: Álvaro García López, Juan Sabuco, Cristina Januário, Jorge Duarte, Jesús M. Seoane, and Miguel A. F. Sanjuán
  **Lugar y Fecha**: URJC, Móstoles, Madrid, Spain, 30 January 2014

- **Seminario**: Máster en Modelización y Física de Sistemas Complejos
  **Presentación oral**: A validated mathematical model of tumor growth.
  **Autores**: Álvaro García López, Jesús M. Seoane, and Miguel A. F. Sanjuán
  **Lugar y Fecha**: URJC, Móstoles, Madrid, Spain, 2015

- **Seminario**: Máster en Modelización y Física de Sistemas Complejos
  **Presentación oral**: Cellular automata models of tumor growth.
  **Autores**: Álvaro García López, Jesús M. Seoane, and Miguel A. F. Sanjuán
  **Lugar y Fecha**: URJC, Móstoles, Madrid, Spain, 2015

- **Seminario**: Seminars on the visit of Prof. Jesús María Sanz Serna to the URJC
  **Presentación oral**: On the fractional cell kill law governing the lysis of solid tumors
  **Autores**: Álvaro García López, Jesús M. Seoane, and Miguel A. F. Sanjuán
  **Lugar y Fecha**: URJC, Móstoles, Madrid, Spain, 2015

- **Seminario**: Seminars on the visit of Prof. Yorke to the URJC
  **Presentación oral**: On the fractional cell kill law governing the lysis of solid tumors
  **Autores**: Álvaro García López, Jesús M. Seoane, and Miguel A. F. Sanjuán
  **Lugar y Fecha**: URJC, Móstoles, Madrid, Spain, 2015

## Proyectos de investigación

- **Título del proyecto**: Dinámica No Lineal de Sistemas Complejos y Aplicaciones Interdisciplinares (FIS2009-09898)
  **Entidad financiadora**: Ministerio de Ciencia e Innovación
  **Duración desde**: 1 de Enero 2010 **hasta**: 31 de Diciembre 2013

**Investigador principal**: Miguel Angel Fernández Sanjuán
**Tipo de paticipación del doctorando**: Miembro investigador
**Cuantía de la subvención**: 194.810, 01 Euros

- **Título del proyecto**: Dinámica No Lineal de Sistemas Complejos (FIS2013-40653-P)
  **Entidad financiadora**: Ministerio de Economía y Competitividad
  **Duración desde**: 1 de Enero 2014 **hasta**: 31 de Diciembre 2016
  **Investigador principal**: Miguel Angel Fernández Sanjuán
  **Tipo de paticipación del doctorando**: Miembro investigador
  **Cuantía de la subvención**: 54.000 Euros

## Estancias de investigación

- **Lugar**: Curitiba, Brasil
  **Centro y Departamento**: Universidad Federal do Paraná
  **Fecha**: Agosto-Noviembre 2015
  **Financiación**: Beca Iberoamérica del Banco Santander (2015)

# Resumen y conclusiones de la tesis en castellano

# Resumen y conclusiones

## Introducción

A pesar de los avances en el tratamiento de algunos cánceres, y de los miles de millones invertidos por el gobierno americano en la lucha contra el cáncer en los últimos cuarenta años, las tasas de mortalidad de una gran parte de ellos apenas si han disminuido. Estos hechos, junto con diversos hallazgos experimentales que han puesto en duda los cimientos de la teoría de la mutación somática, teoría vigente de la carcinogénesis a lo largo de prácticamente el último siglo, han llevado al National Cancer Institute a abrir doce centros de física y oncología. Sin lugar a duda, a dicha decisión han contribuido los hallazgos de la teoría de los sistemas dinámicos y la no linealidad, así como el subsiguiente desarrollo de las ciencias de la complejidad y la biología de sistemas, iniciadas estas últimas a lo largo de los años cincuenta del siglo pasado, mediante la introducción de principios y técnicas matemáticas capaces de modelizar los sistemas biológicos. En dicho contexto, el presente trabajo se centra en el estudio de las interacciones entre las células cancerígenas que integran un tumor y la respuesta inmunológica celular. En una primera toma de contacto, se investiga un modelo en ecuaciones diferenciales ordinarias de tres poblaciones celulares, publicado previamente en la literatura científica. Dichas poblaciones son las células sanas, las células cancerígenas y las células efectoras de la respuesta inmunitaria. El hallazgo de dinámicas caóticas transitorias en dicho modelo, permite utilizar la técnica del control parcial, consiguiendo mantener el tumor oscilando a niveles tolerables y evitando la extinción de células sanas. Una vez familiarizados con el modelo matemático, se desarrolla otro similar, que posteriormente es ajustado a datos experimentales. A tal efecto, se introduce una función matemática capaz de representar la velocidad del lisado de los tumores por los linfocitos T, que posteriormente es estudiada en detalle utilizando modelos de autómatas celulares. Más adelante, poniendo el proceso de lisis de una célula cancerígena en relación con la cinética enzimática, se estudian los límites que ofrece dicha ley matemática, y una última corrección es introducida. La tesis concluye con el estudio de la dinámicas transitorias y asintóticas que resultan de las interacciones entre las células cancerígenas y las células de la respuesta inmunitaria. Extendiendo los modelos de autómatas celulares utilizados previamente, se demuestra la dificultad de observar periodos muy prolongados de latencia tumoral, mediada exclusivamente por el sistema inmunitario.

## Metodología y objetivos

La metodología utilizada a lo largo del trabajo ha sido teórica y matemática, basada tanto en métodos analíticos como computacionales. Los resultados experimentales utilizados en la validación de los modelos se han tomado prestados de artículos publicados en tres revistas: Nature, Science y Cancer Research. Los objetivos que se han propuesto y cumplido a lo largo de esta tesis doctoral se desglosan en los siguientes apartados, mientras que las conclusiones de la presente investigación se

resumen en la última sección.

### Técnica del control parcial aplicada a un modelo de cáncer

Se estudia un modelo en el que el tejido es representado mediante ecuaciones diferenciales ordinarias. En esta primera aproximación se asume, por lo tanto, homogeneidad espacial. Cada una de las tres variables representa a una población celular, a saber, una población de células cancerígenas asociada a la neoplasia, una población de células sanas que tiende a extinguirse en presencia del tumor, y una población de células efectoras de la respuesta inmunitaria. La competición por espacio y por nutrientes entre las células cancerígenas y el tejido sano, así como la acidificación del entorno resultante del metabolismo primitivo de las primeras, se modeliza mediante ecuaciones tipo Lotka-Volterra. La dinámica de la respuesta inmunológica está comprendida por tres términos: uno de reclutamiento de linfocitos a la región del tumor, como consecuencia de la emisión de citocinas; otro de competición por recursos, que permite incluir la inactivación de las células inmunitarias por las células cancerígenas; y, finalmente, un tercero que representa la inactivación de linfocitos independiente de las células cancerígenas, por poder solo lisar un numero finito de veces. Finalmente, un término de lisis representa la destrucción de células cancerígenas por las celulas inmunitarias, también modelado a la Lotka-Volterra.

Se encuentra que, para un sistema inmune muy eficiente en el reclutamiento y un tumor muy agresivo en su crecimiento, el sistema dinámico presenta oscilaciones caóticas de las poblaciones. Variando los parámetros de los modelos, se observa una crisis de frontera que provoca la aparición de transitorios caóticos, después de los cuales el tumor acaba por dominar todo el tejido, con la consiguiente extinción de células sanas. Con el fin de evitar el escape de las células cancerígenas y el sobrecrecimiento del tumor, se aplica una técnica de control, denominada técnica del control parcial. El método del control parcial permite, dado un sistema dinámico que experimenta dinámicas caóticas previas a la ocurrencia de un acontecimiento en particular, mantener dicha dinámica, evitando dicho suceso indeseado. Asumiendo que dicho sistema experimenta también ciertas perturbaciones externas, nuestro método de control es capaz de evitar la ocurrencia del acontecimiento indeseado, en nuestro caso el sobrecrecimiento del tumor, con la consecuente extinción de células sanas, utilizando controles de menor intensidad que dichas perturbaciones.

En última instancia se discute la imposibilidad de aplicar dicho método, dada la complejidad de los sistemas biológicos.

### Validación de un modelo matemático con datos experimentales

En segundo lugar, se procede a una modificación del modelo anterior para ponerlo en concordancia con resultados experimentales, obtenidos en estudios de la respuesta inmune celular al crecimiento tumoral. Para ello, la función matemática que rige el lisado se modifica, siguiendo trabajos anteriores. Tras la validación del modelo utilizando ajustes por mínimos cuadrados, se analiza su espacio de fases y su sensibilidad a las perturbaciones, mediante la variación de sus parámetros. Para ello

se utilizan técnicas habituales en el estudio de los sistemas dinámicos, como son los diagramas de bifurcaciones o el cómputo de conjuntos invariantes asociados a los puntos fijos inestables (sillas) del mismo. Dicho análisis permite establecer un valor estimado del mínimo nivel de ligandos que han de sobreexpresar las células cancerígenas para que la respuesta inmunitaria sea efectiva. Este hecho podría resultar de interés en el desarrollo de futuras inmunoterapias. En lo que a la nueva función matemática concierne, se proponen una serie de hipótesis con el fin de explicar su naturaleza.

En la última parte del trabajo se introducen unos protocolos de quimioterapia, que son representados mediante el Exponential Kill Model. Para representar los resultados experimentales (obtenidos en estudios *in vivo* con ratones), se propone la utilización de retardos en los modelos, capaces de representar la demora que se observa desde que se administran los fármacos, hasta que ejercen sus efectos citotóxicos, sugiriendo que dichas demoras se deben a los complejos procesos farmacocinéticos en la distribución y absorción de tales agentes. Este método supone una simplificación notable, en comparación con otros modelos farmacocinéticos más complejos.

### La expresión matemática que rige el lisado de un tumor

Con el objeto de estudiar la compatibilidad de las hipótesis planteadas anteriormente en relación con la expresión matemática que determina la velocidad con la que un tumor es lisado por el sistema inmunitario, en función de la citotoxicidad intrínseca de los linfocitos y la geometría del mismo, se desarrolla un autómata celular, propuesto en otros trabajos. Dicho modelo es un modelo espacio-temporal, en el que las células ocupan diversas posiciones en una malla cuadrada. Las células pueden proliferar, migrar o morir, en función de la concentración de nutrientes en cada punto del espacio, siguiendo ciertas reglas probabilísticas. La difusión de nutrientes en el dominio del tumor, tales como el oxígeno y la glucosa, es simulada mediante ecuaciones de reacción y diffusión.

Asumiendo que originalmente el espacio está ocupado por tejido sano, y colocando en el centro del dominio una célula mutada, se itera el sistema en el tiempo, generando tumores con distinta geometría. Se aprecia como, al aumentar la tasa metabólica de las células tumorales, la competición por nutrientes entre las mismas produce, por un proceso de retroalimentación positiva, una ruptura de la simetría esférica de los tumores, que adquierien morfologías papilares y filamentosas.

Se aprovechan las diversas morfologías para estudiar las curvas de lisado. A tal efecto, se disponen diversas poblaciones de linfocitos en los dominios del tumor, y se observa el lisado de los mismos al cabo de cierto tiempo (el equivalente a cuatro horas, que es lo acostumbrado en los ensayos de emisión de cromo en inmunología). Para ello, se supone que el tumor no crece durante el proceso de lisado, tal y como ocurre en muchos experimentos en inmunología, en los que las células del tumor se irradian previamente. En todo caso, el tiempo que tarda una célula en dividirse es aproximadamente de un día, por lo cual se puede asumir una aproximación adiabática. Mediante ajuste por mínimos cuadrados entre los resultados *in silico* y el modelo

en ecuaciones diferenciales ordinarias, se observa que los tumores menos esféricos son lisados más rápidamente. Sin embargo, la función matemática utilizada es incapaz de reproducir los resultados del autómata celular cuando se estudian escenarios inmunodeficientes (cuando las células del sistema inmunitario no son capaces de reconocer bien a las células tumorales). Para ello proponemos una modificación de la misma que reproduce los resultados notablemente mejor. Además, ello permite dilucidar el significado biológico de los parámetros que figuran en dicha función, de forma clarividente. Dos de ellos quedan vinculados a la geomtría del tumor, mientras que el tercero queda asociado a la citotoxicidad intrínseca de los linfocitos. Se provee con ello, por vez primera, una medida rigurosa de la citotoxicidad intrínseca.

Finalmente, utilizando la cinética enzimática para representar el proceso celular, se deriva la función matemática de forma analítica. Esta función puede entenderse como una extensión de la cinética de Michaelis-Menten para situaciones en las que la concentración de substrato es equiparable a la de la enzima.

### El decaimiento de tumores

Establecida la función matemática que representa la velocidad con la que las células efectoras de la respuesta inmunitaria lisan un tumor, se procede a investigar sus límites. Para ello, se obtiene de forma analítica la velocidad con la que un tumor es lisado cuando está completamente rodeado de células inmunitarias. Ajustando nuevamente dicha expresión matemática al modelo de autómata celular descrito anteriormente, y haciendo las modificaciones oportunas, se verifica que en dicho caso el decaimiento de un tumor bidimensional sigue una función del tiempo de forma parabólica, lo cual es consistente con el hecho de que, para tumores conexos, el tumor se reduce en superficie, pero através de su frontera unidimensional. Con el objetivo de que se cumplan dichos límites, y para cubrir también tumores disconexos, es preciso introducir una última modificación en la expresión matemática.

### Dinámica de la respuesta celular al crecimiento tumoral

En última instancia, se procede a estudiar la dinámica transitoria y asintótica que resulta de la coevolución del sistema inmunitario y un tumor. Para ello, se introduce una modificación en el modelo de autómata celular, que incluye el flujo de células inmunitarias de la respuesta innata (células NK), y que suelen depositarse de forma natural en los tejidos.

Mediante el desarrollo de nuevas técnicas, como por ejemplo los diagramas de bifurcaciones transitorios, se observan tres regímenes en función de la citotoxicidad intrínseca de las células efectoras. O bien el tumor es eliminado, si los linfocitos son suficientemente efectivos; o bien el tumor se mantiente a bajos niveles, en un estado de equilibrio que puede durar entre cinco y quince años; o bien los tumores escapan a la vigilancia (inmunoevasión). Ello permite correlar de forma fidedigna los resultados del modelo con la teoría de la inmunoedición. Dicha teoría propone que, habida cuenta de la heterogeneidad celular comunmente hallada en los tumores, el sistema inmunológico esculpe su fenotipo seleccionando las poblaciones que son resistentes a

la vigilancia inmunitaria. En un principio las células susceptibles son eliminadas, sobreviviendo únicamente las células parcial y totalmente resistentes. Luego sigue una etapa de equilibrio o latencia, en la que el tumor permanece asintomático durante un periodo más o menos extenso de tiempo. En última instancia, el proceso desemboca en la evasión inmunitaria de las subpoblaciones más resistentes, observándose el recrecimiento del tumor.

Moviéndonos en el espacio de parámetros, se observa que la ventana de equilibrio es notablemente sensible a las modificaciones de los mismos, manifestando la delicadeza de un estado de latencia tumoral prolongado mediado de forma exclusiva por el sistema inmunitario.

## Conclusiones

Las conlusiones principales que se derivan de nuestro trabajo se exponen a continuación.

- La conclusiones más importantes del capítulo segundo son dos. En primer lugar, que es plausible que la utilización de protocolos de inmunoterapia sea capaz de introducir dinámicas caóticas en la dinámica de crecimiento de un tumor. En el segundo, que a pesar de las limitaciones prácticas del método de control utilizado, el trabajo sugiere una interesante alternativa a la aplicada por los tratamientos convencionales, que está siendo estudiada en otros contextos, como por ejemplo en la quimioterapia. Dicha alternativa propone, en lugar de intentar erradicar un tumor, produciendo la expansión subsiguiente de las pequeñas poblaciones resistentes que generalmente suelen sobrevivir al mismo, mantenerlo a unos niveles razonables, y aprovechar la competición interna de las células cancerígenas y posteriores intervenciones para evitar su expansión. Nótese que en tanto que un tumor no metastatice, en muchas ocasiones, no supone un peligro fatal para el paciente.

- En el tercer capítulo se concluye, mediante el ajuste del modelo a datos experimentales, que la velocidad del proceso de lisis de un tumor no puede incrementarse arbitrariamente. Se propone que dicha saturación es el resultado del apiñamiento de los linfocitos, que dejan de estar en contacto con el tumor cuando son muy numerosos. Así mismo, se concluye que la utilización de retardos es capaz de simplicar notablemente los procesos farmacocinéticos, en una buena aproximación.

- La conclusión del capítulo cuarto es que la velocidad con la que el sistema inmunitario lisa un tumor es mayor conforme aumenta el número de células inmunitarias, pero llegado a un punto satura, dado que una vez que las primeras líneas de linfocitos lo cubren, el resto no están en contacto. Consecuentemente, dado el volumen de un tumor, cuanto mayor es la superficie que encierra dicho volumen, mayor es la velocidad con la que éste es lisado, pues hay más lugar de contacto. Por lo tanto, los tumores esféricos son los más difíciles de lisar.

De igual modo, dado un número suficiente de células inmunitarias, la velocidad con la que se lisa un tumor incrementa al aumentar el número de células tumorales, pero una vez que todas las células inmunitarias están ocupadas lisando a sus adversarias, se observa nuevamente saturación.

- En el capítulo quinto se concluye que, cuando la población de células inmunitarias es pequeña en comparación con el tamaño del tumor, se observa que su decaimiento es lineal con el tiempo. Esto es, el tumor decae con velocidad uniforme. Basta considerar el caso límite en el que sólo se tiene un linfocito. Si éste tarda en lisar una célula cancerígena en torno a una hora, entonces la velocidad de decaimiento es aproximadamente de una célula por hora. Sin embargo, cuando el tamaño de la población de células inmunitarias es suficientemente grande, rodeando todo el tumor, éste se va lisando capa a capa. Dado que la superficie de contacto se hace más pequeña a cada paso, la velocidad disimuye a medida que se reduce el tumor. Si el tumor es conexo, el decaimiento de un tumor bidimiensional es parabólico en dicho límite. Sin embargo, si es disconexo y los linfocitos están homogéneamente mezclados con las células que constituyen el tumor, el decaimiento es exponencial, de forma idéntica a un proceso de decaimiento radiactivo. En casos intermedios, la expresión matemática que rige la lisis de un tumor es una función de Hill cruzada. La cinética del proceso es muy similar a una cinética de Michaelis-Menten, pero que aplica tanto al sustrato como a la enzima. Como se acaba de decir, la función matemática resultante es una función de Hill en dos variables, donde los exponentes, al ser menores o iguales a la unidad, manifiestan el carácter no cooperativo del proceso de lisis. Esto es, en lo que a la lisis concierne, las células se estorban o no lo hacen.

- La conclusión del último capítulo es que, si bien el sistema inmune puede mantener un tumor asintomático durante cierto tiempo (hasta unos pocos anõs), es improbable que sea capaz de mantener un estado de latencia tumoral durante periodos muy prolongados (del orden de quince años). Ello se debe a un ajuste relativamente fino entre los procesos que espolean la respuesta inmunitaria (el reclutamiento, fundamentalmente) y el ritmo de crecimiento del tumor, así como del constante desplazamiento que resulta de dicho proceso.